

Aus der Klinik für Kardiologie und Pneumologie  
(Prof. Dr. med. G. Hasenfuß)  
der Medizinischen Fakultät der Universität Göttingen

# **Evaluation of the antifibrotic potential of Serelaxin in two experimental models of cardiac fibrogenesis**

INAUGURAL-DISSERTATION

zur Erlangung des Doktorgrades  
der Medizinischen Fakultät der  
Georg-August-Universität zu Göttingen

vorgelegt von

**Tim Pascal Wilhelmi**

aus

**Wiesbaden**

Göttingen 2022

Dekan: Prof. Dr. med. Wolfgang Brück

### **Betreuungsausschuss**

Betreuerin: Prof. Dr. med. Elisabeth Zeisberg

Ko-Betreuer: Prof. Dr. med. Michael Zeisberg

### **Prüfungskommission**

Referentin: Prof. Dr. med. Elisabeth Zeisberg

Ko-Referentin: Prof. Dr. rer. nat. Susanne Lutz

Datum der mündlichen Prüfung: 21.09.2023

Hiermit erkläre ich, die Dissertation mit dem Titel "Evaluation of the antifibrotic potential of Serelaxin in two experimental models of cardiac fibrogenesis" eigenständig angefertigt und keine anderen als die von mir angegebenen Quellen und Hilfsmittel verwendet zu haben.

Göttingen, den .....

.....  
(Unterschrift)

Die Daten, auf denen die vorliegende Arbeit basiert, wurden publiziert:

**Wilhelmi T**, Xu X, Tan X, Hulshoff MS, Maamari S, Sossalla S, Zeisberg M, Zeisberg EM (2020): Serelaxin alleviates cardiac fibrosis through inhibiting endothelial-to-mesenchymal transition via RFXFP1. *Theranostics* 10, 3905–3924



## Table of contents

<b>LIST OF FIGURES.....</b>	<b>V</b>
<b>LIST OF TABLES.....</b>	<b>VI</b>
<b>LIST OF ABBREVIATIONS .....</b>	<b>VII</b>
<b>1 INTRODUCTION.....</b>	<b>1</b>
<b>1.1 Cardiac fibrosis.....</b>	<b>1</b>
1.1.1 Definition.....	1
1.1.2 Classification, etiology and pathogenesis .....	1
1.1.3 Diagnostic tools to detect cardiac fibrosis.....	4
1.1.4 Therapeutic management .....	5
<b>1.2 Heart failure .....</b>	<b>6</b>
1.2.1 Definition.....	6
1.2.2 Epidemiology .....	6
1.2.3 Etiology.....	7
1.2.4 Classification.....	8
1.2.5 Pathophysiology.....	9
1.2.6 Clinical presentation .....	11
1.2.7 Diagnostic tools .....	11
1.2.8 Therapeutic management .....	12
<b>1.3 Endothelial to mesenchymal transition (EndMT) .....</b>	<b>14</b>
1.3.1 Definition.....	14
1.3.2 Mechanism and induction .....	14
1.3.3 Markers.....	16
1.3.4 EndMT and cardiac fibrosis.....	17
<b>1.4 Serelaxin .....</b>	<b>18</b>
1.4.1 Relaxin.....	18
1.4.1.1 Ligands .....	18
1.4.1.2 Relaxin family peptide receptors .....	20
1.4.1.3 Effector organs and functions.....	21
1.4.2 Serelaxin and fibrosis .....	22
1.4.3 Serelaxin and acute heart failure.....	22
1.4.3.1 Phase I studies.....	23
1.4.3.2 Phase II studies .....	23
1.4.3.3 Phase III studies.....	24
<b>1.5 Notch signaling pathway .....</b>	<b>25</b>
1.5.1 Mechanism.....	25

---

1.5.2	Functions .....	26
1.5.3	Notch signaling and fibrosis .....	26
<b>1.6</b>	<b>Epigenetics.....</b>	<b>26</b>
1.6.1	Definition.....	26
1.6.2	Mechanisms .....	27
1.6.3	Epigenetic modifications and fibrosis .....	28
<b>1.7</b>	<b>Objectives.....</b>	<b>29</b>
<b>2</b>	<b>MATERIALS AND METHODS .....</b>	<b>30</b>
<b>2.1</b>	<b>Materials.....</b>	<b>30</b>
2.1.1	Animals.....	30
2.1.2	Human tissue.....	30
2.1.3	Cell culture.....	30
2.1.4	Instruments.....	31
2.1.5	Commercial kits .....	32
2.1.6	Chemicals and reagents.....	34
2.1.7	Buffers .....	35
2.1.8	Antibodies.....	40
2.1.9	Oligonucleotides (primers).....	41
2.1.10	Other materials.....	43
2.1.11	Software .....	44
<b>2.2</b>	<b>Methods.....</b>	<b>45</b>
2.2.1	Ascending aortic constriction (AAC) .....	45
2.2.2	Osmotic minipump implantation.....	45
2.2.2.1	Application of Serelaxin .....	46
2.2.2.2	Application of Angiotensin-2 (ATII) .....	46
2.2.3	Echocardiographic measurements .....	46
2.2.4	Blood pressure measurement in ATII-treated animals.....	46
2.2.5	Sacrifice and preparation .....	46
2.2.6	Cell culture experiments .....	47
2.2.6.1	Maintenance and harvesting.....	47
2.2.6.2	TGF $\beta$ 1 and Serelaxin treatment.....	47
2.2.6.3	Relaxin family peptide receptor experiments .....	47
2.2.6.4	Notch pathway signaling experiments.....	48
2.2.7	Histological methods .....	48
2.2.7.1	Preparation and processing of tissue sections.....	48
2.2.7.2	Hematoxylin-eosin (HE) staining .....	48
2.2.7.3	Masson-Trichrome staining (MTS).....	49
2.2.8	Immunofluorescence staining.....	49
2.2.9	Immunohistochemistry staining.....	50
2.2.10	Histological quantification of fibrosis and immune staining .....	50
2.2.11	Medium densitometry analysis.....	51
2.2.12	RNA extraction .....	51
2.2.13	Measurement of nucleic acid concentration.....	51
2.2.14	RNA reverse transcription .....	52

2.2.15	Quantitative real-time PCR.....	52
2.2.16	EndMT qPCR array .....	52
2.2.17	Protein extraction .....	53
2.2.17.1	Protein extraction from murine heart tissue .....	53
2.2.17.2	Protein extraction from MCEC and HCAEC .....	53
2.2.18	Determination of the protein concentration .....	53
2.2.19	Western blotting .....	53
2.2.20	Chromatin immunoprecipitation (ChIP) .....	54
2.2.21	Statistical analysis .....	56
<b>3</b>	<b>RESULTS.....</b>	<b>57</b>
<b>3.1</b>	<b>The impact of Serelaxin in pressure overload mouse models .....</b>	<b>57</b>
3.1.1	Cardiac fibrosis and survival in AAC mouse model .....	57
3.1.2	Cardiac phenotype and heart's performance in AAC mouse model.....	59
3.1.3	Fibrosis in Angiotensin-2 mouse model .....	61
<b>3.2</b>	<b>Analysis of EndMT upon Serelaxin treatment .....</b>	<b>63</b>
3.2.1	EndMT in two independent mouse models.....	63
3.2.2	TGF $\beta$ 1-induced EndMT <i>in vitro</i> .....	65
<b>3.3</b>	<b>Role of RXFPs in Serelaxin-induced inhibitory effect on EndMT .....</b>	<b>67</b>
3.3.1	RXFPs in HCAECs.....	67
3.3.2	RXFPs in MCECs .....	67
3.3.3	RXFPs <i>in vivo</i> .....	68
<b>3.4</b>	<b>Evaluation of signaling pathways affected by Serelaxin.....</b>	<b>72</b>
3.4.1	Gene candidates during EndMT .....	72
3.4.2	Validation of EndMT gene candidates <i>in vitro</i> and <i>in vivo</i> .....	73
3.4.3	Expression of Notch pathway proteins <i>in vivo</i> .....	75
3.4.4	Molecular activation of Notch signaling by Serelaxin.....	77
<b>3.5</b>	<b>Serelaxin rescues Rxfp1 expression through histone modifications in Rxfp1 promoter region .....</b>	<b>79</b>
3.5.1	Histone modifications upon Serelaxin treatment .....	79
3.5.2	Serelaxin's influence on histone modifications under Rxfp1 knockdown .....	80
3.5.3	TGF $\beta$ /SMAD2/3 cascade affected by Serelaxin .....	81
<b>4</b>	<b>DISCUSSION .....</b>	<b>84</b>
<b>4.1</b>	<b>Two independent disease models of pressure-overload .....</b>	<b>84</b>
<b>4.2</b>	<b>Serelaxin attenuates cardiac fibrosis and improves overall survival.....</b>	<b>85</b>
<b>4.3</b>	<b>Serelaxin impacts different signaling pathways to inhibit EndMT <i>in vitro</i> and <i>in vivo</i> .....</b>	<b>87</b>
<b>4.4</b>	<b>Epigenetic regulation of Rxfp1 by Serelaxin in endothelial cells .....</b>	<b>90</b>
<b>4.5</b>	<b>Future perspectives and potential applications .....</b>	<b>92</b>

---

<b>5</b>	<b>SUMMARY .....</b>	<b>95</b>
<b>6</b>	<b>REFERENCES .....</b>	<b>96</b>

## List of figures

Figure 1: Classification and pathology of cardiac fibrosis .....	2
Figure 2: Origins of activated cardiac myofibroblasts.....	3
Figure 3: TGF $\beta$ signaling pathway .....	15
Figure 4: Markers of endothelial to mesenchymal transition .....	17
Figure 5: Synthesis of Relaxin .....	19
Figure 6: Signal transduction upon activation of RXFP1 mediated by relaxin. ....	21
Figure 7: Notch signaling pathway .....	25
Figure 8: Experimental design of AAC mouse model .....	57
Figure 9: Serelaxin ameliorates cardiac fibrosis in AAC mouse model.....	58
Figure 10: Serelaxin ameliorates cardiac fibrosis.....	59
Figure 11: AAC-operated mouse hearts showed an enlarged phenotype .....	60
Figure 12: Experimental design of ATII mouse model.....	61
Figure 13: Serelaxin ameliorates cardiac fibrosis in ATII mouse model.....	62
Figure 14: Serelaxin attenuates EndMT in two different mouse models of cardiac fibrogenesis .....	64
Figure 15: Serelaxin does not affect apoptosis in AAC-operated mouse hearts .....	65
Figure 16: Serelaxin partially inhibits TGF $\beta$ 1-induced EndMT in HCAECs MCECs.....	66
Figure 17: Attenuation of TGF $\beta$ 1-induced EndMT by Serelaxin in HCAECs is mediated by RXFP1 .....	68
Figure 18: Serelaxin partially inhibits TGF $\beta$ 1-induced EndMT via Rxfp1 in MCEC.....	69
Figure 19: Serelaxin attenuates EndMT via RXFP1 <i>in vitro</i> and <i>in vivo</i> .....	71
Figure 20: Evaluation of EndMT gene candidates in TGF $\beta$ 1- and Serelaxin-treated HCAECs .....	73
Figure 21: Validation of EndMT gene candidates affected by Serelaxin <i>in vitro</i> and <i>in vivo</i> .....	74
Figure 22: Serelaxin restores expression of Notch1 pathway proteins in AAC-operated hearts .....	76
Figure 23: Reduction of soluble Jagged1 upon TGF $\beta$ 1 treatment in MCECs .....	77
Figure 24: Serelaxin rescues TGF $\beta$ 1-induced inhibition of Notch pathway via Rxfp1 in MCECs .....	78
Figure 25: Experimental validation of Serelaxin's ability to rescue Notch pathway <i>in vitro</i> .....	78
Figure 26: Serelaxin reactivates Rxfp1 expression via histone modifications.....	80
Figure 27: Serelaxin induces cascade of histone modifications by binding to Rxfp1.....	81
Figure 28: Serelaxin impacts histone modifications by inhibiting TGF $\beta$ / SMAD2/3 axis .....	82
Figure 29: Molecular mechanism Serelaxin drives to partially inhibit EndMT and cardiac fibrosis.....	82

## List of tables

Table 1: Cell lines used in this study .....	30
Table 2: Cell culture mediums used in this study.....	31
Table 3: Instruments used in this study.....	31
Table 4: Commercial kits used in this study .....	33
Table 5: Chemicals and reagents used in this study.....	34
Table 6: Ready-to-use buffers used in this study .....	35
Table 7: Preparation of 10x PBS .....	36
Table 8: Preparation of 10x TBS .....	36
Table 9: Preparation of citrate buffer .....	36
Table 10: Preparation of immunohistofluorescence blocking buffer .....	36
Table 11: Preparation of 10 ml NP40 lysis buffer .....	36
Table 12: Preparation of 1000 ml 1x T-BST buffer .....	37
Table 13: Preparation of 400 µl Western blot sample buffer.....	37
Table 14: Preparation of 1000 ml Western blot inner buffer.....	37
Table 15: Preparation of 1000 ml Western blot outer buffer .....	37
Table 16: Preparation of 50 ml Western blot blocking (5%) or washing (2%) buffer .....	37
Table 17: Preparation of 50 ml Western Blot transferring buffer .....	37
Table 18: Preparation of 100 ml ChIP Nuclear preparation buffer.....	38
Table 19: Preparation of 5 ml ChIP Sonication buffer-1 .....	38
Table 20: Preparation of 50 ml ChIP Sonication buffer-2 .....	38
Table 21: Preparation of 250 ml ChIP Dilution buffer .....	38
Table 22: Preparation of 250 ml ChIP IP buffer .....	39
Table 23: Preparation of 50 ml ChIP Wash buffer.....	39
Table 24: Preparation of 250 ml ChIP TE buffer.....	39
Table 25: Primary and secondary antibodies for immunofluorescence used in this study.....	40
Table 26: Primary antibodies for immunohistochemistry used in this study .....	41
Table 27: Antibodies for Western blot used in this study .....	41
Table 28: Antibodies for ChIP assay used in this study.....	41
Table 29: Primers for ChIP-qPCR assay for Rxfp1 used in this study.....	41
Table 30: Primers for qRT-PCR used in this study .....	42
Table 31: Other materials used in this study.....	43
Table 32: Software used in this study.....	44
Table 33: AAC survival differences between both sexes.....	59

## List of abbreviations

AAC	ascending aortic constriction
AAV	adeno-associated virus
ACC	American College of Cardiology
ACE	angiotensin converting enzyme
ADH	antidiuretic hormone
AHA	American Heart Association
AHF	acute heart failure
ALK	activin receptor-like kinase
ANOVA	analysis of variance
AP1	activator protein 1
ARNI	angiotensin-receptor-neprilysin-inhibitor
ATII	angiotensin 2
ATP	adenosine triphosphate
ATR1/2	angiotensin receptor 1/2
$\alpha$ -SMA	$\alpha$ -smooth muscle actin
BCA	bicinchoninic assay
BMP	bone morphogenetic protein
BNP	brain natriuretic peptide
BPG	bisphosphoglycerate
BRD4	bromodomain-containing protein 4
CAD	coronary artery disease
cAMP	cyclic adenosine monophosphate
cDNA	complementary DNA
CD31	cluster of differentiation 31
CM	cardiomyopathy
Col1 $\alpha$ (I)	$\alpha$ -1 type I collagen
CRS	cardiorenal syndrome
CRT	cardiac resynchronisation therapy
C-terminus	carboxyl-terminus
CT	cycle threshold
DAPI	4',6-diamidino-2-phenylindole
DAPT	N-[N-(3,5-Difluorophenacetyl)-L-alanyl]-S-phenylglycine t-butyl ester
ddH <sub>2</sub> O	double-distilled water
Dll	delta-like
DMEM	Dulbecco's modified eagle medium
DMSO	dimethyl sulfoxide
DNA	deoxyribonucleic acid
dNTP	deoxy nucleoside triphosphate
DTT	dichlorodiphenyltrichlorethan
ECG	electrocardiogram
ECM	extracellular matrix
EDV	end-diastolic volume
EDTA	ethylenediaminetetraacetic acid
EF	ejection fraction
EMT	epithelial to mesenchymal transition
EndMT	endothelial to mesenchymal transition
eNOS	endothelial nitric oxide synthase
ERBB3	receptor tyrosine-protein kinase erbB-3

---

Erk	extracellular-signaling-regulated-kinase
ESC	European Society of Cardiology
EtOH	ethanol
EU	European Union
f	female
FBS	fetal bovine serum
FCS	fetal calf serum
FDA	Food and Drug Administration
FS	Fractional shortening
FSP-1	fibroblast specific protein-1
FZD7	frizzled class receptor 7
GAPDH	glyceraldehyd-3-phosphat-Dehydrogenase
GPCR	G protein-coupled receptor
GSC	goosecoid protein
GSK3B	glycogen synthase kinase 3 beta
HCAEC	human coronary artery endothelial cells
HDAC	histone deacetylases
HE	hematoxylin and eosin
HEPES	4-(2-hydroxyethyl)-1-piperazineethanesulfonic acid
HERP	HES-related proteins
HER3	human epidermal growth factor receptor 3
HES1	hairy and enhancer of split-1
HF	heart failure
HFmrEF	heart failure with mildly reduced left ventricular ejection fraction
HFpEF	heart failure with preserved left ventricular ejection fraction
HFrfEF	heart failure with reduced left ventricular ejection fraction
HR	hazard ratio
ICD	implantable cardioverter-defibrillator
IGF	insulin-like growth factor
IL	interleukin
iNOS	inducible nitric oxide synthase
INSL	insulin-like peptide
KD	knockdown
LGR	leucine-rich repeat-containing G-protein-coupled receptors
lncRNA	long non-coding ribonucleic acid
LVIDd	diastolic left ventricular inner diameter
LVIDs	systolic left ventricular inner diameter
m	male
MAPK	mitogen-activated protein kinase
MCEC	mouse cardiac endothelial cells
miRNA	micro ribonucleic acid
MMP	matrix metalloprotease
MRI	magnetic resonance imaging
mRNA	messenger ribonucleic acid
MTS	Masson's trichrome staining
NEM	N-ethylmaleimide
NF- $\kappa$ B	nuclear factor 'kappa-light-chain-enhancer' of activated B-cells
NICD	notch intracellular domain
nNOS	neuronal nitric oxide synthase
NO	nitrogen monoxide
N-terminus	amino-terminus



---

NT-proBNP	N-terminal prohormone of brain natriuretic peptide
NYHA	New York Heart Association
OE	overexpression
ORF	open reading frame
PBS	phosphate buffered saline
PCR	polymerase chain reaction
PC-1	proprotein-convertase 1
PDE	phosphodiesterase
PECAM-1	platelet endothelial cell adhesion molecule-1
PICP	procollagen I C-terminal propeptide
PIIINP	procollagen III N-terminal propeptide
PKA	protein kinase A
PKC	protein kinase C
PW	pulse wave
PWT <sub>d</sub>	diastolic posterior wall thickness
PWT <sub>s</sub>	systolic posterior wall thickness
RAAS	renin-angiotensin-aldosterone-system
RAC1	rac family small GTPase 1
RASAL1	RAS (rat sarcoma) protein activator like 1
RLN	relaxin
RLX030	Serelaxin
RNA	ribonucleic acid
(q)RT-PCR	(quantitative) real-time polymerase chain reaction
RXFP	relaxin family peptide receptor
SDS-PAGE	sodium dodecyl sulphate–polyacrylamide gel electrophoresis
SEM	standard error of mean
SGLT2	sodium/glucose cotransporter 2
shRNA	small hairpin RNA
siRNA	small interfering RNA
SD	standard deviation
SLUG	snail family transcriptional repressor 2
(p)SMAD	phosphorylated SMAD
SNAIL	snail family transcriptional repressor 1
Steap1	six-transmembrane epithelial antigen of prostate 1
ST2	soluble interleukin 1 receptor-like 1
TAC	transverse aortic constriction
T-ALL	T-cell acute lymphoblastic leukaemia
TBS	Tris-buffered saline
TBST	Tris-buffered saline with Tween20
Tet3	tet methylcytosine dioxygenase 3
TGF $\beta$	transforming growth factor $\beta$
TNF $\alpha$	tumor necrosis factor $\alpha$
TSS	transcription starting site
TWIST	twist family basic helix-loop-helix transcription factor 1
VE-cadherin	vascular endothelial cadherin
Vold	diastolic left ventricular volume
Vols	systolic left ventricular volume
vWF	von Willebrand factor
WGA	wheat germ agglutinin
ZEB	zinc finger E-box-binding homebox

# 1 Introduction

## 1.1 Cardiac fibrosis

### 1.1.1 Definition

The heart has a dynamic architecture and, as all organs and tissues, it consists of two principal components: First, residing and mobile cells that fulfill their specific parenchymal or stromal functions. Second, an interstitial, non-cellular space called extracellular matrix (ECM) that contains fibers, enzymes and other macromolecules. ECM serves as a structural and biochemical scaffolding for surrounding cells by being highly durable, mechanically stable and by providing an electrical separation (Baxter et al. 2008; Frantz et al. 2010). With an approximate amount of 85%, the major component of the human adult cardiac ECM is collagen type I, followed by collagen type III (approximately 11%) (Bashey et al. 1992). The synthesis and turnover of collagen is predominantly regulated by cardiac fibroblasts (Kong et al. 2014).

Cardiac fibrosis is a crucial feature of nearly every form of chronic heart disease (Boudoulas and Hatzopoulos 2009). Regardless of their cellular origin, activated cardiac fibroblasts mediate fibrogenesis by an excessive extracellular deposition of connective tissue (Zeisberg and Kalluri 2010; Kong et al. 2014). The fibrotic heart exhibits an altered ratio of collagen type I to collagen type III, depending on the etiology of cardiac fibrosis. An increased level of collagen type I was observed in myocardial infarction, whereas an upregulation of collagen type III occurred in patients suffering from ischemic cardiomyopathy (Mukherjee and Sen 1991; Mukherjee and Sen 1993; Kong et al. 2014). The process described above is called myocardial remodeling and leads to an increased wall stiffness, reduced contractility and a disturbed electrical integrity. Myocardial remodeling results in chamber dilation, cardiomyocyte hypertrophy and cardiac arrhythmia. Ultimately, these pathological conditions lead to congestive heart failure (HF) (Weber et al. 1988; Sabbah et al. 1995; Cohn et al. 2000; Schotten et al. 2004; Brown et al. 2005).

### 1.1.2 Classification, etiology and pathogenesis

Myocardial fibrosis can be subdivided into two types, namely interstitial and replacement fibrosis (**Figure 1**) (Anderson et al. 1979; Ambale-Venkatesh and Lima 2015). The two forms of myocardial fibrosis are induced in several models of HF.

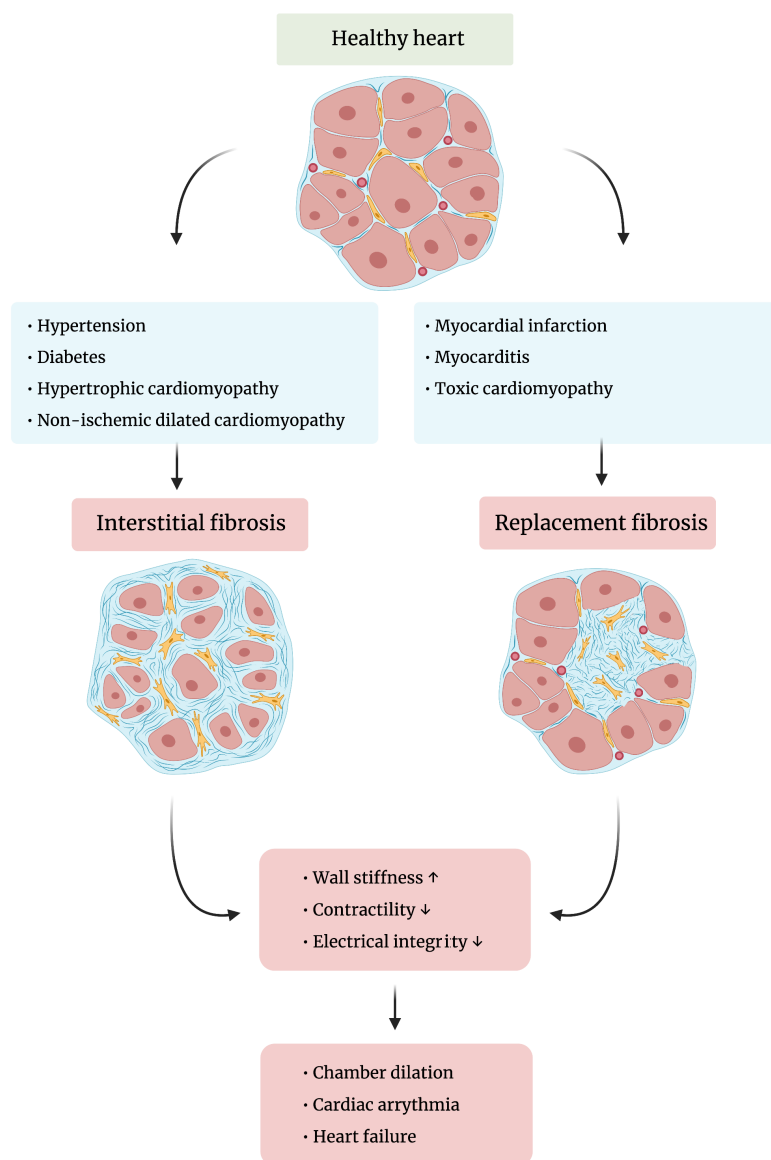


**Figure 1: Classification and pathology of cardiac fibrosis** Systematic scheme of the two main histological forms of cardiac fibrosis with their respective etiologies, common pathological consequences and clinical manifestations (modified from Sweeney et al.(2020); created with BioRender.com).

Interstitial fibrosis functions as a diffuse adaptive response. It ensures an initial preservation of cardiac structure and function. Its subtypes include reactive and infiltrative interstitial fibrosis. The former is present in many types of diseases including hypertension, diabetes, non-ischemic dilated cardiomyopathy, hypertrophic cardiomyopathy, sarcoidosis, and chronic renal insufficiency. The latter is relatively rare. It occurs as result of progressive interstitial deposition of insoluble proteins occurring, for example, in amyloidosis or glycosphingolipids as it is the case with Anderson-Fabry disease (Hashimura et al. 2017; Liu et al. 2017). Replacement fibrosis compensates a lack of cells in areas of cardiomyocyte necrosis and mainly occurs after myocardial infarction. Moreover, replacement fibrosis is associated with conditions such as sarcoidosis, myocarditis, toxic cardiomyopathies and chronic renal insufficiency (Burt et al. 2014; Liu et al. 2017). In our study, ascending aortic constriction (an animal model of left ventricular pressure overload) is utilized, which is

similar to aortic stenosis. It is characterized by both reactive interstitial fibrosis and replacement fibrosis (Isoyama and Nitta-Komatsubara 2002).

The cellular initiators of cardiac fibrosis are myofibroblasts. They are not physiologically present until their precursor cells are activated and subsequently differentiate into myofibroblasts. Myofibroblasts are activated for multiple reasons such as pressure overload, myocardial injuries, viral infections, toxic molecules and genetic abnormalities (Bernaba et al. 2010; Creemers and Pinto 2011; Lindner et al. 2014; Shinde and Frangogiannis 2014; Liu et al. 2017). Although the distinct sources of activated cardiac fibroblasts remain unclear, several origins have been identified (**Figure 2**). Traditionally, it is understood that activated myofibroblasts derive from resident fibroblasts by activation and proliferation upon pathological stimuli (Moore-Morris et al. 2014). Mollmann et al. (2006) found that under myocardial infarct conditions most myofibroblasts derived from hematopoietic progenitor cells. Zeisberg et al. (2007b) drew a different conclusion by lineage tracing, whereby the implicated fibroblasts derived from endothelial cells via endothelial to mesenchymal transition (EndMT). Cells of the embryonic epicardium that undergo epithelial to mesenchymal transition (EMT) during development are also recognized as an origin of myofibroblasts (Muñoz-Chápuli et al. 2001). Pericytes that rest in the perivascular surrounding of cardiac vessels appear to be another important source of cardiac myofibroblasts (Kramann et al. 2015).

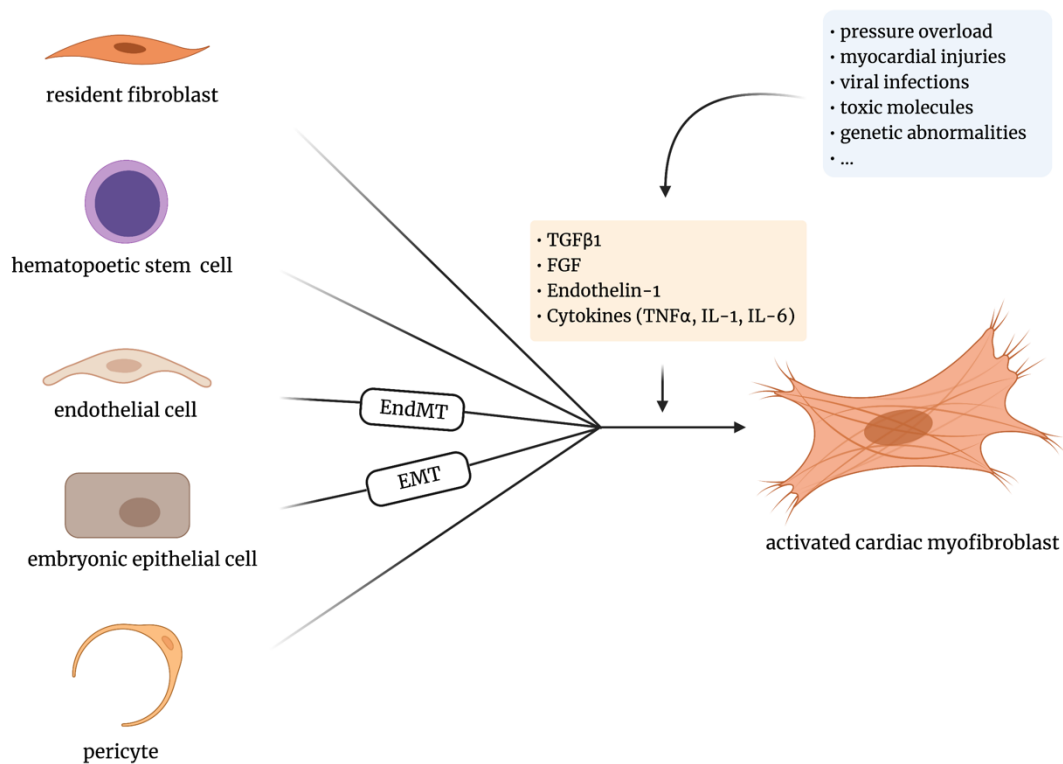


**Figure 2: Origins of activated cardiac myofibroblasts** In the context of different diseases, stimulation by various molecular factors can lead to differentiation or transition of resident fibroblasts, hematopoietic stem cells, endothelial cells (EndMT), embryonic epithelial cells (EMT) or pericytes to activated cardiac myofibroblasts (created with BioRender.com).

The activation of cardiac myofibroblasts is mediated by mechano-sensitive adhesion proteins including Integrins and Cadherins, as well as molecular signaling (Schroer and Merryman 2015). Investigating the wide range and complex interaction of molecular pathways that activate myofibroblast such as transforming growth factor beta 1 (TGF $\beta$ 1), fibroblast growth factor, endothelin-1 and cytokines (e.g. TNF $\alpha$ , IL-1 and IL-6) have helped to understand the initiation, progression and regression of cardiac fibrosis (Rogler et al. 2001; Shi-Wen et al. 2004; Zent and Guo 2018). Activated fibroblasts from failing or infarcted hearts show typical changes such as increased migration and synthesis of collagen, expression of  $\alpha$ -smooth muscle actin, and pro-inflammatory cytokine secretion (Squires et al. 2005; Flack et al. 2006).

### 1.1.3 Diagnostic tools to detect cardiac fibrosis

Various methods of diagnosing cardiac fibrosis are established and available. The current gold standard is a histological quantification of the amount of collagen and the description of type and extent of cardiac fibrosis based on an endomyocardial biopsy. The biopsy can be obtained during open heart surgery, myectomy or with catheter-based procedures (Jellis et al. 2010; Pattanayak and Bleumke 2015).

Alongside the biopsy analysis, there are several non-invasive diagnostic tools, which allow an indirect identification of cardiac fibrosis. A simple and readily available instrument is the electrocardiogram which visualizes QRS prolongation, frequent ventricular premature beats and ventricular tachycardia caused by cardiac fibrosis (Loring et al. 2013). Increased left ventricular end diastolic diameter, decreased ejection fractions, systolic desynchrony, and elevated filling pressures can be detected by ultrasonic cardiogram. However, given their low specificity, these techniques are only of limited use for a definitive diagnosis.

In addition, a cardiac MRI scan is a diagnostic technique that maps the heart tissue composition and function after application of Gadolinium-based contrast agents (Everett et al. 2016). In absence of contrast injection, it is considered a non-invasive procedure. However, it is an expensive technique that requires a high level of expertise and skills for image generation and analysis (Graham-Brown et al. 2017).

Although there is extensive clinical data published on a number of circulating biomarkers that reflect cellular and molecular response, correlating with the quantity of fibrotic heart tissue, such as Galectin-3 (secreted by inflammatory cells and fibroblasts), ST2 (soluble interleukin 1 receptor-like 1), microRNA, pro-collagen type I (PICP) and amino-terminal pro-peptide of pro-collagen type III (PIIINP), the studies lack specific proof that they are proportionally correlated to myocardial fibrosis (Prockop and Kivirikko 1995; Ho et al. 2012; Yancy et al. 2013; Thum 2014; López et al. 2015; Passino et al. 2015).

### 1.1.4 Therapeutic management

The development of cardiac fibrosis can be understood as excessive scarring that cannot contain itself. For that reason, the modification of scar properties plays a decisive role in anti-fibrotic therapy, especially after myocardial infarction (Rog-Zielinska et al. 2016). Since the remodeling process of the heart ultimately leads to HF, cardiac fibrosis therapy is currently limited to guideline-compliant treatment of HF. The four medicinal first-line interventions are beta-blockers, ACE inhibitors, aldosterone antagonists and SGLT2 inhibitors (McDonagh et al. 2021). Beta blockers have anti-arrhythmic effects against arrhythmia that can be caused by cardiac fibrosis, and, in this way, decrease the risk of sudden cardiac death (Al-Gobari et al. 2013). ACE inhibitors target the renin-angiotensin-aldosterone system and inhibit cardiac remodeling (Ertl and Frantz 2005). By inhibiting the binding of angiotensin 2 (ATII) to its specific angiotensin receptor 1 (ATR1) on myofibroblasts, Losartan suppresses the function of TGF $\beta$ 1 to prevent the activation of myofibroblasts (Sun 1998). Eplerenon has been shown to suppress fibrosis formation by blocking the aldosterone pathway (Neefs et al. 2017).

However, to date no specific therapy is clinically available to halt the progression of cardiac fibrosis. Nevertheless, several pre-clinical and clinical studies have attempted to address fibrogenesis and its progression either by targeting collagen synthesis or its degradation. Collagen synthesis includes an intracellular and an extracellular part. Within the fibroblasts, pre-collagen is synthesized, combined to form triple helices, and gets chemically modified by enzymes such as the lysyl oxidase. After being secreted to the extracellular space, the pre-collagen microfibrils are cross-linked to form the final collagen structure. Torasemide, a loop diuretic, is reported to inhibit lysyl oxidase and thereby limits the speed by which collagen is crosslinked (López et al. 2009).

Furthermore, Torasemide treatment reduced TGF $\beta$ 1 signaling pathway activation and thus ameliorated cardiac fibrosis in patients with chronic HF (López et al. 2007). Another attempt targeted TGF $\beta$ 1 signaling by a specific antibody. Its administration led to a decreased collagen synthesis. However, systemic off target effects could not be excluded by addressing the reduction of cardiac fibrosis (Wynn and Ramalingam 2012).

In recent years, injectable biomaterials that control cardiac fibrosis have sparked interest. In a rat model of chronic myocarditis, Gelatin hydrogel sheets that contain a hepatocyte growth factor improved cardiac function and decreased fibrosis by activating matrix metalloprotease (MMP) 1 to increase collagen degradation (Nakano et al. 2014).

Cardiac fibrogenesis is driven by the activation and proliferation of cardiac fibroblasts. Since they form the largest population in fibrotic areas of the heart, the idea of reprogramming these cells to generate cardiomyocytes and replace cardiac scars has attracted greater interest among researchers. Several groups successfully attempted to reprogram residual fibroblasts

to induce cardiomyocytes in murine hearts by retroviral transduction and thereby reduce the extent of fibrosis (Inagawa et al. 2012; Qian et al. 2012; Miyamoto et al. 2018).

Recently, a variety of non-coding RNA such as micro-RNA (miRNA) and long non-coding RNA (lncRNA) have been identified to modulate fibrosis. Silencing of miRNA-21 and miRNA-34 have been shown to reduce fibrosis (Thum et al. 2008; Huang et al. 2014). However, miRNA-29 was shown to extensively increase collagen synthesis (van Rooij et al. 2008). Additionally, distinct fibrosis-related genes can be regulated by lncRNAs such as Wisper and MIAT (Micheletti et al. 2017; Qu et al. 2017). These data suggest that non-coding RNAs are suitable targets for regulating the development and progression of cardiac fibrosis.

Recently, it has been shown that epigenetic changes (see section 1.6) regulate pro-fibrotic genes in fibroblasts and immune cells (Felisbino and McKinsey 2018). Mocetinostat, an inhibitor of histone deacetylase, rejected an activation of fibroblast and thereby ameliorated cardiac fibrosis in preliminary studies (Nural-Guvener et al. 2014). Furthermore, an inhibitor of the epigenetic reader bromodomain-containing protein 4 (BRD4) suppressed profibrotic transcriptional networks in HF in mice that underwent myocardial infarction (Duan et al. 2017). All described data is generated from preclinical studies; however, the results are promising in terms of developing an instrument for clinical treatment of cardiac fibrosis.

## 1.2 Heart failure

### 1.2.1 Definition

HF describes all those conditions by which the heart's performance is insufficient for a regular blood circulation. It is caused by abnormalities in the structure and/or function of the heart, which leads to decreased cardiac output and/or an increase in filling pressures of the heart at rest or during exercise. Decreased cardiac output and increased filling pressures result in back pressure and accumulation of water throughout the body, which can be observed in the form of edema e.g., on the legs and in the lungs. The subsequent pulmonary water retention manifests as a subjective shortness of breath called dyspnea. Therefore, the symptomatic treatment primarily aims to relieve the heart by fluid dehydration (Ponikowski et al. 2016; Herold 2020).

### 1.2.2 Epidemiology

The specificity of epidemiological data depends on the population that is included in the definition. The prevalence of HF is largely age-dependent and averages at approximately 2%. In the 5th decade HF occurs in around 1%, in the 6th decade 4% and in the 8th decade up to 10% (Mosterd and Hoes 2007). With the increase in life expectancy, the incidence of the disease rises alongside. Although the overall prevalence of HF is only slightly at the expense

of the male sex ( $m : f = 1,1 : 1$ ), the lifetime risk of HF at 55 years of age, is 33% for men compared to 28% for women (Bleumink et al. 2004; Herold 2020).

With HF as the most common cause of hospitalization among adults and the third most common cause of death in Germany it has far-reaching health-economic consequences as the highest costs for the system arise from hospital admissions. The median survival after the first inpatient decompensation is 2.5 years while it decreases to 1.5 years after the second. In the best-case scenario, therapies used for HF should not only be symptomatic, but also reduce the frequency of hospital admissions. The effect on the frequency of hospital admissions is therefore assessed in approval-relevant studies (Zugck et al. 2010; Herold 2020; Wirtz et al. 2020)

### 1.2.3 Etiology

The heart's pumping function can be restricted for several different reasons. The reasons can be broadly assigned to three main principles: systolic ventricular dysfunction, diastolic ventricular dysfunction and cardiac arrhythmia. Multiple rare etiologies exist beside these categories.

Essentially, a systolic ventricular dysfunction can be characterized by three states, to which specific etiologies can be assigned:

First, a reduced cardiac contractility and stroke volume which mainly occur during coronary artery diseases (CAD) and myocardial infarction (50%) as well as cardiomyopathies (CM; 15%) such as dilated CM and end stage hypertrophic CM. Additionally, myocarditis can cause a systolic ventricular dysfunction (Zabalgaitia et al. 2001; Ammirati et al. 2018; Vikhorev and Vikhoreva 2018).

Second, a constant and excessive ejection capacity caused by pendulum volume, which occurs during valve vicia such as aortic regurgitation (Starling et al. 1991).

And third, an increased pumping resistance because of a flow obstruction. This is mainly caused by arterial hypertension, pulmonary hypertension and stenosis vicia such as aortic stenosis (Herold 2020).

A diastolic ventricular dysfunction is characterized by reduced diastolic elasticity and, as a result, reduced filling of the ventricles. Reduced diastolic elasticity occurs, for example, in left ventricular concentric hypertrophy, arterial hypertension, constrictive pericarditis, restrictive CM or pericardial tamponade (Mandinov 2000; Herold 2020).

Cardiac arrhythmia, more precisely bradycardia and tachycardia of any origin can cause HF. The most common representative is tachyarrhythmia absoluta during atrial fibrillation (Kantharia 2010).

Finally, there are less frequent etiologies like systemic diseases with cardiac involvement (such as sarcoidosis, amyloidosis, hemochromatosis and pheochromocytoma), connective



tissue disorders (mainly systemic lupus erythematosus), electrolyte imbalances (in particular hypocalcemia and hypophosphatemia from any cause), vitamin and nutrient deficiency (severe thiamine or selenium deficiency), tumors of the heart (e.g. atrial myxoma), infiltration by other malignancies, side effects of medicines (e.g. anthracyclines), drug abuse (especially cocaine, but also excessive alcohol abuse), endocardial diseases as well as acute and chronic kidney failure as part of the renocardiac syndromes (Burchell 1960; Lip et al. 2000; Ponikowski et al. 2016).

#### 1.2.4 Classification

Classifications of HF are useful and necessary for the diagnosis, specific therapy, and prognosis for HF patients. Additionally, classifications facilitate a clear assignment of patient groups in the context of clinical studies. HF can be differentiated according to various criteria:

An important distinction by stages of HF is named after the New York Heart Association (NYHA). It places patients in one of four categories based on the patient's subjective physical discomfort and ability to perform.

NYHA I is defined as HF without physical limitations. Daily physical exertion does not cause inadequate exhaustion, arrhythmia, shortness of breath or angina pectoris.

NYHA II includes patients with a slight reduction of physical performance. There are no symptoms during rest or little movement. Excessive physical exertion (e.g., walking uphill or climbing stairs) causes exhaustion, arrhythmias, shortness of breath or angina pectoris.

NYHA III describes HF with a severe impairment of physical performance during normal activity. The patient does not report symptoms when resting. Little physical exertion (e.g., walking on the flat) causes exhaustion, arrhythmia, shortness of breath or angina pectoris.

NYHA IV is defined as HF with discomfort during any physical activity and when resting including being bedridden.

Depending on the success of the therapy and progression a change in the patients' NYHA stage is possible. A classificatory focus on symptoms means that patients who only become symptom-free after drug therapy can be classified in NYHA I (as asymptomatic HF). Because most clinical studies on HF refer to the NYHA stages, the classification system is now the basis for a majority of the recommendations in guidelines on HF (Ponikowski et al. 2016; Caraballo et al. 2019).

The American Heart Association (AHA) and the American College of Cardiology (ACC) propose similar classifications based on stages, however less commonly used by practitioners compared to the NYHA classification. Both AHA and ACC classifications also include risk factors and further diagnostic indications of HF (Yancy et al. 2013).

The diagnostic HF classification of the European Society of Cardiology is another classification based on stages. The classification system draws on the ejection fraction which is defined as the quotient of the stroke volume and the end-diastolic volume in percent. The classification distinguishes between three forms of HF:

The first form is described as heart failure with reduced left ventricular ejection fraction (HFrEF) characterized by an EF < 40% and symptoms of HF.

An intermediated form is heart failure with mildly reduced ejection fraction (HFmrEF) characterized by an EF of 40 – 49%, symptoms of HF, increased natriuretic peptides (BNP > 35 pg/ml and/ or NT-proBNP > 125 pg/ml) and additional structural or functional disorders of the left ventricle visualized by echocardiography.

The third form is heart failure with preserved ejection fraction (HFpEF) characterized by an EF of  $\geq$  50%, symptoms of HF, increased natriuretic peptides (BNP > 35 pg/ml and/ or NT-proBNP > 125 pg/ml) and structural or functional disorders of the left ventricle visualized by echocardiography. Simply speaking, HFrEF is a systolic dysfunction while HFpEF can be seen as diastolic disorder (Ponikowski et al. 2016; McDonagh et al. 2021).

Another possibility of classification references the HF location by chamber. The distinction is made between left, right and global HF. Isolated right HF is rather rare (cor pulmonale, right heart infarction, arrhythmogenic cardiomyopathy, pulmonary arterial hypertension, pulmonary embolism, etc.). Symptoms of right HF occur more frequently during left HF due to the backflow of blood into the right heart (Herold 2020).

Finally, HF can be divided by temporality (acute vs. chronic) and the clinical condition of the patient (compensated vs. decompensated). HF is compensated for as long as the symptoms occur under physical or emotional stress. Decompensated HF causes symptoms during rest. Acute heart failure (AHF) is characterized by the rapid development or deterioration and can be life-threatening. AHF links to a frequent need for stationary admission. It is usually the worsening of a pre-existing chronic HF, referred to as acute to chronic decompensation, and less often an initial manifestation of HF (*de novo*). Apart from a few exceptions such as myocarditis, peripartum cardiomyopathy and Takotsubo cardiomyopathy, most underlying diseases are associated with irreversible damage to the heart function, so that the HF is chronic and progressive. The history of HF diseases is typically not linearly progressive but erratic. Acute decompensations significantly deteriorate a patient's long-term prognosis (Ponikowski et al. 2016; McDonagh et al. 2021).

### 1.2.5 Pathophysiology

The pathophysiology of HF is complex, not least because multiple regulatory mechanisms seek to counteract the cardiac dysfunction (partly successfully) and thereby cause subsequent problems. To describe the pathophysiology of HF, the systolic should be considered separately from the diastolic subtype because of their different pathogenesis.

During systolic dysfunction, which leads to HF<sub>r</sub>EF, any kind of damage to the myocardium results in the decrease of contractility. The contractility of the heart, also known as inotropy, describes the force and speed with which muscle fibers shorten and is the dominant determinant of systolic ejection capacity. The decline in cardiac output leads to the insufficient perfusion of organs, which in turn causes the activation of various neurohumoral hormone systems. The aim of the activation is to maintain the supply of blood to important organs such as the brain and kidneys. The process of activation can be divided into four mechanisms that are at play:

First, an activation of the sympathetic nervous system with consecutive catecholamine release, which leads to an increment of the heart rate and peripheral resistance.

Second, the renin-angiotensin-aldosterone (RAAS) system is activated alongside. Angiotensin leads to an increase in afterload through vasoconstriction while aldosterone leads to an increase in preload through sodium and water reabsorption.

Third, the antidiuretic hormone (ADH) – a vasopressor released from the pituitary gland – further increases water retention and elevates the preload as well.

And fourth, a dilation of the atria and ventricles causes the release of natriuretic peptides which have a vasodilatory and natriuretic-diuretic effect. Furthermore, they have an inhibitory influence on the sympathetic and RAAS. Therefore, the natriuretic peptides develop beneficial effects on the insufficient heart and can be seen as an approach in both diagnosis and therapy (Katz 2018; Herold 2020).

A diastolic dysfunction that leads to HF<sub>p</sub>EF is present when the ventricle cannot be filled with blood to a sufficient extent (end-diastolic volume; EDV) by an acceptable low pressure. This process is principally dependent on three determinants:

An early diastolic relaxation caused by the active molecular dissociation of the myofilaments, a passive stiffness of the ventricle being influenced, *inter alia*, by the composition of the ECM and its interaction with the cardiomyocytes as well as a synchronous actions of the atria, which can be disturbed by arrhythmias.

Within the framework of an HF<sub>p</sub>EF, a disruption of these determinants leads to a filling of normal EDV that is only possible with increased filling pressures – even during rest. During physical exercise the disruption of determinants is compensated by an increase in heart rate, in turn, reducing the duration of the diastole, which leads to a further backlog of blood in the atrium and a decrease in the EDV. As a result of this vicious circle, the stroke volume decreases and, as mentioned above, the organs are insufficiently supplied with blood and oxygen (Kass et al. 2004; Herold 2020).

### 1.2.6 Clinical presentation

HF clinically depends on the part of the heart that is affected. However, there are common signs of left and right HF. The most common symptoms are nocturia, fatigue/weakness, and sympathetic over-activity manifesting in tachycardia and arrhythmia (Watson et al. 2000).

In the context of left HF, a distinction is made between backward failure and forward failure. While the former is an increased backlog of blood, the latter describes an insufficient ejection of blood. Backward failure leads to dyspnea (from exertional dyspnea to orthopnea), tachypnea, (mostly nocturnal) coughing attacks with dyspnea ("cardiac asthma"), cyanosis, pulmonary congestion up to pleural effusions and pulmonary edema. Forward failure results in renal perfusion and function reduction ("cardiorenal syndrome with low output"), insufficient cerebral perfusion with various manifestations (Inamdar and Inamdar 2016).

Right HF manifests itself almost exclusively as backward failure which leads to an increase in hydrostatic pressure in the capillaries and thus results in interstitial edema. Interstitial edema results in symptoms such as ankle edema, increase of the central venous pressure with visible venous congestion (e.g., visible neck veins), congested liver ("cirrhose cardiaque") with hepatomegaly, icterus and ascites as well as congestion of other organs, e.g., congestive gastritis (nausea, loss of appetite) or congestive kidney (impaired kidney function). The most common scenario in daily clinical practice, is global HF that shows signs of both left and right HF (Konstam et al. 2018).

### 1.2.7 Diagnostic tools

HF cannot be reliably diagnosed solely based on clinical symptoms and signs. For a diagnosis there must be objective evidence of underlying functional and structural disorders. The diagnostic criteria of the various forms of HF have already been introduced in Section 1.2.4. In the following, different types of examination are briefly presented.

A standard 12-lead resting electrocardiogram (ECG) forms the basic element of a HF assessment. In addition to the identification of a potential cause (bradycardia, tachycardia), ECG can provide therapy-relevant findings such as the heart rate as a therapy target, atrial fibrillation as an indication for anti-coagulation or bundle branch block as an indication for cardiac resynchronization therapy (CRT) (Madias 2007).

Brain natriuretic peptide (BNP) is synthesized and secreted by myoendocrine cells, specialized cardiomyocytes of the myocardium when the heart is exposed to increased wall tension. It is initially available as a precursor peptide proBNP from which the biologically inactive N-terminal prohormone of brain natriuretic peptide (NT-proBNP) is split off in a 1:1 ratio during secretion. The concentration of NT-proBNP correlates with the severity of the ventricular dysfunction. This diagnostic tool shows a high negative predictive value, so it allows to rule out HF. Due to the low positive predictive value, however, slightly elevated

natural peptides cannot confirm the diagnosis of HF. In addition, the values can be severely impacted by age, kidney function and obesity (McCullough et al. 2002; Palazzuoli et al. 2010)

Echocardiography is the method of choice for the assessment of systolic and diastolic dysfunction of both left and right ventricles. For the condition of a systolic dysfunction, the assessment focus rests on the planimetric determination of the ejection fraction (Ponikowski et al. 2016). Furthermore, echocardiography can assess the presence of hypertrophy, wall movement disorders, right heart burden, valve vicia and pericardial effusion (Herold 2020). Generally, diastolic dysfunction is diagnosed by two echocardiographic parameters, namely the transmitral flow using pulsed wave Doppler (E and A wave) and measuring the tissue velocities in the mitral annulus using myocardial tissue Doppler (E' and A' wave). From this, the quotient  $E/E'$  can be calculated as a surrogate for left ventricular filling pressure. If the quotient is elevated, it indicates an increased filling pressure. A diastolic dysfunction can be proven together with a decreased value of E' (Paulus et al. 2007).

Aside from echocardiography, there are further imaging techniques available. The widespread, inexpensive, and radiation-free transthoracic sonography displays and assesses signs of HF such as pleural effusions, pulmonary venous congestion and pulmonary edema. The chest x-ray in posteroanterior view enables the distinction from pneumological differential diagnoses, to demonstrate cardiac enlargement in the case of eccentric hypertrophy and to roughly assess individual ventricles and supplying vessels (Sartini et al. 2017). The cardiac MRI is a growing and promising area of cardiac diagnostics, not least because it offers the possibility of generating live recordings. The MRI diagnostic tool is essential for the diagnosis of individual underlying diseases such as myocarditis, certain cardiomyopathies and for vitality and ischemia diagnosis. However, given the extensive effort, high costs and lack of widespread availability, it is not of significant importance in basic diagnostics (Peterzan et al. 2016). Finally, in the case of clinical suspicion of CAD and for the evaluation of certain therapies, invasive diagnostics in the form of coronary angiography can be helpful (Ponikowski et al. 2016; McDonagh et al. 2021).

### 1.2.8 Therapeutic management

General therapy goals in HF comprise, in the short-term, an alleviation or elimination of clinical symptoms and, in the medium-term, improved disease control by prescribing a suitable symptomatic drug therapy or by optimizing an existing therapy. In principle, it is the cause of the HF that needs to be treated (e.g., optimal therapy adjustment of arterial hypertension or therapy of the causal cardiac arrhythmia). In addition to general therapeutic tools such as modifying risk factors, three pillars of specific therapy are available: drugs, non-surgical device therapies and heart transplantation (Ponikowski et al. 2016; McDonagh et al. 2021).

So far, a disease-modifying drug effect with reduced mortality has only been proven for HF<sub>r</sub>EF, as in the case of ACE inhibitors (alternatively AT1 receptor blockers), beta blockers,

mineralocorticoid receptor antagonists, angiotensin-receptor-neprilysin-inhibitors (ARNI) and sodium dependent glucose co-transporter 2 (SGLT2) inhibitors. Diuretics, digitalis glycosides and ivabradine improve symptoms and partially lower hospitalization rates (Swedberg et al. 2010; Ponikowski et al. 2016). ACE inhibitors, AT1 receptor blockers, mineralocorticoid receptor antagonists and ARNI intervene in the RAAS, whereby the latter additionally inhibits the degradation of natriuretic peptides. Beta blockers inhibit the activating effects of adrenaline and noradrenaline on the  $\beta$ -adrenoceptors, and thus reduce the stimulating effect of the sympathetic system on the heart. SGLT2 inhibitors are promising drugs that have originated from diabetes therapy but have recently shown impressive cardio- and reno-protective effects in clinical studies. SGLT2 inhibitors have been upgraded to first line therapy of HFrEF in the updated ECS guidelines of 2021. According to preliminary data, a clinical trial (EMPEROR-Preserved) promises results that could possibly lead to the approval of SGLT2 inhibitors for the treatment of HFpEF. SGLT2 inhibitors would be the first ever approved drugs for this disease (Anker et al. 2021; McDonagh et al. 2021).

Most diuretics increase the flow of urine through saluresis, i.e., through the increased excretion of electrolytes (especially  $\text{Na}^+$ ,  $\text{Cl}^-$ ), which also causes water to be excreted. Digitoxin and digoxin are cardiac glycosides that inhibit sodium / potassium ATPase in the cardiomyocytes. As a result, the intracellular sodium content increases, the effective gradient of the sodium/ calcium anti-porter is reduced, and the calcium content increases intracellularly. This leads to an increase in the force of contraction (positive inotropic) and a slowdown in the conduction of excitation in the heart (negative dromotropic). Ivabradine works through lowering the heart rate by blocking the  $I_f$ -channel in the pacemaker cells of the sinus node (Karow 2019).

There are essentially two systems available for non-surgical device therapy for chronic HF:

CRT, which, in the case of a complete bundle branch block, synchronizes the atrioventricular and interventricular contraction processes, leads to reverse remodeling and consequently results in a decrease of the ventricular volume. Lastly, CRT leads to an increase in pumping power and lowers lethality (Cleland et al. 2006).

An implantable cardioverter-defibrillator (ICD), which is recommended for secondary prophylaxis after resuscitation due to ventricular fibrillation and for primary prophylaxis. Implanting an ICD reduced overall mortality by 23% (Schaer et al. 2014).

Surgically, heart transplantation is available as an *ultima ratio* for the treatment of end-stage HF. This is subject to defined criteria and is carried out at selected clinical centers (Mehra et al. 2006).

## 1.3 Endothelial to mesenchymal transition (EndMT)

### 1.3.1 Definition

Endothelial to mesenchymal transition (EndMT) describes a biological process in which endothelial cells lose their morphological characteristics and specific properties, such as apical-basal polarity and cell-cell junctions, and progressively transdifferentiate into a mesenchymal, fibroblast-like phenotype including a spindle-shaped morphology, increased cell motility and resistance to senescence and apoptosis (Roy et al. 2015). This process is important in a physiological cell transformation mechanism during embryonic heart development and it enables the formation of the heart valves and the endocardial cushion from endocardial cells of the atrioventricular canal (Eisenberg and Markwald 1995). In addition, EndMT contributes to numerous genetically determined as well as acquired diseases such as malignant disorders, diabetes mellitus, atherosclerosis and pulmonary arterial hypertension (Arciniegas et al. 2007; Zeisberg et al. 2007a; Li et al. 2009; Cao et al. 2014; Boström et al. 2016). Furthermore, EndMT has gained attention because of its contribution to fibrogenesis in multiple organs such as heart, lung, kidney and liver (**Figure 2**) (Zeisberg et al. 2007b; Zeisberg et al. 2008; Choi et al. 2016; Peng et al. 2016; Ribera et al. 2017).

### 1.3.2 Mechanism and induction

Several stimuli have been shown to induce EndMT. Mahler et al. (2014) observed shear stress to stimulate EndMT during aortic valve disease. Another important stimulus is hypoxia. It has been shown to cause EndMT in pulmonary artery cells (Zhu et al. 2006). Rieder et al. (2011) gave strong evidence that exposure to inflammatory stress causes endothelial cells to undergo EndMT. Furthermore, studies found an induction of EndMT due to fatty acid metabolism and high glucose levels (Yu et al. 2017; Xiong et al. 2018).

Even though the exact molecular mechanisms regulating EndMT are not yet fully known, multiple signaling pathways have been proven to initiate and progress EndMT during both physiological and pathological conditions, among which TGF $\beta$  signaling is particularly relevant. TGF $\beta$  is involved in cell proliferation, differentiation and apoptosis and it is considered as the major inducer of EndMT (Arciniegas et al. 1992). There are three isoforms in vertebrates that together make up the TGF $\beta$  family: TGF $\beta$ 1, TGF $\beta$ 2, and TGF $\beta$ 3. While TGF $\beta$ 2 mainly mediates developmental EndMT (Azhar et al. 2009), TGF $\beta$ 1 induces EndMT during tumor development (Wawro et al. 2018) and fibrogenesis (Sime et al. 1997; Nakajima et al. 2000). The effects of TGF $\beta$ 3 on EndMT are relatively unknown. All effects of these growth factors are mediated by specific membrane-bound glycoprotein receptors, which are divided into two subfamilies, type I and II, based on their different structural and functional properties. Both, type I and II, have serine/threonine kinase activity. Receptor characterizations revealed different protein structures, based on which they are divided into five type II and seven type I receptors. The different combinations of the receptors

determine the specificity to their ligands. Under physiological conditions TGF $\beta$  binds to TGF $\beta$  receptor type II which phosphorylates and thereby activates TGF $\beta$  receptor type I (van Meeteren and ten Dijke 2012).

In endothelial cells, TGF $\beta$  has two type I receptors interacting with one TGF $\beta$  type II receptor. The first type I receptor also known as ALK1 (activin receptor-like kinase-1) activates SMAD (SMAD family member) 1/5/8 signaling by phosphorylation. Phosphorylated SMAD1/5/8 subsequently induce endothelial cell proliferation and migration. The second type I receptor ALK5 recruits and phosphorylates SMAD2/3 which in turn thereby inhibit endothelial proliferation and migration (Goumans et al. 2003; Lin et al. 2012). Phosphorylated SMAD2 and 3 form a larger complex with SMAD4, the common-mediator (Co) SMAD. The complex translocates to the nucleus and regulates the expression of numerous transcription factors such as SNAIL (snail family transcriptional repressor 1), SLUG (snail family transcriptional repressor 2), and TWIST (twist family basic helix-loop-helix transcription factor 1). These transcription factors have in common that they repress the endothelial gene expression and promote the expression of mesenchymal markers and therefore can be utilized as predictors of EndMT (**Figure 3**). Beside these prominent representatives, other transcriptional factors such as Zinc finger E-box-binding homebox 1 (ZEB1) and 2 (ZEB2) were previously investigated in various studies to facilitate EndMT (Elliott et al. 2003; Peinado et al. 2004; Yang et al. 2004; Lee et al. 2015; Levet et al. 2015; Gong et al. 2017).

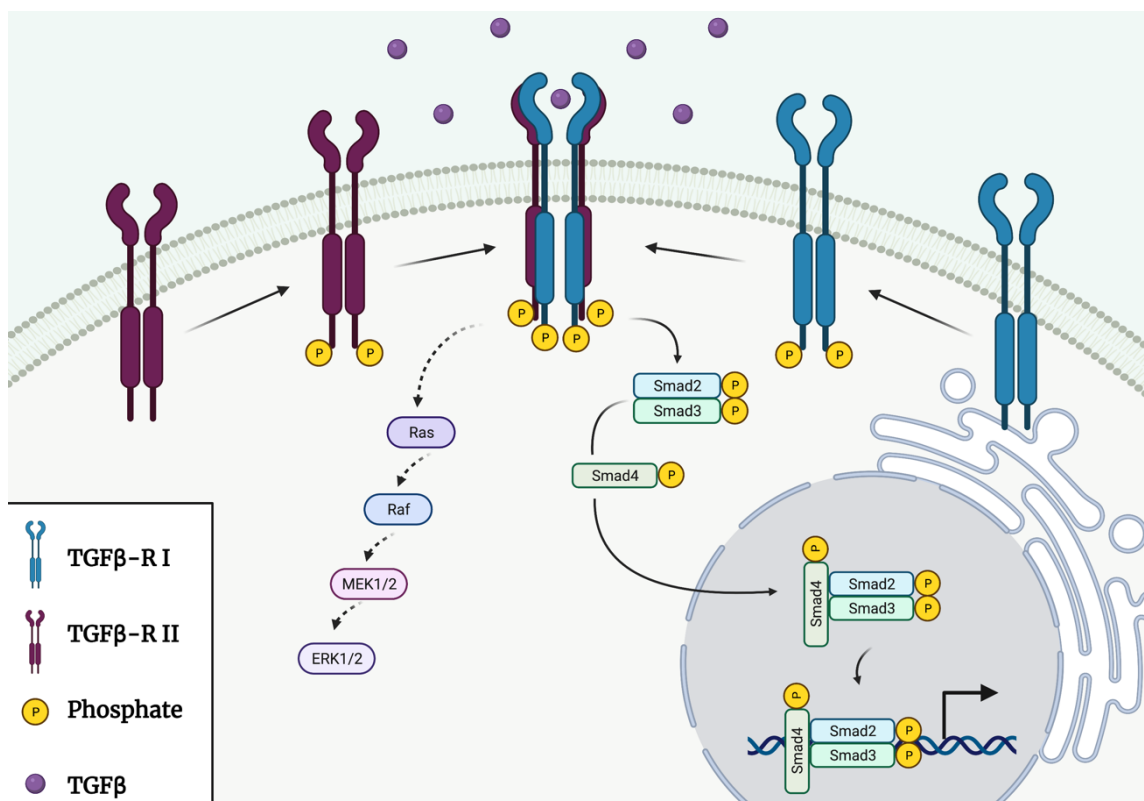


**Figure 3: TGF $\beta$  signaling pathway** The activated TGF- $\beta$  receptor complex mediates its signal transduction via multiple mechanisms. After phosphorylation and consecutive activation of the SMAD proteins, the targeted gene expression is affected (modified from Weiss and Attisano (2013); created with BioRender.com)



In addition to TGF $\beta$  receptor type I and II, TGF $\beta$  can bind to other receptors such as betaglycan and endoglin. These receptors are expressed in endothelial cells and when binding to TGF $\beta$  they can modulate the response of TGF $\beta$  to its origin receptors (Wong et al. 2000). Other pathways can independently, or synergistically with TGF $\beta$ , regulate EndMT during both developmental and pathological conditions. The following molecular pathways should be mentioned here: Notch signaling has been described to mediate EndMT during heart development by activating SNAIL (Timmerman et al. 2004; Chang et al. 2011). Previous studies have shown that Wnt/ $\beta$ -catenin signaling has been implicated in EndMT during valve diseases and after myocardial infarction (Aisagbonhi et al. 2011; Zhong et al. 2018). Furthermore, BMP (bone morphogenetic protein) signaling plays an important role regarding EndMT as BMPs are members of the TGF $\beta$  superfamily and consequently mediate their downstream effects via activation of SMAD molecules. BMP6 promotes developmental tube formation while other BMPs were able to induce EndMT during tumor angiogenesis and development of pulmonary hypertension (Valdimarsdottir et al. 2002; Teichert-Kuliszewska et al. 2006; Heinke et al. 2008).

### 1.3.3 Markers

To prove and objectify EndMT, markers that characterize the process have to be available. Essentially, three methods can be used for this purpose: 1) a quantification of the above-mentioned transcription factors during EndMT, as well as the detection of 2) suppression of epithelial respectively endothelial cell-specific genes and 3) induction of genes that testify to the acquirement of mesenchymal characteristics (**Figure 4**).

The paracellular endothelial barrier consists of occludent and adherent contacts. Occludent contacts ensure a diffusion barrier. Adherent contacts ensure the necessary strength of adhesion so that occludent contacts can be formed and maintained. A loss of these endothelial characteristics can be shown by the suppression of VE-cadherin. VE-cadherin mediates the strong adhesion of endothelial cells by binding with the extracellular domain and by being anchored intracellularly to the actin cytoskeleton via adapter molecules (Frid et al. 2002; Lopez et al. 2009). The suppression of cluster of differentiation 31 (CD31), which is also called platelet endothelial cell adhesion molecule 1 (PECAM-1), equally indicates a loss of endothelial cell properties. During inflammatory processes, PECAM-1 initiates the adhesion of leukocytes to endothelial cells and the subsequent transmigration. Given the high expression density on endothelial cells and lack of expression on non-endothelial cells such as fibroblasts, PECAM-1 is frequently used to characterize endothelial cells and EndMT (DeLisser et al. 1997; Woodfin et al. 2007; Piera-Velazquez and Jimenez 2012). Other endothelial cell markers are collagen IV, an integral component of the endothelial basement membrane and the von Willebrand factor (vWF), a glycoprotein that is produced and stored in endothelial cells and mediates platelet adhesion to collagen in the injured vessel wall (Medici and Kalluri 2012).

The expression of mesenchyme-characteristic genes is also a necessary marker for EndMT among which fibronectin, vimentin, fibroblast-specific protein-1 (FSP-1) and alpha-smooth muscle actin ( $\alpha$ -SMA) are the most commonly used markers.  $\alpha$ -SMA is one of six different actin protein isoforms and builds intracellular microfilaments. It is widely used as a marker for myofibroblasts. However, given their insufficient specificity and sensitivity, all mesenchymal markers receive criticism from researchers and practitioners. As previously described, not all cardiac fibroblasts that derived from EndMT, express FSP-1. FSP-1 is a member of the S100 protein calcium-binding family that functions in motility and invasion in smooth muscle cells and macrophages. Vimentin, one of the intermediary filaments, that occurs in the cell skeleton and exists in the plasma of mesenchymal cells, can also be detected in endothelial cells (Frid et al. 2002; Zeisberg et al. 2007a; Zeisberg et al. 2007b; Chen et al. 2009; Zeisberg and Neilson 2009; Zeisberg and Kalluri 2010; Rieder et al. 2011; Dave and Bayless 2014; Ranchoux et al. 2015; Zhang et al. 2016).

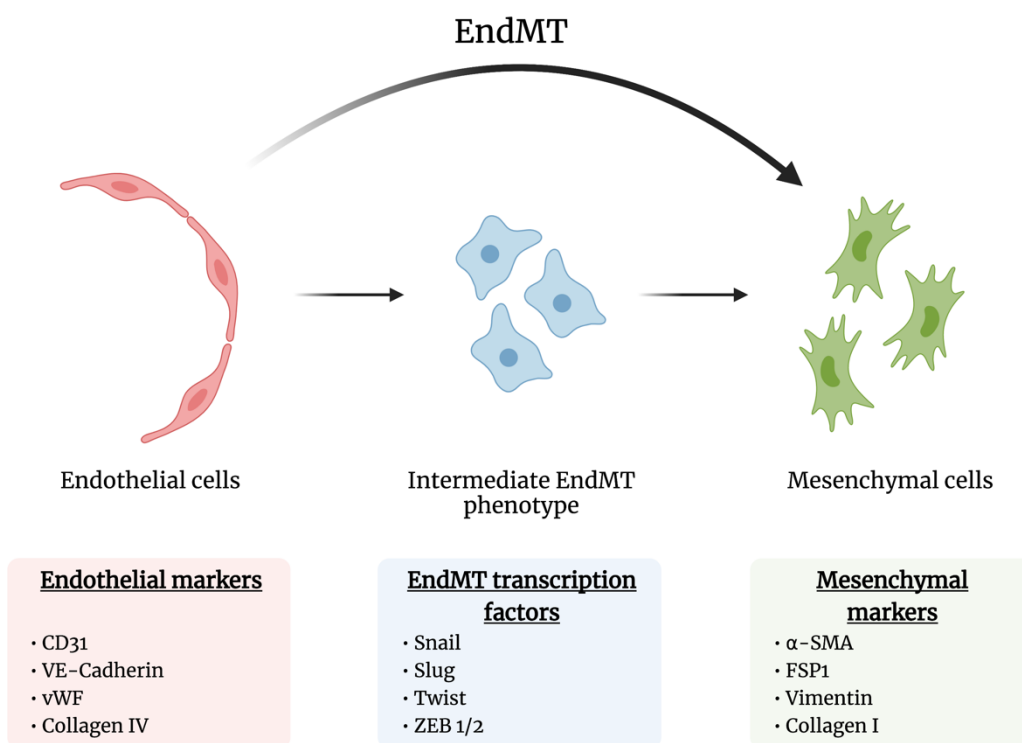


**Figure 4: Markers of endothelial to mesenchymal transition** EndMT describes the transition from endothelial cells to mesenchymal cells via an intermediate phenotype. Specific markers can be assigned to each of these three states (modified from Piera-Velazquez and Jimenez (2019); created with BioRender.com).

### 1.3.4 EndMT and cardiac fibrosis

Cardiac fibrosis is predominantly driven by activated fibroblasts whose origins vary. Zeisberg et al. (2007b) were the first to show “that cardiac fibrosis is associated with the emergence of fibroblasts originating from endothelial cells, suggesting an endothelial-mesenchymal transition (EndMT) similar to events that occur during formation of the atrioventricular cushion in the embryonic heart”. They proved that the inhibition of TGF $\beta$ 1-induced EndMT

ameliorates the progression of cardiac fibrosis (Zeisberg et al. 2007b). Today, aberrant EndMT is recognized as a key mechanism of cardiac fibrogenesis as shown in a variety of rodent animal models (Xu et al. 2015a; Wei et al. 2018; Cheng et al. 2021). An estimated 30% of fibroblasts are derived from EndMT during fibrogenesis. Interestingly, the proportion of EndMT-derived fibroblasts depends on the extent of the cardiac fibrosis itself (Yoshimatsu and Watabe 2011).

## 1.4 Serelaxin

### 1.4.1 Relaxin

The peptide hormone Relaxin secreted by vertebrates during pregnancy was firstly described and named by Frederick Lee Hisaw in 1926. He injected serum from a pregnant guinea pig into a non-pregnant female animal and showed that Relaxin led to an elongation of the pubic ligament and a widening of the symphysis cleft in the serum-treated guinea pig (Hisaw 1926). In addition to these functions, Fevold et al. (1930) described various other, primarily pregnancy-related effects of Relaxin such as widening of the birth canal, inhibition of spontaneous contractions of the myometrium, and induction of growth and differentiation of the mammary glands.

#### 1.4.1.1 Ligands

Relaxin is a 6.3 kDa peptide hormone that belongs to a group of seven Relaxin family peptides, which are part of the insulin superfamily (Bani 1997). This family of structurally related hormones include two subfamilies: First, insulin as well as insulin-like growth factor 1 and 2 (IGF-1 and IGF-2) and second, Relaxin-1, Relaxin-2, Relaxin-3, Leydig cell insulin-like (INSL3), early placenta insulin-like (INSL4), INSL5 and INSL6 (Humbel 1990; Wilkinson et al. 2005).

Structurally and functionally, Relaxin occupies an independent position within the family of insulin-like molecules. Relaxin is synthesized as a prohormone and consists of a signal peptide, B-chain, C-peptide and an A-chain (from the N' - to the C' - terminus). Due to its much longer C-peptide, preprorelaxin is about twice as large as preproinsulin (Gast 1983). The signal peptide is enzymatically cleaved and converts the preprorelaxin into the prorelaxin. Catalyzed by the prohormone convertase PC-1, the C-peptide is split off. During this step mature Relaxin is produced analogously to the processing of insulin (**Figure 5**). The presence of the Relaxin A- and B-chains and their correct conformation are essential for the Relaxin bioactivity. The A- and B-chain are characteristically linked by two disulfide bridges. Another disulfide bridge is located within the A-chain (Bryant-Greenwood and Schwabe 1994; Bani 1997). The guanidino side groups of two amino acids, which protrude like spikes from the surface of the B-chain, the so-called “two-prong”, interact directly with the membrane Relaxin receptor (Büllesbach et al. 1992). The A-chain is essential for the

three-dimensional conformation and bioactivity of the hormone. A chemical modification of certain amino acids in this chain as well as the chemical synthesis of Relaxin derivatives, in which certain amino acids have been replaced, result in a complete loss of the receptor binding (Büllesbach and Schwabe 1988; Büllesbach et al. 1992). The Relaxin peptides show a recognizable heterogeneity in the amino acid sequence within the different mammalian species. However, almost all peptides retain a highly conserved Arginine-rich motif in the B-chain (Bathgate et al. 2013).

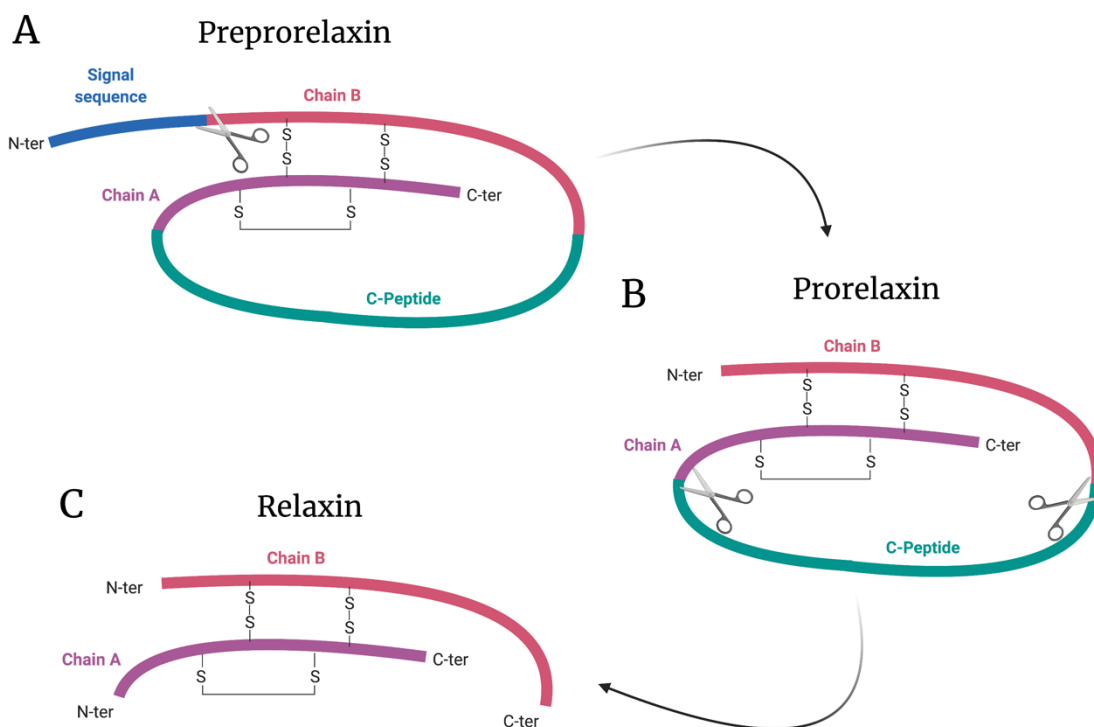


**Figure 5: Synthesis of Relaxin** (A)The preprohormone, characterized by the three-domain structure and disulfide bridges within and between the domains, is intracellularly, enzymatically processed to (B) prorelaxin and finally cleaved to mature heterodimeric (C) Relaxin (created with BioRender.com).

With Relaxin-H1, -H2 and -H3 three isoforms of Relaxin are known in humans. The proteins encoded by three Relaxin genes (RLN1, RLN2, RLN3). The occurrence of Relaxin-H2 is limited to humans and the great apes and corresponds to Relaxin-1 in other mammals such as mice. Relaxin-H1 and -H2 are located on the short arm of chromosome 9 (9p24), whereas Relaxin-H3 is located on chromosome 19 (Hudson et al. 1983).

Relaxin's expression was originally observed in the pregnant female reproductive tract; especially in corpus luteum, endometrium, mammary gland and placenta (O'Byrne et al. 1978; Yki-Järvinen et al. 1985; Gunnarsen et al. 1996). However, the expression of its mRNA and protein has since been detected in non-pregnant female as well as in male tissue, for example brain, thymus, heart, kidney, lung, spleen, skin and prostate tissue (Sokol et al. 1989; Osheroff and Ho 1993; Bathgate et al. 2002).

#### 1.4.1.2 Relaxin family peptide receptors

For a long time, attempts to find the corresponding receptors to Relaxin peptides led to little. Initially, it was assumed that Relaxin mediated the activation of a tyrosine kinase receptor - analogously to the mode of action of insulin (Palejwala et al. 1998). By observing that INSL3 knockout mice showed the same phenotype of abnormal testis descent as mice with malfunction of G protein-coupled receptors (GPCR), it was suggested that the target of Relaxin family peptides are GPCR (Overbeek et al. 2001). Today it is well known that Relaxin mediates its pleiotropic effects via seven-transmembrane GPCR, which were previously also known as leucine-rich repeat-containing G-protein-coupled receptors (LGR). The receptors have a molecular weight of 60-80 kDa and consist of approximately 400-500 amino acids. The C-terminal end is located intracellularly and is connected to the extracellularly located N-terminus via the seven-transmembrane domain (Iyengar 1993).

These so-called Relaxin family peptide receptors (RXFP) include four highly conserved GPCR, which can be subdivided into two groups based on their architecture and signaling properties. RXFP1 (LGR7) and RXFP2 (LGR8) lead to an activation of adenylate cyclase via  $G_s$  protein coupling and result in an increase of intracellular cAMP and an activation of phosphoinositide 3-kinase. Additionally, they increase phosphorylation of mitogen-activated protein kinases (MAPK) as well as nitrogen oxide (NO) synthesis (**Figure 6**). RXFP1 is the cognate receptor for Relaxin-H2 and Relaxin-H3 while RXFP2 is preferentially bound by INSL3, Relaxin-H2 and Relaxin-H3 (Hsu et al. 2002; Kumagai et al. 2002; Nistri and Bani 2003). Despite the close similarity between their suitable ligands, RXFP1/RXFP2 and RXFP3/RXFP4 receptors are structurally not highly related. RXFP3 (GPCR 135) and RXFP4 (GPCR 142) are associated to small peptide receptors and lead to the inhibition of adenylate cyclase via  $G_i$  protein. Thereby, they decrease intracellular cAMP levels, increase phosphorylation of extracellular-signaling-regulated-kinase 1 and 2 (Erk1/2) and activate AP1-linked reporter genes as well as  $\text{NF}\kappa\text{B}$ . RXFP3 provides the binding site for Relaxin-H3 and RXFP4 for INSL5 and Relaxin-H3 (Bathgate et al. 2013).

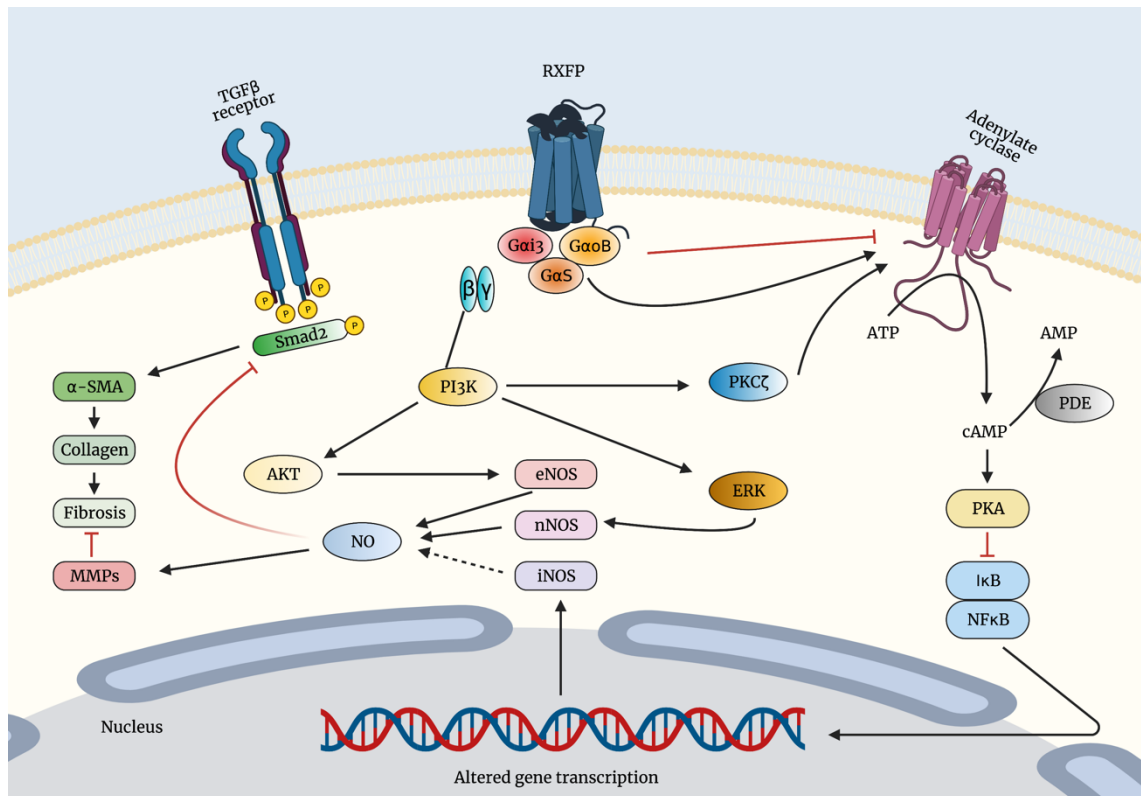


**Figure 6: Signal transduction upon activation of RXFP1 mediated by relaxin** The antifibrotic effect of Relaxin is mediated by RXFP1, which leads to an induction of the expression of eNOS, nNOS, iNOS and a subsequent increased synthesis of NO. NO increases the expression of MMPs, which contribute to a reduction in fibrosis. In addition, there is an inhibition of pSMAD2 and thus a direct inhibition of the TGFβ signal cascade (modified from Bathgate et al. (2013), created with BioRender.com).

#### 1.4.1.3 Effector organs and functions

Physiologically, Relaxin certainly plays an important role during pregnancy. Synthesized primarily in the corpus luteum, Relaxin's highest plasma levels are reached at ovulation, in the case of pregnancy during the first trimester and lastly during delivery. Alongside an increase in flexibility and elasticity of the interpubic ligaments as well as softening of the pubic symphysis and the cervix, Relaxin mediates an adaptation to hemodynamic changes that occur during pregnancy by increasing cardiac output, renal blood flow and arterial compliance (Conrad et al. 2004; Conrad and Novak 2004; Neill and Knobil 2006). In males, Relaxin's source appears to be the prostate and it is suggested that it could be purified from seminal plasma. The precise function remains unknown, though hypothesized to be involved in sperm implantation. The treatment of human sperm with Relaxin increased motility and induced a hyperactivation of sperm (Ferlin et al. 2012).

Apart from its diverse functions in the reproductive tract, Relaxin has been shown to have an influence on the formation and expansion of tumors. It is expressed by endometrial, mammary thyroid and prostate tumors (Tashima et al. 1994; Hombach-Klonisch et al. 2006; Kamat et al. 2006; Thompson et al. 2006). Interestingly, blocking of either Relaxin or RXFP1 in patients with prostate tumors caused a significant reduction of cancer growth (Vinall et al.

2006). Because of its ability to reduce collagen and to increase the expression of MMPs, Relaxin has an antifibrotic effect on connective tissue metabolism. It displays profibrotic changes induced by TGF $\beta$ . These effects are mediated through an activation of the NO pathway that cause decrease in Smad2 phosphorylation and nuclear localization (Mookerjee et al. 2009). As a result of these effects, several studies have examined Relaxin's ability to treat connective tissue disorders such as scleroderma (Khanna et al. 2009).

#### 1.4.2 Serelaxin and fibrosis

Serelaxin (RLX030, *Novartis Pharma*) is the recombinant form of human Relaxin-H2, which is currently the only known circulating Relaxin peptide in human plasma (Bathgate et al. 2006). As previously mentioned, Relaxin can affect connective tissue metabolism. Relaxin was identified in *Rln1* gene knockout mice as a naturally occurring regulator of collagen turnover in the heart (Du et al. 2003). In cardiac fibroblasts, Relaxin reduced fibroblast activation and fibroblast differentiation. Consequently, Relaxin decreased the expression of collagen type I and III. Additionally, it increased the expression of MMP-2 (Samuel et al. 2004). In a model for cardiomyopathy, Relaxin treatment reduced ventricular collagen, myocardial stiffness and diastolic dysfunction (Samuel et al. 2008). In a mouse model of isoprenaline-induced cardiac injury, Serelaxin had an antifibrotic effect (Samuel et al. 2014). Studies that utilized pressure overload in mouse models revealed that the application of Serelaxin improved left ventricular fibrosis as well as cardiac magnetic resonance-derived myocardial deformation parameters (McCarthy et al. 2017; Lapinskas et al. 2020). However, the detailed molecular mechanisms are not clear to date.

Serelaxin gained attention not only in reference to cardiac fibrosis but also fibrosis in other organs. There is evidence for Serelaxin as a therapeutic for lung fibrosis as recently reviewed by Lam et al. (2018): The combination of Serelaxin with rosiglitazone treatment significantly reduced hepatic fibrosis (Bennett et al. 2017). In a randomized, double-blind, placebo-controlled trial, patients suffering from scleroderma, which is characterized by skin fibrosis, were subcutaneously treated with Serelaxin over 24 weeks. They showed a significant reduction of skin thickening and improved mobility upon application of Serelaxin compared to the placebo group (Seibold et al. 2000). Giam et al. (2018) suggested that Serelaxin has the potential to exert nephroprotective effects in patients with dilated cardiomyopathy by reducing tubulointerstitial and glomerular fibrosis by half.

#### 1.4.3 Serelaxin and acute heart failure

During pregnancy - with the decisive contribution of Relaxin - the systemic peripheral resistance decreases with a simultaneous slight increase in cardiac output and a significant increase in renal plasma flow and the glomerular filtration rate. Such changes appear therapeutically desirable, especially in the case of HF. For this purpose, *Novartis Pharma* developed Serelaxin (brand name Reasanz) by recombinant DNA technology in a bacterial

expression system. It is identical in amino acid sequence and structure to the naturally occurring Relaxin-H2 and marketed in Russia for the treatment of AHF. Serelaxin has undergone several clinical trials in patients with AHF in Europe, the United States and Asia. (European Medicines Agency 2014; Michael Seganish et al. 2017; Metra et al. 2019).

#### 1.4.3.1 Phase I studies

*RLX.CHF.001* was a phase I open label single center safety and hemodynamic pilot study in 16 patients with stable congestive HF. Serelaxin was intravenously administered for 24 hours in 8-hour intervals at escalating doses of 10, 30, 100, 250, 480 and 960 µg/kg/day. Pulmonary capillary wedge pressure, cardiac output/cardiac input, systemic vascular resistance, serum creatinine, blood urea nitrogen and uric acids were the observed parameters. Additionally, an exploratory phase I study took place (*CRLX030.A2103*). Here, safety, tolerability, pharmacokinetics and pharmacodynamics of intravenous infusions of Serelaxin at three dose levels were observed in 32 Japanese and 8 Caucasian male and female healthy subjects. Both studies examined safety and tolerability (European Medicines Agency 2014).

#### 1.4.3.2 Phase II studies

In addition to two smaller phase II multicenter, randomized, double-blind, parallel group, placebo-controlled studies that evaluated hemodynamic effects of Serelaxin in 70 subjects with AHF (*CRLX030.A2201*) and renal hemodynamic effects of Serelaxin in 88 patients suffering from chronic HF (*CRLX030.A2202*), *PRE-RELAX-AHF (RLX.CHF.003.PRE)* was the predominant phase II study for Serelaxin treatment. The multicenter, randomized, double-blind, placebo-controlled safety and efficacy trial, included 234 randomized patients hospitalized with AHF, dyspnea, congestion on chest radiograph, increased BNP or NT-proBNP normal to elevated blood pressure (>125 mmHg), and mild to moderate renal impairment. The dose-finding study evaluated several clinical outcomes, including improvement in dyspnea, in-hospital outcomes, cardiovascular and all-cause mortality. Serelaxin was intravenously applied over 48 hours in 10, 30, 100 or 250 µg/kg/day. Dyspnea improved with Serelaxin compared to the placebo, as assessed on a Likert scale (40% vs 23%;  $p = 0.044$ ). The length of stay was 10.2 days (SD 6.1) for Relaxin-treated patients versus 12.0 days (SD 7.3) for the placebo group. The number of days alive and out of hospital were 47.9 (SD 10.1) with Serelaxin versus 44.2 (SD 14.2) with the placebo treatment. Cardiovascular death or readmission because of heart or renal failure at day 60 was reduced with Relaxin (2.6% vs 17.2%;  $p = 0.053$ ). The number of serious adverse events was similar between groups. In summary, this study proved the safety and beneficial effects on dyspnea and other clinical outcomes, resulting in a further phase III study (Teerlink et al. 2009; European Medicines Agency 2014).



### 1.4.3.3 Phase III studies

The first phase III trial RELAX-AHF (*RLX.CHF.003*) was designed as a multicenter, randomized, double-blind, placebo-controlled study with the aim to confirm the safety and efficacy observed in Pre-RELAX-AHF. Here, 1161 patients hospitalized with AHF (defined as dyspnea at rest or with minimal exertion), congestion on the chest radiograph, increased BNP or NT-proBNP, normal to elevated blood pressure ( $>125$  mmHg), and mild to moderate renal impairment (estimated creatinine clearance of 30-75 ml/min/1.73 m<sup>2</sup>) were randomly assigned within 16 hours after presentation. Serelaxin was given as an intravenous infusion (30 µg/kg/d) when hospitalized for up to 48 hours in addition to loop diuretics and other drugs. At the same time, the comparison was made with a placebo in addition to standard therapy. Acute dyspnea (one of the primary endpoints), quantified by using the visual analog scale, was significantly improved within the first five days of administering Serelaxin. Serelaxin also significantly reduced the early worsening (period up to day 5) of a decompensated HF - measured by clinical signs, symptoms and an escalation of therapy (e.g., diuretics, vasopressors). The other primary endpoint, which recorded an improvement in the symptom of dyspnea after six, twelve and 24 hours (Likert scale), was not significantly influenced. Secondary endpoints such as the combined endpoint cardiovascular death or re-hospitalization or acute kidney failure within 60 days of index presentation and the combined endpoint “days alive out of hospital up to day 60” did also not change significantly. However, therapy with Serelaxin was associated with a significant reduction in other endpoints (shorter length of stay in hospital, shorter length of stay in the intensive care unit or the cardiac care unit, less administration of loop diuretics, etc.). Additionally, renal dysfunction was associated with lower cardiovascular and all-cause mortality in Serelaxin-treated patients as compared to placebo-treated patients (Teerlink et al. 2013; Liu et al. 2016).

The suggested evidence of not only relief of symptoms but also a significant improvement of outcomes in patients with AHF prompted the executive committee in collaboration with *Novartis Pharma* to fund a second phase III trial (RELAX-AHF-2) with 6545 patients. The inclusion criteria remained the same, although the treatment protocol was changed in the way that the administration of Serelaxin now had to begin no more than four hours after randomization. The two primary endpoints were the worsening of HF at five days and death from cardiovascular causes at 180 days. Worsening of HF was reached at a rate of 6.9% in the Serelaxin treated group and 7.7% in the placebo group (HR: 0.89;  $p = 0.19$ ). Death from cardiovascular causes at 180 days occurred in 8.7% of the patients in the Serelaxin group compared to 8.9% in the placebo group (HR: 0.98;  $p = 0.77$ ). Secondary endpoints included death from any cause at 180 days, the length of the index hospital stay and death from cardiovascular causes or rehospitalization for HF or renal failure at 180 days. None of the additional endpoints was tested for significance. Despite the fact that the FDA initially rated Serelaxin as a “breakthrough therapy”, the regulatory authorities refused to approve Serelaxin after *Novartis Pharma* announced that RELAX-AHF-2 did not meet its primary endpoints (Miyares and Davis 2013; Metra et al. 2019).

## 1.5 Notch signaling pathway

### 1.5.1 Mechanism

The Notch signaling pathway is named after its receptor "Notch". The notch gene was discovered in a fruit fly (*Drosophila melanogaster*), in which a mutation had caused "notches" in its wings. In most animals, the highly conserved cell signaling system enables cell-to-cell communication between neighboring cells through the interaction of the Notch receptor on the surface of one cell and its ligands. The Notch signaling pathway is particularly important during embryonic development, but also in the adult organism, especially for cell differentiation. In mammals there are four known Notch receptors (Notch1, Notch2, Notch3 and Notch4) and five ligands (Jagged1, Jagged2 and Delta-like (Dll) 1, Dll3, and Dll4) (Harper et al. 2003).

The Notch1 signaling pathway is activated via its ligand Jagged1 that binds to the extracellular domain of the Notch1 receptor. This leads to cleavage of the Notch intracellular domain (NICD) by a  $\gamma$ -secretase. NICD translocates into the nucleus where it binds to the transcriptional regulator CSL (for CBF-1, Su(H), and LAG-1). The binding results in the displacement of co-repressors previously bound to CSL and recruitment of co-activators. The co-activators induce the expression of the Hairy-Enhancer of Split (HES) and HES-related proteins (HERP) gene families (**Figure 7**) (Harper et al. 2003).

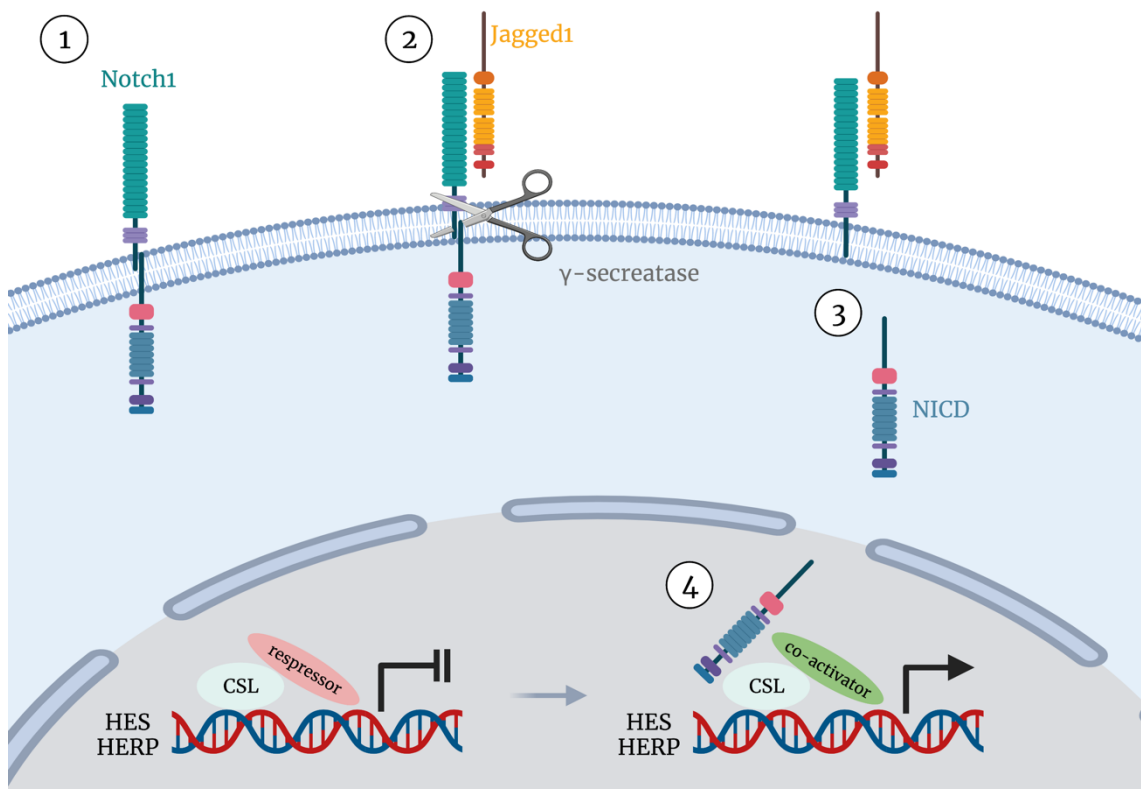


**Figure 7: Notch signaling pathway** After Jagged1 binding to Notch1, the receptor is cleaved by  $\gamma$ -secretase. The intracellular part (NICD) translocates into the nucleus and acts together with CSL and other co-activators

as a transcription factor and thus initiates the expression of HES and HERP (modified from Yamaguchi et al. (2008), created with BioRender.com).

### 1.5.2 Functions

Associated with embryogenesis, the Notch signaling pathway is involved in the development of all organs and tissues and significantly determines the shape of organs by means of cell-to-cell interaction via lateral inhibition. During bone development, the Notch signaling pathway leads to the expansion of bone marrow that houses the hematopoietic stem cells. It is the site where hematopoiesis takes place. The parathyroid hormone causes the osteoblasts of the bone marrow niche to express Jagged, which stimulates the Notch receptor of the stem cells and leads to their expansion and self-renewal. In this way, an increased need for hematopoietic stem cells (for example after blood loss) can occur in the adult organism (Harper et al. 2003; Zanotti and Canalis 2017). However, the Notch signaling pathway is also involved in many diseases, such as leukemia (e.g., T-ALL), a variety of solid cancers, multiple sclerosis or the Fallot tetralogy (Louvi and Artavanis-Tsakonas 2012).

### 1.5.3 Notch signaling and fibrosis

Recently, Notch signaling has been shown to play a role not only in developmental EndMT during embryonic formation of the heart but also in pathogenic EndMT during fibrogenesis (Nistri et al. 2017). In this aspect, Notch has been reported to preserve endothelial cell properties and attenuate EndMT, which in turn can be affected by Relaxin (High and Epstein 2008; Zhou et al. 2015). Moreover, Notch inhibits the development of cardiomyocytes and TGF $\beta$ -mediated cardiac fibrosis in transgenic mice overexpressing the Notch ligand Jagged1 (Nemir et al. 2014). Zhou et al. (2019) could proof that Notch signaling influenced differentiation of fibroblasts into myofibroblasts by antagonizing TGF $\beta$ 1/SMAD3 signaling (Zhou et al. 2019).

## 1.6 Epigenetics

### 1.6.1 Definition

The word “epigenetic” means “in addition to changes in genetic sequence”. In 1942 – when the structure of DNA was still unknown – Conrad Waddington coined the term “epigenetics” and defined it as “the branch of biology which studies the causal interactions between genes and their products which bring the phenotype into being”. Today epigenetics is seen as the field that addresses the question of factors, content and processes of genetics that influence the activity of genes and thus the development of a cell (Waddington 1968; Weinhold 2006). A wide variety of drivers behind epigenetics is known or suspected including hormones, viruses, radioactivity, and agents such as tobacco smoke, pesticides, and diesel exhaust. In the last decade knowledge in epigenetics has grown exponentially and

epigenetics play a central role in the emergence and development of diseases including cardiovascular and autoimmune illnesses as well as cancers of almost all types (Weinhold 2006).

### 1.6.2 Mechanisms

Epigenetic phenomena do not change the base sequence of DNA, but the chemical structure of DNA bases and/or chromatin, the proteins that bind to DNA. The most important epigenetic modifications are DNA methylation and histone modification. DNA methylation is catalyzed by DNA methyltransferase enzymes and involves the attachment of methyl groups to the base cytosine in certain gene areas, the so-called CpG islands. These are DNA segments in which the base sequence cytosine-guanine, more precisely cytosine phosphatidyl-guanosine, or CpG for short, occur particularly often. Around 70% of gene promoter regions lie within CpG islands. Methylated cytosines within the promoter region recruit gene suppressor proteins and hamper the binding of transcriptional factors to DNA. By these mechanisms, DNA methylation results in gene silencing (Saxonov et al. 2006; Moore et al. 2013).

Usually, DNA is not found unpacked within the cell nucleus but is bound to histones. Eight different histone proteins, two molecules each of histone 2A, histone 2B, histone 3 and histone 4 form the core of a nucleosome, which is wrapped by a small section of a DNA strand. Histone modifications are chemical changes in the histones that influence the chromatin structure and as a result transcription. They are found both at the unstructured N- and C-terminal ends of histone proteins and in the globular area within the nucleosome core (Zentner and Henikoff 2013). Histone modifications are named as follows:

- 1) The name of the histone (e.g., H3),
- 2) The modified amino acid in one-letter code (e.g., K4 for a lysine in position 4),
- 3) The type of modification (methylation: me, phosphorylation: p, acetylation: ac, ubiquitination: ub). In the case of methylated lysine or arginine, the number of methyl groups is also mentioned (e.g., trimethylation: me<sub>3</sub>).

Accordingly, a trimethylation of the lysine at position 4 of histone 3 is called H3K4me<sub>3</sub>. In our work, four major epigenetic histone modifications (methylation or acetylation) are particularly relevant: H3K4me<sub>3</sub> and H3K27ac are enriched around the transcription start sites (TSS) and active enhancers. They directly recruit the transcription complex and activate expression. H3K9me<sub>3</sub> is enriched in pericentromeric heterochromatin and thus acts as transcriptional repressor. H3K27me<sub>3</sub> is associated with heterochromatin and recruits a protein complex that inhibits RNA polymerase II elongation and in this way silences genes (Kimura 2013).

### 1.6.3 Epigenetic modifications and fibrosis

Several small-molecule inhibitors of epigenetic regulators have already been approved for therapy for oncology and non-oncology indications (Shortt et al. 2017). However, there is no approval for the treatment for HF or cardiac fibrosis, even though studies show a large number of molecular associations between cardiac fibrosis and epigenetic modulations: Silencing of a histone deacetylase in a rat model of oxidative and inflammatory stress attenuated the concentration of pro-inflammatory cytokines in plasma, decreased inflammatory cell infiltration and cardiac interstitial collagen deposition, and reduced passive diastolic stiffness in perfused hearts (Iyer et al. 2010). Xu et al. (2015b) showed that aberrant promoter methylation of RASAL1, a RAS-GTPase-activating protein, and thus suppression of its gene expression, results in EndMT contributing to cardiac fibrosis. Application of BMP7 was able to reverse the aberrant methylation through Tet3-mediated hydroxymethylation and thereby ameliorated experimental cardiac fibrosis in a pressure overload mouse model.

## 1.7 Objectives

The development and progression of cardiac fibrosis in the context of numerous cardiac and systemic diseases remains an enormous medical and socio-economic challenge, which underlines the importance of finding treatment solutions for patients. The administration of Serelaxin showed a significant improvement in dyspnea and a reduction of the early worsening of HF in clinical trials but could not significantly affect hospitalization or systolic parameters such as cardiac output. The fact that Serelaxin improved the symptoms of dyspnea (but not the cardiac output) suggests a possible influence of Serelaxin on the ventricular wall tension (and/ or the atria) as well as on cardiac fibrosis. The results of the clinical studies demand that the relevance of Serelaxin and its exact (functional) mechanism require further investigation and constitute the starting point for this study. Serelaxin had an anti-fibrotic impact on kidney and heart fibrosis in an experimental model of spontaneously hypertensive rats (Lekgabe et al. 2005). However, this study could not provide any insight into the pathomechanism. *In vitro* studies showed an anti-TGF $\beta$ /SMAD3-mediated preventive effect of Relaxin on the activation of fibroblasts (Sassoli et al. 2013). This suggests an inhibitory influence of Serelaxin on the equally SMAD3-mediated, profibrotic mechanisms including EndMT. In developing the findings of previous studies this project has three main objectives:

First, to systematically evaluate a possible effect of Serelaxin on specific subtypes of cardiac fibrosis.

Second, to investigate if Serelaxin influences EndMT *in vitro* and *in vivo* using experimental mouse models.

Third, to evaluate Serelaxin's potential antifibrotic mode of action and identify possible signaling pathways involved.

## 2 Materials and methods

### 2.1 Materials

#### 2.1.1 Animals

All animal experiments complied with ethical regulations and were conducted according to the animal experimental protocols, which were approved under file number G13.1325 by the Institutional Review Board of the University of Göttingen and the responsible government authority of Lower Saxony (Germany). All animal procedures conformed to the guidelines from Directive 2010/63/EU of the European Parliament on the protection of animals used for scientific purposes.

In this study all operations and treatments were performed on mice with a C57BL/6N background. C57BL describes the common, black-coated inbred strain of laboratory mice originally generated in 1921 by C. C. Little at the Bussey Institute for Research in Applied Biology while the sub-strain "6" was the most popular of all surviving sub-strains (Festing 1979). The letter "N" is the laboratory code and stands for the National Institutes of Health (NIH). All experimental mice cohorts were of mixed sex and operated at the age of 12 weeks. Animal surgery procedures are described in the respective method sections.

#### 2.1.2 Human tissue

All procedures were performed conforming to the World Medical Association Declaration of Helsinki. The permission to use human tissue was approved by the local ethics committee. Left ventricular myocardial tissue was obtained from end-stage HF patients at the time of heart transplantation or from donors without heart disease when the heart could not be transplanted for technical reasons.

#### 2.1.3 Cell culture

All cell lines and cell culture mediums used in this work are listed below in alphabetical order alongside their suppliers and the ordering numbers.

**Table 1: Cell lines used in this study**

Name	Species	Provider	Ordering number
HCAEC	human	Genlantis, San Diego, California, USA	PH30005AK
MCEC	murine	Cedarlane, Burlington, Canada	CLU510

Table 2: Cell culture mediums used in this study

Medium	Provider	Ordering number
DMEM	Life Technologies, Gibco, Carlsbad, California, USA	41965-039
Endothelial Cell Basic Medium	Genlantis, San Diego, California, USA	PM210500
FCS	Sigma-Aldrich, St. Louis, Missouri, USA	F4135-500ML
HCAEC Growth Medium	Genlantis, San Diego, California, USA	PM212500
HEPES Solution 1M	Thermo Fisher Scientific, Waltham, Massachusetts, USA	15630080
OPTI-MEM I (1X)	Life Technologies, Gibco Carlsbad, California, USA	31985-062

### 2.1.4 Instruments

All instruments used in this work are listed below in alphabetical order alongside their function and suppliers.

Table 3: Instruments used in this study

Function	Instrument	Provider
-20°C laboratory freezer	Mediline Lgex 3410	Liebherr, Bulle FR, Switzerland
-80°C laboratory freezer	MDF-U54V	Sanyo Biomedical, Wood Dale, Illinois, USA
Autoclaving	Autoclave LGAK0027	Teenomara Deutschland GmbH, Fernwald, Germany
Cell culture hood	BIOWIZARD	Kojair, Mänttä-Vilppula, Finland
Centrifugation of 1.5/2ml tubes	<ul style="list-style-type: none"> <li>▪ MiniSpin Centrifuge 5452</li> <li>▪ Centrifuge 5424 R</li> </ul>	Eppendorf, Hamburg, Germany
Centrifugation of 15/50ml tubes	Rotanta 460 R	Hettich, Tuttlingen, Germany
Centrifugation of qRT-PCR plates	PerfectSpin P	Peqlab Biotechnology, Erlangen, Germany
CO <sub>2</sub> Incubator	MCO-20AIC	Sanyo, Moriguchi, Osaka, Japan
Confocal microscope	FluoView FV100	Olympus, Shinjuku, Tokyo, Japan
Counting cells	Countess automated cell counter	Invitrogen, Life Technologies, Carlsbad, California, USA
Drying	Heated cabinet	Heraeus, Hanau, Germany
Flame sterilization	Fireboy	Integra, Hudson, New Hampshire, USA
Fluorescence analysis	Fluorescence camera ColorView	Olympus, Shinjuku, Tokyo, Japan
Heating block	Thermomixer comfort	Eppendorf, Hamburg, Germany
Ice machine	AF 80 Flake Ice Maker	Scotsman-Ice, Vernon Hills, Illinois, USA
Microscope	BX43	Olympus, Shinjuku, Tokyo, Japan
Microscope	Axiovert S100 TV	ZEISS, Oberkochen, Germany
Microscope	Nikon Eclipse T5100	Nikon, Minato, Tokyo, Japan
Microtome	Leica RM2165	Leica Microsystems, Wetzlar, Germany



Function	Instrument	Provider
Mixing and heating	ThermoMixer comfort	Eppendorf, Hamburg, Germany
Nitrogen tank	APOLLO	Messer, Griesheim, Germany
Nucleic acid concentration measuring	NanoDrop 2000	Thermo Fisher Scientific, Waltham, Massachusetts, USA
Paraffin Embedding	Leica 1120 H	Leica Microsystems, Wetzlar, Germany
Pipet Aid	Pipetus	Hirschmann, Eberstadt, Germany
Platform shaking	Rotamax 120	Heidolph, Schwabach, Germany
Power Supply	MP 300V Power Supply	Major Science, Saratoga, California, USA
Power Supply	Electrophoresis Power Supply	Rettberg, Goettingen, Germany
Protein transferring	Fastblot B44	Biometra, Goettingen, Germany
Real-time PCR cyclers	StepOnePlus Real-Time PCR System	Applied Biosystems, Waltham, Massachusetts, USA
Safety cabinets	NuAire Biological Safety cabinet	NuAire, Plymouth, Massachusetts, USA
Sonicating	Ultrasonic Liquid Processors S-400	Misonix Sonicators, Newtown, Connecticut
Steaming	Steam cooker 3216	BRAUN GmbH, Kronberg, Germany
Tissue disruption	TissueLyser LT	Qiagen, Hilden, Germany
Tissue floating	Tissue flotation bath GFL 1052	GFL-GmbH, Burgwedel, Germany
Tube rolling	Tube Roller Mixer SRT6	Bibby Scientific, Stuart, Staffordshire, UK
Vacuum pump	Vacusafe	Integra, Hudson, New Hampshire, USA
Vortexing	Vortex Genie 2	Bender & Hobein AG, Zurich, Switzerland
Warming up	Water bath WNB-7	Memmert GmbH, Schwabach, Germany
Weighing	Top Loading Balances TE2101	Sartorius, Goettingen, Germany
Western blot developing	ChemiDoc MP System	Bio-Rad, Munich, Germany
Western Blot imaging	ChemiDoc MP System	Bio-Rad, Munich, Germany

### 2.1.5 Commercial kits

All commercial kits used in this work are listed below in alphabetical order alongside their suppliers and ordering numbers.

Table 4: Commercial kits used in this study

Kit	Ingredients	Provider	Ordering number
<b>Chemiluminescent Kit</b>	<ul style="list-style-type: none"> <li>▪ Solution A</li> <li>▪ Solution B</li> </ul>	Santa Cruz Biotechnology, Santa Cruz, California, USA	sc-2048
<b>DNeasy Blood &amp; Tissue Kit</b>	<ul style="list-style-type: none"> <li>▪ Buffer ATL, AL, AE</li> <li>▪ Buffer AW1, AW2</li> <li>▪ Proteinase K</li> <li>▪ DNeasy Mini Spin Columns in 2 ml Collection Tubes</li> <li>▪ Collection Tubes</li> </ul>	Qiagen, Hilden, Germany	69506
<b>Pierce BCA Protein Assay</b>	<ul style="list-style-type: none"> <li>▪ BCA Reagent A</li> <li>▪ BCA Reagent B</li> <li>▪ Albumin Standard Ampules (2 mg/ml)</li> </ul>	Thermo Fisher Scientific, Waltham, Massachusetts, USA	23225
<b>PureLink RNA Mini Kit</b>	<ul style="list-style-type: none"> <li>▪ Lysis Buffer</li> <li>▪ Wash Buffer I</li> <li>▪ Wash Buffer II</li> <li>▪ RNase-Free Water</li> <li>▪ Spin Cartridges</li> <li>▪ Collection Tubes</li> <li>▪ Recovery Tubes</li> </ul>	Ambion, Carlsbad, California, USA	12183025
<b>RT<sup>2</sup> First Strand Kit</b>	<ul style="list-style-type: none"> <li>▪ Buffer GE</li> <li>▪ Buffer BC3</li> <li>▪ Reverse Transcriptase RE3</li> <li>▪ Control P2</li> <li>▪ Nuclease-Free Water</li> </ul>	Qiagen, Hilden, Germany	330404
<b>Superscript II Reverse Transcriptase</b>	<ul style="list-style-type: none"> <li>▪ Superscript II, Reverse Transcriptase</li> <li>▪ 5X First Strand Buffer</li> <li>▪ 0.1 M DTT (1,4-Dithiothreitol)</li> <li>▪ RNaseOUT</li> </ul>	Invitrogen, Life Technologies, Carlsbad, California, USA	18064-071
<b>Trichrome Stain (Masson) Kit</b>	<ul style="list-style-type: none"> <li>▪ Aniline Blue Solution</li> <li>▪ Biebrich Scarlet-Acid Fuchsin Solution</li> <li>▪ Phosphomolybdic Acid Solution</li> <li>▪ Phosphotungstic Acid Solution</li> </ul>	Sigma-Aldrich, St. Louis, Missouri, USA	HT-15-1KT
<b>VECTASTAIN Elite ABC-HRP Kit</b>	<ul style="list-style-type: none"> <li>▪ Reagent A</li> <li>▪ Reagent B</li> <li>▪ biotinylated horse anti-mouse/rabbit IgG</li> <li>▪ normal horse serum</li> </ul>	Vector Laboratories, Burlingame, California, USA	PK-6200

Kit	Ingredients	Provider	Ordering number
<b>Weigert's Iron Hematoxylin Solution Set</b>	<ul style="list-style-type: none"> <li>▪ Weigert's iron hematoxylin solution, Part A</li> <li>▪ Weigert's iron hematoxylin solution, Part B</li> </ul>	Sigma-Aldrich, St. Louis, Missouri, USA	HT-1079-1Set

### 2.1.6 Chemicals and reagents

All chemicals and reagents used in this work are listed below in alphabetical order alongside their suppliers and ordering numbers.

Table 5: Chemicals and reagents used in this study

Name	Provider	Ordering number
<b>20× LumiGlo and 20× Peroxide</b>	Cell Signaling Technology, Danvers, Massachusetts, USA	7003
<b>3XFlagNICD1 Plasmid</b>	Addgene, Watertown, Massachusetts, USA	20183
<b>Acetic acid solution</b>	MERCK, Darmstadt, Germany	1.37035.2500
<b>Angiotensin 2 powder (50mg)</b>	Sigma-Aldrich, St. Louis, Missouri, USA	A9525-50mg
<b>Bouin's solution</b>	Sigma-Aldrich, St. Louis, Missouri, USA	HT10132-1L
<b>Chloroform</b>	Sigma-Aldrich, St. Louis, Missouri, USA	C2432-500ML
<b>Dako AEC Substrate Chromogen Ready-to-Use</b>	Agilent Dako, Santa Clara, California, USA	K3464
<b>DAPI</b>	ROTH, Karlsruhe, Germany	6335.1
<b>DAPT (<math>\gamma</math>-secretase inhibitor)</b>	MERCK, Darmstadt, Germany	D5942-5MG
<b>Dimethyl sulfoxide (DMSO)</b>	Sigma-Aldrich, St. Louis, Missouri, USA	D8418-50ML
<b>DNase I</b>	Sigma-Aldrich, St. Louis, Missouri, USA	D5307
<b>Eosin G solution (pH5)</b>	ROTH, Karlsruhe, Germany	X883.2
<b>EtOH 100%</b>	ROTH, Karlsruhe, Germany	9065.2
<b>Fast SYBR Green Master Mix Real-Time PCR</b>	SA Biosciences, Qiagen, Frederick, Maryland, USA	4385617
<b>Formaldehyde</b>	ROTH, Karlsruhe, Germany	P087.3
<b>Glycine</b>	MERCK, Darmstadt, Germany	1.04201.0100
<b>H<sub>2</sub>O<sub>2</sub></b>	ROTH, Karlsruhe, Germany	8070.4
<b>Isoflurane</b>	Abbvie, North Chicago, Illinois, USA	B506
<b>LGR7 (RXFP1) Human Tagged ORF Clone</b>	OriGene Technologies, Rockville, Maryland, USA	RC211338L3
<b>Linear polyacrylamide</b>	MERCK, Darmstadt, Germany	56575-1ML
<b>Lipofectamine 2000</b>	Invitrogen, Life Technologies, Carlsbad, California, USA	11668019
<b>Mayer's hemalum solution</b>	ROTH, Karlsruhe, Germany	T865.2
<b>Novex Sharp Pre-Stained Protein Standard</b>	Invitrogen, Life Technologies, Carlsbad, California, USA	LC5800

Name	Provider	Ordering number
<b>Phenol:Chloroform:Isoamyl Alcohol 25:24:1 saturated with 10 mM Tris and 1 mM EDTA</b>	Sigma-Aldrich, St. Louis, Missouri, USA	P2069-100ML
<b>Protein-G sepharose</b>	GE Healthcare, Life Sciences, Chicago, Illinois USA	17-0618-01
<b>Proteinase-K</b>	Peqlab, VWR Life Science, Radnor, Pennsylvania, USA	04-1075
<b>Recombinant human TGFβ1 (10 µg)</b>	R&D Systems, Minneapolis, Minnesota, USA	240-B010/CF
<b>RNase A</b>	Thermo Fisher Scientific, Waltham, Massachusetts, USA	EN0531
<b>Serelaxin (4,75 mg/ml)</b>	Novartis, Basel, Switzerland	Not publicly available
<b>shRNA_RXFP1</b>	OriGene Technologies, Rockville, Maryland, USA	TL301865
<b>shRNA_RXFP4</b>	OriGene Technologies, Rockville, Maryland, USA	TL301862
<b>siRNA_Rxfp1</b>	OriGene Technologies, Rockville, Maryland, USA	SR419891
<b>Stop Solution (DNase I)</b>	Sigma-Aldrich, St. Louis, Missouri, USA	S4809
<b>Trizol</b>	Life Technologies, Gibco, Carlsbad, California, USA	15596026
<b>Trypsin EDTA Solution</b>	Sigma-Aldrich, St. Louis, Missouri, USA	T4049-100ml
<b>Xylol</b>	ROTH, Karlsruhe, Germany	9713.3

### 2.1.7 Buffers

Detailed information on **ready-to-use buffers** utilized in this work are listed below in alphabetical order alongside their suppliers and ordering numbers.

**Table 6: Ready-to-use buffers used in this study**

Buffer	Provider	Ordering number
<b>10× Reaction Buffer (DNase I)</b>	Sigma-Aldrich, St. Louis, Missouri, USA	R6273
<b>Phosphate buffered saline (PBS) for cell culture (1×)</b>	Life Technologies, Gibco, Carlsbad, California, USA	14190-094
<b>Restore Western Blot Stripping Buffer</b>	Thermo Fisher Scientific, Waltham, Massachusetts, USA	21059

Detailed information on the substances required for the preparation of **general buffers** that were used in this study are listed below in alphabetical order alongside the respective quantity, supplier and ordering number.

Table 7: Preparation of 10x PBS

Ingredient	Quantity	Provider	Ordering number
HCl	to pH = 7.25	ROTH, Karlsruhe, Germany	X942.2
K <sub>2</sub> HPO <sub>4</sub> •3H <sub>2</sub> O	2 g	ROTH, Karlsruhe, Germany	6878.2
KCl	2 g	MERCK, Darmstadt, Germany	TA698936
Na <sub>2</sub> HPO <sub>4</sub> • 2H <sub>2</sub> O	11.5 g	ROTH, Karlsruhe, Germany	4984.1
NaCl	80 g	ROTH, Karlsruhe, Germany	P029.3
ddH <sub>2</sub> O	1000 ml	Provided by the UMG	

Table 8: Preparation of 10x TBS

Ingredient	Quantity	Provider	Ordering number
NaCl	87 g	see above	see above
Tris	24.23 g	ROTH, Karlsruhe, Germany	5429.2
ddH <sub>2</sub> O	1000 ml	see above	see above

Detailed information on the substances required for the preparation of **immunohistochemistry and immunofluorescence buffers** that were used in this study are listed below in alphabetical order alongside quantity, supplier and ordering number.

Table 9: Preparation of citrate buffer

Ingredient	Quantity	Provider	Ordering number
Target Retrieval Solution, pH 6 (10x)	10 ml	Agilent Dako, Santa Clara, California, USA	S1699
ddH <sub>2</sub> O	90 ml	see above	see above

Table 10: Preparation of immunohistofluorescence blocking buffer

Ingredient	Quantity	Provider	Ordering number
Albumin Fraction V	0.5 g	ROTH, Karlsruhe, Germany	8076.3
PBS	50 ml	10x PBS stock	-

Detailed information on the substances required for the preparation of **Western blot buffers** that were used in this study are listed below in alphabetical order alongside quantity, supplier and ordering number.

Table 11: Preparation of 10 ml NP40 lysis buffer

Ingredient	Quantity	Provider	Ordering number
cOmplete ULTRA Tablets (protease inhibitor)	1 tablet	Hoffmann La-Roche AG, Basel, Switzerland	5892970001
NP40 Cell Lysis Buffer	10 ml	Life Technologies, Carlsbad, California, USA	FNN0021

Table 12: Preparation of 1000 ml 1x T-BST buffer

Ingredient	Quantity	Provider	Ordering number
TBS	100 ml	generated in Zeisbergs Lab (see above)	
Tween 20%	1 ml	ROTH, Karlsruhe, Germany	9127.2
ddH <sub>2</sub> O	900 ml	see above	see above

Table 13: Preparation of 400 µl Western blot sample buffer

Ingredient	Quantity	Provider	Ordering number
NuPAGE LDS Sample Buffer	200 µl	Invitrogen, Life Technologies, Carlsbad, California, USA	NP0007
β-Mercaptoethanol	80 µl	ROTH, Karlsruhe, Germany	4227.3
ddH <sub>2</sub> O	180 µl	see above	see above

Table 14: Preparation of 1000 ml Western blot inner buffer

Ingredient	Quantity	Provider	Ordering number
NuPAGE MOPS SDS Running Buffer (20×)	50 ml	Novex, Life Technologies, Carlsbad, California, USA	NP0001
β-Mercaptoethanol	1 ml	see above	see above
ddH <sub>2</sub> O	950 ml	see above	see above

Table 15: Preparation of 1000 ml Western blot outer buffer

Ingredient	Quantity	Provider	Ordering number
NuPAGE MOPS SDS Running Buffer (20×)	50 ml	see above	see above
ddH <sub>2</sub> O	950 ml	see above	see above

Table 16: Preparation of 50 ml Western blot blocking (5%) or washing (2%) buffer

Ingredient	Quantity	Provider	Ordering number
Milk powder (2% for washing / 5% for blocking)	1 g ≅ 2% 2.5 g ≅ 5%	ROTH, Karlsruhe, Germany	T145.2
TBST	50 ml	generated in AG Zeisberg (see above)	

Table 17: Preparation of 50 ml Western Blot transferring buffer

Ingredient	Quantity	Provider	Ordering number
Methanol (10%)	5 ml	ROTH, Karlsruhe, Germany	8388.6
NuPAGE Transfer Buffer (20×)	2.5 ml	Thermo Fisher Scientific, Waltham, Massachusetts, USA	NP0006
ddH <sub>2</sub> O	42.5 ml	see above	see above

Detailed information on the substances required for the preparation of **Chromatin immunoprecipitation buffers** that were used in this study are listed below in alphabetical order alongside quantity, supplier and ordering number.

Table 18: Preparation of 100 ml ChIP Nuclear preparation buffer

Ingredient	Quantity	Provider	Ordering number
EDTA (pH 8.0) 0.5 M	4 ml	Invitrogen, Carlsbad, California, USA	Y02353
NaCl 5 M	3 ml	see above	see above
NaF 0.5 M	4 ml	Sigma-Aldrich, St. Louis, Missouri, USA	201154-500G-D
NP-40 (10%)	5 ml	see above	see above
Tris (pH 7.5)	5 ml	see above	see above
Triton-X-100 (10%)	10 ml	MERCK, Darmstadt, Germany	11332481001
ddH <sub>2</sub> O	69 ml	see above	see above

Table 19: Preparation of 5 ml ChIP Sonication buffer-1

Ingredient	Quantity	Provider	Ordering number
EDTA (pH 8.0) 0.5 M	0.1 ml	see above	see above
SDS powder	0.05 g	Thermo Fisher Scientific, Waltham, Massachusetts, USA	BP166-100
Tris-HCl (pH 8.0) 1 M	0.25 ml	Thermo Fisher Scientific, Waltham, Massachusetts, USA	15568025
ddH <sub>2</sub> O	up to 5 ml	see above	see above

Table 20: Preparation of 50 ml ChIP Sonication buffer-2

Ingredient	Quantity	Provider	Ordering number
EDTA (pH 8.0) 0.5 M	2 ml	see above	see above
NaCl 5 M	1.5 ml	see above	see above
NaF 0.5 M	2 ml	see above	see above
NP-40 (10%)	5 ml	see above	see above
Tris-HCl (pH 8.0) 1 M	2.5 ml	see above	see above
ddH <sub>2</sub> O	37 ml	see above	see above

Table 21: Preparation of 250 ml ChIP Dilution buffer

Ingredient	Quantity	Provider	Ordering number
EDTA (pH 8.0) 0.5 M	10 ml	see above	see above
NaCl 5 M	7.5 ml	see above	see above
NaF 0.5 M	10 ml	see above	see above
NP-40 (10%)	25 ml	see above	see above
Sodium deoxycholate (10%)	12.5 ml	Sigma-Aldrich, St. Louis, Missouri, USA	D6750-100G
Tris-HCl (pH 8.0) 1 M	12.5 ml	see above	see above
ddH <sub>2</sub> O	172.5 ml	see above	see above

Table 22: Preparation of 250 ml ChIP IP buffer

Ingredient	Quantity	Provider	Ordering number
EDTA (pH 8.0) 0.5 M	10 ml	see above	see above
NaCl 5 M	7.5 ml	see above	see above
NaF 0.5 M	10 ml	see above	see above
NP-40 (10%)	25 ml	see above	see above
Sodium deoxycholate (10%)	12.5 ml	see above	see above
Sodium dodecyl sulfate (SDS; 10%)	2.5 ml	Thermo Fisher Scientific, Waltham, Massachusetts, USA	28312
Tris-HCl (pH 8.0) 1 M	12.5 ml	see above	see above
ddH <sub>2</sub> O	170 ml	see above	see above

Table 23: Preparation of 50 ml ChIP Wash buffer

Ingredient	Quantity	Provider	Ordering number
EDTA (pH 8.0) 0.5 M	2 ml	see above	see above
LiCl 8 M	3.125 ml	MERCK, Darmstadt, Germany	L7026-100ML
NaF 0.5 M	2 ml	see above	see above
NP-40 (10%)	5 ml	see above	see above
Sodium deoxycholate (10%)	5 ml	see above	see above
Tris-HCl (pH 8.0) 1 M	5 ml	see above	see above
ddH <sub>2</sub> O	27.875 ml	see above	see above

Table 24: Preparation of 250 ml ChIP TE buffer

Ingredient	Quantity	Provider	Ordering number
EDTA (pH 8.0) 0.5 M	0.5 ml	see above	see above
Tris-HCl (pH 8.0) 1 M	2.5 ml	see above	see above
ddH <sub>2</sub> O	247 ml	see above	see above



### 2.1.8 Antibodies

All antibodies used in this work are listed below by order of their intended method of use. They are presented in alphabetical order alongside their respective species, supplier, ordering number and dilution factors.

Table 25: Primary and secondary antibodies for immunofluorescence used in this study

Antibody	Species	Provider	Ordering number	Dilution
<b><math>\alpha</math>-SMA, anti-mouse</b>	Rabbit	Abcam Biochemicals, Cambridge, UK	Ab32575	1:100
<b>Alexa Fluor 488, anti-rabbit</b>	Donkey	Life Technologies, Invitrogen, Carlsbad, California, USA	R37118	1:200
<b>Alexa Fluor 568, anti-goat</b>	Donkey	Life Technologies, Invitrogen, Carlsbad, California, USA	A11057	1:200
<b>Alexa Fluor 568, anti-mouse</b>	Donkey	Life Technologies, Invitrogen, Carlsbad, California, USA	A10037	1:200
<b>Alexa Fluor 568, anti-rabbit</b>	Donkey	Life Technologies, Invitrogen, Carlsbad, California, USA	A10042	1:200
<b>CD31, anti-mouse</b>	Goat	Santa Cruz Biotechnology, Santa Cruz, California, USA	SC1306	1:50
<b>Coll<math>\alpha</math>(I)</b>	Rabbit	Abcam Biochemicals, Cambridge, UK	Ab34710	1:200
<b>JAGGED1</b>	Rabbit	Santa Cruz Biotechnology, Santa Cruz, California, USA	SC8303	1:50
<b>NICD</b>	Rabbit	Abcam Biochemicals, Cambridge, UK	Ab52627	1:50
<b>NOTCH1</b>	Rabbit	Abcam Biochemicals, Cambridge, UK	Ab8925	1:100
<b>RXFP1, anti-mouse</b>	Rabbit	Santa Cruz Biotechnology, Santa Cruz, California, USA	SC50528	1:50
<b>wheat germ agglutinin, Alexa Fluor 488 conjugate, anti-mouse</b>	-	Life Technologies, Invitrogen, Carlsbad, California, USA	W11261	1:1000

Table 26: Primary antibodies for immunohistochemistry used in this study

Antibody	Species	Provider	Ordering number	Dilution
Cleaved Caspase 3	mouse	Cell Signaling Technology, Danvers, Massachusetts, USA	9661	1:200

Table 27: Antibodies for Western blot used in this study

Antibody	Provider	Ordering number	Dilution
CD31	Abcam Biochemicals, Cambridge, UK	Ab28364	1:1000
JAGGED-1	Santa Cruz Biotechnology, Santa Cruz, California, USA	Sc-8303	1:200
RXFP1	Abnova, Taipei, Taiwan	PAB16536	1:1000
RXFP4	Sigma-Aldrich, St. Louis, Missouri, USA	SAB4501495	1:1000
SMAD2/3	Cell Signaling Technology, Danvers, Massachusetts, USA	12747T	1:1000
$\alpha$ -TUBULIN	Sigma-Aldrich, St. Louis, Missouri, USA	T5168	1:4000

Table 28: Antibodies for ChIP assay used in this study

Antibody	Provider	Ordering number	Dilution
H3K27ac	Active Motif, Carlsbad, California, USA	39133	1:400
H3K27me3	Active Motif, Carlsbad, California, USA	39155	1:400
H3K4me3	Active Motif, Carlsbad, California, USA	39159	1:400
H3K9me3	Active Motif, Carlsbad, California, USA	39765	1:400
pSMAD2/3	Cell Signaling Technology, Danvers, Massachusetts, USA	5678	1:300

### 2.1.9 Oligonucleotides (primers)

All primers used in this work are listed below by order of their method of use. They are presented in alphabetical order alongside sequence (5' → 3'), species and supplier.

Table 29: Primers for ChIP-qPCR assay for Rxfp1 used in this study

Primer	Sequence 5' → 3'	Provider
Amplicon 1	F: TGCTCAACTTTCCAAACAGA R: ATGCTTTTGTGGCACAGCTA	Microsynth AG, Balgach, Switzerland
Amplicon 2	F: CCATGCTTGGGATTTACCTC R: TGCTCTGACAAAAGCCTTCAC	Microsynth AG, Balgach, Switzerland
Amplicon 3	F: ATGAGGGAGGGACACAGAGA R: ACAGCTCACAGTGGTTGTGC	Microsynth AG, Balgach, Switzerland
Amplicon 4	F: TGGTGTGGGGATTGAACCTCA R: GACTTCATGCATGTGGAGGC	Microsynth AG, Balgach, Switzerland

Table 30: Primers for qRT-PCR used in this study

Gene	Sequence 5' → 3'	Species	Provider
<i>CD31</i>	F: CCAAAGCCAGTAGCATCATGGTC R: GGATGGTGAAGTTGGCTACAGG	Mus musculus	Primer Design, Chandler's Ford, UK
<i>ErbB3</i>	F: TCACACTCAGCCCGTTTAGA R: AGGTGCTGGGTTTCCCTTCTC	Mus musculus	OriGene Technologies, Rockville, Maryland, USA
<i>Fzd7</i>	F: TCAGCTGGAGGAAAAAGACG R: GTGCTGGACGCGGAGAGT	Mus musculus	OriGene Technologies, Rockville, Maryland, USA
<i>Gapdh</i>	undisclosed	Mus musculus	Primer Design, Chandler's Ford, UK
<i>Gsc</i>	F: CATGTAGGGCAGCATCTGGT R: CAGCAGTGTCTCTGCGTC	Mus musculus	OriGene Technologies, Rockville, Maryland, USA
<i>Gsk3b</i>	F: GTGGTTACCTTGCTGCCATC R: GACCGAGAACCACCTCTTT	Mus musculus	OriGene Technologies, Rockville, Maryland, USA
<i>Jagged1</i>	F: AACCTGTAACATAGCCGAAAC R: GTAAAGGACTCGCCGTTGAC	Mus musculus	Primer Design, Chandler's Ford, UK
<i>Notch1</i>	F: TGCCCGTCTTGAAATGTAGG R: GGCAGTGTCTTTCCCAGA	Mus musculus	Primer Design, Chandler's Ford, UK
<i>Rac1</i>	F: TCTCCAGGAAATGCATTTGGT R: AGATGCAGGCCATCAAGTGT	Mus musculus	OriGene Technologies, Rockville, Maryland, USA
<i>Rxfp1</i>	F: ATTTCTCTCTGCTGTGCTGACT R: CGGCTGTGCGTGCTTATTG	Mus musculus	Primer Design, Chandler's Ford, UK
<i>Rxfp2</i>	F: ACGAACTCCACCTTCCTAACG R: AAAATGTCTTCTCTGGAACAAAACC	Mus musculus	Primer Design, Chandler's Ford, UK
<i>Rxfp3</i>	F: AACCCGATCCTCTACTGCTTAG R: GCATGTTGGTGAGCGAAGG	Mus musculus	Primer Design, Chandler's Ford, UK
<i>Rxfp4</i>	F: AGGTAAGTGTGGTCAGCGTGTG R: CCAGTGGAAGTCCATGTCTGAC	Mus musculus	OriGene Technologies, Rockville, Maryland, USA
<i>Slug</i>	F: CGCTCCTTCCGGTCAAGA R: AGGTATAGGGTAACTTTCATAGAGATA	Mus musculus	Primer Design, Chandler's Ford, UK
<i>Snail</i>	F: GTGCCACCTCCAAACCC R: AAGGACATGCGGGAGAAGG	Mus musculus	Primer Design, Chandler's Ford, UK
<i>Steap1</i>	F: CAAACCCAGAACAACCTTTGGA R: TCGTCTCTCCCGAGTCCTTA	Mus musculus	OriGene Technologies, Rockville, Maryland, USA
<i>Twist</i>	F: TGATAGAAGTCTGAACACTCGTTTG R: GGCTGATTGGCAAGACCTCT	Mus musculus	Primer Design, Chandler's Ford, UK
<i>CD31</i>	F: AAGGAACAGGAGGGAGAGTATTA R: GTATTTTGCTTCTGGGGACACT	Homo sapiens	Primer Design, Chandler's Ford, UK
<i>GAPDH</i>	undisclosed	Homo sapiens	Primer Design, Chandler's Ford, UK
<i>RXFP1</i>	F: GCTGTATGCCATGTCAATCATT R: TCTCCACGAAACTTTAGGTCAA	Homo sapiens	Primer Design, Chandler's Ford, UK

Gene	Sequence 5' → 3'	Species	Provider
<i>RXFP2</i>	F: GATCACTCCTTCATGCCAAAAAG R: TGTCACCACAGTTCTCTTCGT	Homo sapiens	Primer Design, Chandler's Ford, UK
<i>RXFP3</i>	F: ACCAAATCAGTGACCATCGTT R: GCGTTGAAC TTGATGAGGATG	Homo sapiens	Primer Design, Chandler's Ford, UK
<i>RXFP4</i>	F: CCTGTCACTACTTGCTTGGCAC R: TCAACCGCAGATCCCTGAAGGT	Homo sapiens	OriGene Technologies, Rockville, Maryland, USA
<i>SLUG</i>	F: ACTCCGAAGCCAAATGACAA R: CTCTCTCTGTGGGTGTGTGT	Homo sapiens	Primer Design, Chandler's Ford, UK
<i>SNAIL</i>	F: GGCAATTTAAACAATGTCTGAAAAGG R: GAATAGTTCTGGGAGACACATCG	Homo sapiens	Primer Design, Chandler's Ford, UK
<i>TWIST</i>	F: CTCAAGAGGTCGTGCCAATC R: CCCAGTATTTTTATTTCTAAAGGTGTT	Homo sapiens	Primer Design, Chandler's Ford, UK

### 2.1.10 Other materials

All material used in this work that has not been included in previous tables is listed below in alphabetical order alongside suppliers and ordering numbers.

Table 31: Other materials used in this study

Material	Provider	Ordering number
6-well cell culture plate	Corning, Corning, New York, USA	353046
ALZET Osmotic Pumps <ul style="list-style-type: none"> <li>▪ 0.25 µl/hr</li> <li>▪ 0.11 µl/hr</li> </ul>	ALZET, Cupertino, California, USA	<ul style="list-style-type: none"> <li>▪ 1002</li> <li>▪ 1004</li> </ul>
Cell culture flask T-75	MERCK, Darmstadt, Germany	EP0030711017-80EA
Cell scraper	Techno Plastic Products AG, Trasadingen, Switzerland	99004
Cellstar tubes 15 ml	Greiner bio-one, Kremsmünster, Austria	188271
Cellstar tubes 50 ml	Greiner bio-one, Kremsmünster, Austria	227261
culture dish 10 cm	Corning, Corning, New York, USA	430167
Dako Pen	Agilent Dako, Santa Clara, California, USA	S2002
Disposable scalpel	Feather, Kita-Ku, Osaka, Japan	02.001.30.022
EMT Signaling Pathway PCR array	SABiosciences, QIAGEN, Frederick, Maryland, USA	PAHS-090Z
Immu-Mount	Fisher Scientific, Hampton, New Hampshire, USA	9990402
MicroAmp Fast 96-Well Reaction Plate (0.1 ml)	Applied Biosystems, Darmstadt, Germany	4346907
Microscope Slides	Gerhard Menzel GmbH, Braunschweig, Germany	J1800AMNZ
Nitrocellulose blotting membrane	GE Healthcare, Life Sciences, Chicago, Illinois USA	10600002

Material	Provider	Ordering number
NuPage 4-12% Bis-Tris-Gel	Invitrogen, Life Technologies, Carlsbad, California, USA	NP0336BOX
Parafilm	Bemis, Neenah, Wisconsin, USA	PM-999
Pasteur pipets glass	Brand, Sigma-Aldrich, St. Louis, Missouri, USA	747720
Pipette 10 $\mu$ l	Eppendorf, Hamburg, Germany	M20389B
Pipette 100 $\mu$ l	Eppendorf, Hamburg, Germany	O30293G
Pipette 1000 $\mu$ l	Eppendorf, Hamburg, Germany	O48499G
Pipette 2.5 $\mu$ l	Eppendorf, Hamburg, Germany	I26186H
Pipette tips 10/20 $\mu$ l	Starlab GmbH, Hamburg, Germany	S1120-3710
Pipette tips 200 $\mu$ l	Starlab GmbH, Hamburg, Germany	S1111-0700
Pipette tips 1000 $\mu$ l	Starlab GmbH, Hamburg, Germany	S1111-6700
Safe Lock Tubes 1.5 ml	Eppendorf, Hamburg, Germany	0030120.086
Safe Lock Tubes 2 ml	Eppendorf, Hamburg, Germany	0030120.094
Serological pipette 10 ml	Sarstedt, Nümbrecht, Germany	86.1254.001
Serological pipette 25 ml	Sarstedt, Nümbrecht, Germany	86.1685.001
Serological pipette 5 ml	Sarstedt, Nümbrecht, Germany	86.1253.001

### 2.1.11 Software

Any software used in the present work is listed below in alphabetical order alongside the supplier.

Table 32: Software used in this study

Software	Provider
BioRender	Biorender, Toronto, Canada
cellSens Dimension 1.6	Olympus SIS, Muenster, Germany
FluoView FV1000	Olympus, Shinjuku, Tokyo, Japan
GraphPad Prism 6.0	GraphPad Software, La Jolla, California USA
Illustrator CS5	Adobe, San Jose, California, USA
Image Lab 5.21	Bio- Rad Laboratories, Hercules, California, USA
ImageJ 1.49q	NIH, Bethesda, Maryland, USA
MS Office	Microsoft, Redmond, USA
Photoshop CS6	Adobe, San Jose, California, USA
StepOnePlus Software v2.3	Applied Biosystems, Darmstadt, Germany

## 2.2 Methods

### 2.2.1 Ascending aortic constriction (AAC)

12-week-old C57BL/6N mice (each group was composed of male and female mice), weighing between 25-30 g were anesthetized with a mixture of medetomidine (0.5 mg/kg), midazolam (5 mg/kg) and fentanyl (10 mg/kg) at 0.1 ml NaCl intraperitoneally before surgery. AAC was carried out as previously performed and described in several studies (Jiang et al. 2007; Takahashi et al. 2007; Zeisberg et al. 2007b). The aorta can be constricted on different levels: ascending, transverse, and descending part. Constriction of the ascending aorta does induce significant and fast pressure overload on the left ventricle by mimicking aortic stenosis. This causes a high degree of hypertrophy and cardiac fibrosis (Tarnavski et al. 2004). A sham operation was performed under the same conditions except for the aortic banding. AAC and sham operations were performed by either veterinarian Kirsten Koschel or PostDoc Xingbo Xu. Both have been trained in this technique and gained sufficient experience in the procedure. Tim Wilhelmi had been able to assist in the procedures and make appropriate pre- and post-procedures. In particular, postoperative subcutaneous analgesic administration was performed by Tim Wilhelmi.

Aortic pressure gradients were determined by echocardiography to verify aortic constriction. All mice were sacrificed four weeks after operation.

### 2.2.2 Osmotic minipump implantation

The Alzet osmotic minipump consists of an outer semipermeable membrane, a salt chamber with a highly concentrated sodium chloride solution and the inner flexible impermeable membrane, which encloses the medication filling space. Given the osmotic pressure difference, body fluid flows through the semipermeable membrane to the salt chamber. With a continuous increase in volume, the osmotic pressure transfers the medication in the filling space into the animal body via an outlet opening at the pump pole. The constant pumping rate is thus determined by the water permeability of the outer membrane and is not influenced by the molecular weight or the physical or chemical properties of the solutions that are dispensed. The pumps were introduced into the animals immediately after the AAC surgery respectively during ATII surgery. The anesthesia was carried out with 2% (vol / vol) isoflurane in oxygen (1 l / minute) through a nasal mask and was controlled by checking the pain stimuli. The animal was fixed on a warming plate. After depilation and disinfection, the skin in the middle of the dorsal neck was opened in an approximately 1 cm long extension and detached laterally from the muscle fascia. Then the sterile osmotic minipump was inserted into the skin pockets towards the lumbar region. The skin incision was closed by sutures. The anesthesia was terminated, and the animals were monitored until full awakening. The procedure was performed by either veterinarian Kirsten Koschel or PostDoc Xingbo Xu.

### 2.2.2.1 Application of Serelaxin

The animals were treated with Serelaxin in targeted drug doses of 50, 200 and 500 µg/kg body weight/day. To ensure a constant release of Serelaxin, osmotic minipumps were implanted subcutaneously on the back of the wild-type mice. The model A1002 was applied for the 14-day treatment and A1004 for the 28 day treatment. Before implantation, the pump was filled with Serelaxin and PBS using a cannula according to the volume size of 100 µl and the respective concentration. Subsequently, it was equilibrated in PBS overnight at 37°C. For the control groups, the pumps were provided with 100 µl of PBS. With a pump rate of 0.25 µl per hour, 6 µl of this solution were continuously dispensed by osmosis per day for 14 or 28 days.

### 2.2.2.2 Application of Angiotensin-2 (ATII)

ATII in a concentration of 1.5 mg/kg per day plus either Serelaxin (500 µg/kg bodyweight) or PBS as a vehicle control were administered to animals via osmotic minipumps. The model A1002 was applied for the 14 days treatment, A1004 for the 28 days treatment.

### 2.2.3 Echocardiographic measurements

Pressure gradients were measured with a Vevo 2100 system with a 30-MHz respiration- and ECG-controlled probe under anesthesia with 1.5% isoflurane by inhalation during the whole procedure. The ascending aorta was visualized with 2-D and color flow imaging. The distal ascending aortic flow velocity (distal to constriction in AAC mice) was measured by a pulsed wave (PW) Doppler to assess the pressure gradient, which was estimated using the modified Bernoulli equation ( $pressure\ gradient = 4 * velocity^2$ ). The investigator, Dr. Fouzi Alnour, was blinded with respect to treatment.

### 2.2.4 Blood pressure measurement in ATII-treated animals

One week before implantation of the osmotic minipump as well as at the end of the experiment, the mice's blood pressure was determined as a control parameter for the ATII application drawing on the tail cuff method established in our group. The mice were fixed in a plastic tube and the measuring apparatus fixed to the tail. After several measurement runs, an average value was calculated. The measurement took about 10 minutes per animal and, because of the very low stress level on the animal, the procedure required neither analgesia nor sedation.

### 2.2.5 Sacrifice and preparation

After the 14th or 28th postoperative day, the mice were briefly anesthetized by using isoflurane and then killed through cervical dislocation by either Mrs. Sarah Rinkleff or Tim Wilhelmi. During the dissection, the thorax was opened with a longitudinal sternotomy and the heart was removed. It was washed in PBS and halved with the aid of a scalpel, one part

being placed in a cryo-tube and briefly stored in liquid nitrogen before cryopreserved for long-term storage at  $-80^{\circ}\text{C}$ ; and one part being distributed on embedding cassettes and fixed in 4% formaldehyde solution.

### 2.2.6 Cell culture experiments

#### 2.2.6.1 Maintenance and harvesting

Human coronary artery endothelial cells (HCAECs) and mouse cardiac endothelial cells (MCECs) were held in flasks, on plates or six-well-plates that were stored at  $37^{\circ}\text{C}$  in an incubator that supplied 5%  $\text{CO}_2$ . For maintaining the culture, the cells were supplied with a growth medium (500 ml DMEM, 25 ml FBS (5%), and 5 ml 1 M HEPES (1%)). The medium was changed every two days, i.e. the old medium was discarded, the cells were washed with PBS and new medium was supplied. When more than 90% of the container's ground was confluent, Trypsin was added for three minutes to detach the cells. As a next step, Trypsin was neutralized by a growth medium, and all cells were suspended and pipetted into a 15 ml Falcon tube. After centrifugation at 1,000 rpm for five minutes at room temperature, the supernatant was discarded, and the cell pellet was either resuspended and equally distributed in three new flasks for subcultures or collected for further experiments.

#### 2.2.6.2 TGF $\beta$ 1 and Serelaxin treatment

To induce EndMT *in vitro* a special protocol was used in this study. After plating 40,000 cells per well of a six-well-plate in growth medium on the first day, the cells were starved with basal medium (DMEM) on the second day. On the third day, this medium was exchanged for treatment medium which contained growth and basal medium (1:5) supplemented by 10 ng TGF $\beta$ 1 per 1 ml treatment medium. Cells were then harvested after two or four days. In some experiments, cells were treated with Serelaxin which was solved in treatment medium and applied in different concentrations ranging from 20 ng/ml to 200 ng/ml following the same basic procedure.

#### 2.2.6.3 Relaxin family peptide receptor experiments

Transfection experiments were performed in HCAECs and MCECs seeded onto 10 cm plates and cultured overnight. The next day, the cells were transfected with Lipofectamine 2000 according to the manufacturer's instructions (Xu et al. 2015c). Briefly, 2.5  $\mu\text{g}$  of shRNA-plasmid or 40 pmol of siRNA were mixed with Lipofectamine 2000 in a ratio of 1:2 in a total volume of 500  $\mu\text{l}$  of Opti-MEM. The DNA-Lipofectamine complex was formed after a 20-minute incubation period at room temperature and subsequently added to the cells in an endothelial cell basic medium. The medium was replaced by a growth medium after three hours of incubation.

For the *RXFP1* overexpression experiment, cells were treated either with a 2.5  $\mu\text{g}$  *RXFP1* human tagged ORF clone or an empty vector as control in basal medium. In both cases,



knockdown, and overexpression TGF $\beta$ 1 treatment started the next day and cells were collected for gene expression analysis four days after.

#### 2.2.6.4 Notch pathway signaling experiments

For the *NICD* overexpression assay, MCECs were treated with 2.5  $\mu$ g of a vector containing a murine notch 1 intracellular domain or an empty vector as a control. TGF $\beta$ 1 treatment started the next day and cells were collected for gene expression analysis four days after.

The treatment with the  $\gamma$ -secretase inhibitor N-[N-(3,5-difluorophenacetyl)-L-alanyl]-S-phenylglycine t-butyl ester (DAPT) that blocks Notch signaling was performed according to a previously described protocol (Chigurupati et al. 2007). Briefly, MCECs were cultured for an additional 24 hours in a serum-free basal medium in the presence of either 10  $\mu$ M DAPT or DMSO as a control. Afterwards cells were harvested as described above.

### 2.2.7 Histological methods

#### 2.2.7.1 Preparation and processing of tissue sections

The fixation of the heart was carried out in 4% formaldehyde overnight to prevent autolytic processes after death and to maintain the tissue morphology. This leads to the formation of methyl bridges between free amino groups of the proteins and thus to their blocking. The resulting protein crosslinking aims at better retention of tissue structure. The next day, the biopsates were embedded in paraffin. For this purpose, the tissue samples were initially watered for four hours under running tap water to wash out the fixative. The heart samples were then embedded in paraffin in a Leica tissue infiltration machine using an ascending series of alcohols (1 x 50%, 1 x 70%, 1 x 80%, 2 x 95%, 2 x 100%, 2 x chloroform, and 3 x paraffin for one hour each). They were then placed in the paraffin station, poured into paraffin blocks, and cooled down on the cooling plate. Tissue sections of 3  $\mu$ m thickness could be made from each block using a microtome. These were first transferred to a water bath for better unfolding and then transferred to SuperFrost slides. To improve the adhesion of the tissue to the slides, they were dried overnight at 37°C. The histological slides were stored in special boxes at room temperature until further histological processing. Before each histological staining, the tissue sections were first deparaffinized for 10 minutes in 100% xylol and then passed through the following descending alcohol (EtOH) series: 2 x 5 minutes EtOH 100%, 1 x 5 minutes EtOH 80%, 1 x 5 minutes EtOH 50%, 1 x 5 minutes EtOH 30%. Finally, the sections were placed in distilled water for five minutes for further hydration.

#### 2.2.7.2 Hematoxylin-eosin (HE) staining

The hematoxylin-eosin staining is a standard method in the histological laboratory. The aim is to show morphological tissue structures and assess pathological changes in the tissue section. The basophilic cell nuclei are stained blue with iron hematoxylin. Cytoplasm is azido- or eosinophilic and stained red with eosin. For nuclear staining, the sections were first placed

in Mayer's hemalum solution for five minutes and blued under running tap water. The plasma was then stained in the eosin solution (pH5) acidified with 100% acetic acid. Finally, the sections were briefly dehydrated twice using an ascending series of alcohols (EtOH 96% and EtOH 100%) and clarified 2 x 5 minutes in xylol. The slides were mounted with the ImmoMount medium.

#### 2.2.7.3 Masson-Trichrome staining (MTS)

The MTS is widely utilized to differentiate connective tissue and to quantify the degree of fibrosis in different organ parenchyma such as heart or kidney (Tampe et al. 2014; Xu et al. 2015b). The cell nuclei turn brownish-black and the cytoplasm red. The collagen fibers are stained in blue. Following the deparaffinization, the sections were fixed in the preheated Bouins solution at 56°C for 15 minutes, cooled in tap water for ten minutes and placed under running tap water to wash out the yellow color. Furthermore, the preparations for nuclei staining were immersed in Weigert's iron hematoxylin solution for five minutes, washed again for five minutes under running tap water and finally rinsed three times with distilled water. The tissue sections were then immersed in the acid Fuchsin solution for five minutes and rinsed with distilled water three more times. After, the sections were treated with a phosphomolybdic-phosphotungstic solution (prepared by mixing one volume of both acids with two volumes of water) for another five minutes. The preparations were then incubated in aniline blue for collagen detection. The colors were easily washed out by briefly immersing them in 1% acetic acid and distilled water. Finally, the sections were briefly dehydrated twice using an ascending series of alcohols (EtOH 96% and EtOH 100%) and clarified 2 x 5 minutes in xylol. Finally, the sections were mounted with the ImmoMount medium.

#### 2.2.8 Immunofluorescence staining

Antibodies with coupled fluorescent dye are used in immunofluorescence, to localize proteins and thus specific structures in cells as well as tissues. The indirect immunofluorescence method was used for the immunofluorescence staining performed in this study. For this purpose, the antibody that binds to the specific protein (epitope) is unlabeled. The actual coloring takes place in the second step. A second antibody labeled with fluorochrome binds specifically to the first antibody. For that, paraffin-embedded heart tissue was sectioned at 3 µm thickness, deparaffinized and rehydrated by xylol and graded alcohol series prior to staining as described above. An antigen retrieval was performed with citrate buffer for 40 minutes at 95°C in a steamer and thereafter washed with PBS for ten minutes. The slides were blocked in 1% BSA in PBS at room temperature for 30 minutes before incubating with a primary antibody at 4°C overnight in a humid chamber. The fluorochrome-labeled secondary antibody was added and incubated at room temperature for 45 minutes. The cell nucleus was visualized with DAPI (1 mg/ml) in PBS (1:1000 dilution) at room temperature for five minutes. Microscopic pictures were acquired using an Olympus Confocal Microscope FV-1000 and the Fluoview program and processed by Photoshop CS6

software. The primary and secondary antibodies used in this study with dilution factors are listed above (Table 25).

### 2.2.9 Immunohistochemistry staining

In immunohistochemistry, the antigen to be examined is brought together with a specific antibody which is directly conjugated with an enzyme. The antibody – and thus the enzyme – binds to the antigen, and the unbound antibody is rinsed off. In a further step, the antibody-bound enzyme is mixed with substrate which reacts with the enzyme to form a dye, which allows to visually detect the antigen. To carry out immunohistochemistry in this study, VECTASTAIN Elite ABC-HRP Kit was used. Slides were prepared and antigen retrieval was performed as described in 2.2.8. Peroxidase blocking was carried out with 0.3% H<sub>2</sub>O<sub>2</sub> at room temperature for 30 minutes and followed by three washing steps with PBS for five minutes each. A further blocking was performed with two drops of horse normal serum in 10 ml PBS in a humid chamber at room temperature for 20 minutes. The block was then slightly discarded, and the primary antibody was pipetted on the slides and incubated at 4°C overnight. The next day, slides were washed with PBS for five minutes, three times each. Subsequently, a secondary antibody was added and incubated in a humid chamber for 30 minutes at room temperature. After another washing step with PBS, two drops of reagent A were diluted in 5 ml PBS and then gently mixed with two drops of reagent B. This mixture was pipetted on the slides and incubated in a humid chamber for 30 minutes at room temperature. Hereupon, the slides were washed once more with PBS and an ACE substrate was supplied for exactly 15 minutes and consequently washed with PBS. For staining of the nucleus, Mayer's hemalum solution was added for four minutes and blued for five minutes by tap water. Finally, the slides were mounted with ImmoMount medium and quantified under the microscope. All kit ingredients and antibodies used in this method are listed above (Table 26).

### 2.2.10 Histological quantification of fibrosis and immune staining

The percent area of left ventricular myocardial fibrosis was assessed in MTS slides using cellSens software. Perivascular fibrosis was defined as fibrotic lesions surrounding vessels with a minimum diameter of 100 µm.

Immune staining was evaluated under the microscope (using a fluorescence camera at 400x magnification for immunofluorescence). For each tissue section, 10 fields of view at the left ventricular myocardium were analyzed. The percentage of antigen-positive squares could be determined with the aid of a foil grid with 638 x 10 mm<sup>2</sup> squares. The number of positive squares was quantified, the mean was divided by the total number of foil grid squares (638) and multiplied by a factor of 100.

### 2.2.11 Medium densitometry analysis

MCECs were treated with TGF $\beta$ 1, and untreated cells were used as control. After four days the medium was collected, all soluble proteins were precipitated by acetone. The samples were prepared by following the Western blotting protocol and transferred to a cellulose membrane. The membrane was then stained with Ponceau S, a negative stain binding non-covalently to positive and non-polar regions in the protein. It generates reddish pink protein bands with a clear background. After, the membrane was transferred to 5 ml of Ponceau S solution and orbitally shaken for five minutes at room temperature. After rinsing the membrane with deionized water, it was washed three times for five minutes each to remove the background staining. To de-stain the membrane entirely from protein, it was washed with 0.1 N NaOH solution for five minutes. The wash solution was discarded, and the washing procedure with 0.1 N NaOH was repeated once after. After three more washing steps with deionized water for five minutes each, the membrane was dried and quantified.

### 2.2.12 RNA extraction

Total RNA was extracted from either cells or shredded tissue by PureLink RNA kit following the manufacturer's protocol. Tissue was first shredded using a TissueLyser LT machine in 30 Hz for 5 minutes. All subsequent steps were performed using disposable RNase-free pipette tips and micro-centrifuge tubes. First, the sample was incubated with 1 ml of Trizol for five minutes at room temperature and chloroform was added. Second, the tube was shaken vigorously for 15 seconds, incubated for three minutes at room temperature, and centrifuged for 15 minutes at 12,000 g at 4°C. The aqueous phase containing the RNA was transferred into another tube and ethanol was added up to a concentration of 35% in the total sample. The mixture was then vortexed well and transferred to the spin cartridge which was centrifuged for 15 seconds at 12,000 g. The flow-through was discarded and the cartridge was washed three times. After drying the membrane by centrifugation for one minute at 12,000 g, the spin cartridge was transferred into a recovery tube. By elution with 30-50  $\mu$ l of nuclease-free water, incubation for one minute at room temperature and centrifugation for two minutes at 12,000 g, the RNA was collected in the recovery tube. Upon determination of the concentration – as described below – the sample was either kept on ice to be used for immediate further experiments or stored at -80°C.

### 2.2.13 Measurement of nucleic acid concentration

The NanoDrop 2000 spectrophotometer was used for the photometric determination of the concentration of the isolated RNA or DNA. We applied 1  $\mu$ l of the nucleic acid eluate to the sample holder and measured the absorption in relation to the nuclease-free water. To ensure the quality of the sample, the quotient of the absorption coefficients was defined at 260 nm and 280 nm. A value of 2.0 corresponds to pure RNA; 1.8 indicates pure DNA. Deviations above the respective values indicate a possible protein contamination.

### 2.2.14 RNA reverse transcription

Prior to cDNA synthesis using the SuperScript II system, 1 µg of total RNA was digested by DNase at room temperature for 15 minutes to remove any genomic DNA. Therefore, 1 µl of DNase I, 1 µl of 10X reaction buffer and nuclease-free water were mixed bringing the total reaction volume to 10 µl. Afterwards, the reaction was stopped by adding 1 µl of Stop Buffer and heating it up to 70°C for ten minutes. The sample was then chilled on ice for two minutes. 1 µl of oligo (dT) primers as well as 1 µl dNTP 10 mM were added and incubated at 65°C for five minutes. After placement on ice, 4 µl of 5X First-Strand Buffer, 2 µl of DTT and 1 µl of RNaseOUT were added and mixed gently, followed by an incubation period of two minutes at 42°C. Finally, 1 µl of SuperScript II Reverse Transcriptase was added and the sample was incubated at 42°C for 50 minutes, then at 70°C for 15 minutes. The sample was then diluted by a 1:10 ratio and either used for immediate further experiments or stored at -20°C.

### 2.2.15 Quantitative real-time PCR

Quantitative real-time polymerase chain reaction (qRT-PCR) is an amplification method for nucleic acids that is based on the principle of the conventional polymerase chain reaction but also enables the quantification of the DNA. The measurement occurs in the form of a specific fluorescence signal, which depends on the amount of PCR product formed. The product-dependent fluorescence signal is provided by specific DNA-binding fluorescent dyes. For the qRT-PCRs in this study, SYBER-Green I was used, which is a dye that binds in the minor groove of double-stranded DNA independently of the sequence. It fluoresces proportionally. As a result, the amount of PCR products can be measured after each cycle and compared with a fluorescence threshold value at which the fluorescence signal clearly stands out from the background signal. The number of cycles that reaches this threshold value is referred to as the threshold cycle or  $C_T$  value. Hence, the more cDNA is contained, the lower the  $C_T$  value.

The reaction was performed with a SYBR Master Mix in 20 µl of final reaction volume. 2 µl of diluted cDNA (1:20) was used as a template. The reaction ran on a StepOne Plus real-time PCR system with real-time PCR primers (sequences listed in Table 30). Measurements were standardized to the GAPDH reaction using  $\Delta\Delta C_T$  methods. Therefore, the  $C_T$  values of the target gene and the reference were first subtracted from one another ( $\Delta C_T$ ). By forming the difference between the two  $\Delta C_T$  values of the individual groups (e.g., treated vs untreated)  $\Delta\Delta C_T$  can be calculated. The value obtained is inserted into the equation **n-fold expression =  $2^{-\Delta\Delta C_T}$** .

### 2.2.16 EndMT qPCR array

A human EMT Signaling Pathway PCR array was used to analyze the expression changes of genes related to EndMT in HCAECs. 5 µg of total RNA was used for first-strand cDNA

synthesis with the RT<sup>2</sup> first strand kit. The PCR array was carried out following the manufacturer's instructions using the ready-to-use RT<sup>2</sup>-qPCR master mix. 20 µl master mix was added into each well containing pre-dispensed, gene-specific primer pairs and ran on a StepOne Plus realtime PCR system. Data analysis was performed using the web-based standard RT PCR array suite.

### 2.2.17 Protein extraction

#### 2.2.17.1 Protein extraction from murine heart tissue

For protein extraction, a tissue piece of approximately 4 mm<sup>3</sup> in size was separated from the whole heart sample, transferred to a 2 ml Eppendorf tube together with 350 µl NP40 lysis buffer. It was stored for 40 minutes on ice and vortexed every 10 minutes for 10 seconds. The homogenate was then fragmented in the sonicator for a reliable sample digestion (15 seconds on alternately with 15 seconds off). After sonication for 90 seconds the lysate was centrifuged for 10 minutes at 4°C. The supernatant was pipetted into a 1.5 ml Eppendorf tube and used for immediate further experiments or stored at -80°C.

#### 2.2.17.2 Protein extraction from MCEC and HCAEC

After the end of the *in vitro* experiment, the cell lawn was washed with 3 ml PBS and removed from the base of the cell culture bottle or the 6-well-plate by gently pipetting the content with a 1 ml pipette. This was followed by centrifugation and cell lysis by adding 150 µl of cell lysis buffer over 30 minutes on ice and regularly vortexed every ten minutes. After another centrifugation at 4°C and 8000 rpm the supernatant could be removed, collected into a 1.5 ml Eppendorf tube, and used for further experiments or stored at -80°C.

### 2.2.18 Determination of the protein concentration

To determine the protein concentration in the supernatant, the Pierce BCA Protein Assay Kit was used. The principle of this method is based on a combined reaction in which Cu<sup>2+</sup> is initially reduced to Cu<sup>+</sup> in an alkaline medium in the presence of protein. The reduced copper ion forms a purple and water-soluble chelate complex with two molecules of bicinquinonic acid (BCA). This complex shows a strong absorption at 562 nm. The extinction of the color complex is proportional to the protein concentration and can be detected colorimetrically using the NanoDrop 2000 spectrophotometer. The amount of protein is determined relative to a BSA standard curve.

### 2.2.19 Western blotting

The isolated protein samples were diluted to a concentration of 25 µg and mixed with a loading buffer at a ratio of 1:1 and inactivated at 95°C for 5 minutes. As a result, both hydrogen bonds and disulfide bridges of the proteins were broken and exposed the amino acid sequences in their primary structure. Accumulation of the SDS hides the intrinsic charge

of the proteins leading to an omnipresent negative charge and thus allows an exclusive separation according to the size of the polypeptide chains. After cooling down on ice and a short spin down, the protein samples were loaded on a 4 - 12% SDS/PAGE gel and placed in the Western Blot machine filled with running buffer. The machine then ran at 80 V for 15 minutes and after that at 130 V for about two hours. As a next step, the gel was transferred onto a nitrocellulose membrane. Both, the gel and the membrane, were coated with three layers of filter soaked in transferring buffer. A semidry transfer was then performed with 150 mA for 15 minutes and 250 mA for 45 minutes. After blocking with 5% dry milk in TBST solution, the membrane was incubated with a primary antibody solution (diluted in 2% dry milk in TBST, see Table 27) at 4°C overnight. The next day, after washing for three times with 2% dry milk in TBST for 10 minutes, the membrane was incubated with a horseradish peroxidase (HRP)-coupled secondary antibody diluted in 2% dry milk in TBST for one hour at room temperature and finally washed three times with 2% dry milk in TBST for 10 minutes each. The detection of protein was carried out by using 20x LumiGLO reagent and 20x peroxidase in a ratio of 1:1. HRP catalyzes the reaction of luminol (LumiGlo) with peroxidase ( $H_2O_2$ ) to form an excited intermediate dianion, 3-aminophthalate. It emits light (chemiluminescence) while it returns to its basic energetic state. This chemiluminescence is quantified in the ChemiDoc system and Image Lab software and is proportional to the amount of protein on the membrane. The densitometric evaluation of the Western blot images was carried out with the ImageJ program. To normalize the membrane, it was restained with antibodies against the housekeeping protein GAPDH. The membrane was incubated for 60 minutes at room temperature with the stripping buffer from Thermo Scientific on the roller. After washing the membrane for three times in TBST for 5 minutes, it was blocked in 5% BSA for one hour at room temperature and incubated with the primary antibody against GAPDH in 2% BSA overnight at 4°C. The next day, after washing three times, the membrane was incubated with the HRP-conjugated secondary antibody in 5% BSA for one hour at room temperature. After washing three times in TBST for 5 minutes each, the amount of GAPDH was detected again using the ChemiDoc system.

### 2.2.20 Chromatin immunoprecipitation (ChIP)

The aim of chromatin immunoprecipitation (ChIP) is to determine whether some proteins bind parts of the chromatin of living cells or tissues. The method works with regard to crosslinking *in vivo*. After the cells have been lysed, the lysate is loaded onto so-called beads, on which the precipitation occurs. This process takes place *in vitro*. The general principle of chromatin immunoprecipitation is based on holding the protein-DNA bonds that exist at a given point in time by fixing them with formaldehyde. The cells are then destroyed, and the chromatin is shattered into pieces, i.e. several hundred base pairs in length using ultrasound. Those pieces of DNA that have bound the desired protein are immunoprecipitated (isolated) with an antibody specific to the protein. The isolated DNA-protein complexes are dissolved. The identity of the respective pieces of DNA can be obtained by qRT-PCR using primers

that are specific to the suspected DNA region. Chromatin immunoprecipitation for histone modifications in MCECs was performed as previously described (Nagarajan et al. 2015) and involved five main steps:

#### Cross linking and cell harvest:

Before performing ChIP, cells had been plated and treated on 10 cm plates. Firstly, the media was removed, 8 ml of 1% formaldehyde (in PBS) was added and it was incubated for ten minutes at room temperature. As a next step, formaldehyde was quenched by adding 980  $\mu$ l 1.25 M Glycine and incubated for five minutes on a low-speed shaker at room temperature. Cells were washed two times with ice-cold PBS. After removal of PBS and addition of 1 ml cold Nuclear Preparation Buffer the cells were scraped and pipetted up and down several times. The cell lysate was centrifuged at 12,000 g for two minutes at 4°C and the supernatant was discarded. Subsequently, the remaining nuclear pellet was washed with 1 ml Nuclear Preparation Buffer, spun down at 12,000 g for two minutes at 4°C and the supernatant was finally removed.

#### Sonication:

The pellet was completely resuspended in 150  $\mu$ l cold freshly prepared Sonication buffer-1 and incubated at 4°C on a rotating wheel for 15 minutes. As a next step, 150  $\mu$ l cold Sonication buffer-2 was added and briefly spun. The sample was sonicated in 30 cycles with 30 seconds on/off duty time at high power. Finally, the supernatant was taken after centrifugation at 12,000 g for ten minutes at 8°C.

#### Preclearing:

The supernatant was then diluted by adding 600  $\mu$ l of Dilution buffer. As a next step, Sepharose was prepared by washing swollen Sepharose in EtOH three times with the Dilution buffer and centrifuging it at 1,000 g for two minutes. 100  $\mu$ l of Sepharose 50% slurry in Dilution buffer was supplemented with cut off tips and incubated for one hour at 4°C on a rotating wheel. Afterwards, the sample was centrifuged at 12,000 g for two minutes at 4°C and the supernatant was collected. Multiple chromatin samples of 100  $\mu$ l and 10  $\mu$ l of 10% input were aliquoted and snap-frozen in liquid nitrogen.

#### Immunoprecipitation:

After thawing the aliquots on ice, 400  $\mu$ l of IP buffer as well as 1-2  $\mu$ g antibody was added, and everything was incubated overnight on a rotating wheel at 4°C. The same day Protein-G sepharose beads were blocked overnight by adding BSA. The next day 30  $\mu$ l of well mixed Protein-G sepharose was added to the sample with cut off tips and incubated for one to two hours on a rotating wheel at 4°C. Afterwards, it was centrifuged at 2,000 g for two minutes at 4°C. ChIP immune complexes were washed twice with 1 ml ice cold IP buffer supplied with protease inhibitors A/L, NEM and BGP by centrifuging at 2,000 g at 4°C and supernatant was removed. Subsequently, the washing steps were repeated three times with



1 ml ice cold IP buffer and twice with ice cold TE buffer. After the last washing step, the complete supernatant was removed, and the sample was kept on ice.

#### DNA isolation by phenol-chloroform extraction

50  $\mu$ l of Tris 10 mM pH 8 containing RNase A 0.2  $\mu$ g/ $\mu$ l was added to both the samples and input. The mixture was incubated for 30 minutes at 37°C. Then, 50  $\mu$ l of Sonication buffer-1 and 1  $\mu$ l Proteinase-K were added and incubated overnight at 65°C with 800 rpm. The supernatant was kept after centrifugation at 2,000 g for two minutes at room temperature. 100  $\mu$ l of 10 mM Tris pH 8 was supplied on the beads, vortexed ten seconds and then incubated for ten minutes at 65°C with 800 rpm. Afterwards, the sample was centrifuged again at 5,000 g for two minutes at room temperature and the supernatant was added to the supernatant that was kept from the previous step. After adding 10  $\mu$ l 8 M LiCl, 4  $\mu$ l linear polyacrylamide and 200  $\mu$ l phenol/ chloroform/ isoamyl alcohol (25:24:1), the sample was vortexed for 30 seconds and centrifuged at full speed for ten minutes. Next, the aqueous phase was collected in a fresh low binding Eppendorf tube. The organic phase was extracted back by adding 200  $\mu$ l of 10 mM Tris pH 8 and 0.4 M LiCl, vortexed for 30 seconds and finally centrifuged for 5 minutes at full speed. The remaining aqueous phase was added to the previously collected aqueous phase. By adding 1 ml 70% Ethanol and after an incubation period of two hours at -80°C, the DNA was precipitated. After melting, the sample was centrifuged at with 15,000 g for 30 minutes at 4°C and rinsed with 1 ml 70% Ethanol. After centrifugation under the same conditions for five minutes all the ethanol was removed. Then the samples were dried at room temperature for 30 minutes and the DNA was resuspended in 40  $\mu$ l of nuclease free water. After measuring DNA concentration, a qRT-PCR was performed with the respective primers (Table 29) to quantify histone alterations.

#### **2.2.21 Statistical analysis**

Means were calculated and plotted along with standard error bars. All statistical analyses were done using GraphPad Prism software version 6.0 (GraphPad). All data were first analyzed by Student's t-test for single comparison. One-way ANOVA with Bonferroni post-hoc analysis was used for comparing multiple groups. Significant differences between means are considered statistically significant when the p-value is smaller than 0.05. A p <0.05 was marked with \*, p <0.01 with \*\*, p <0.001 with \*\*\* and p <0.0001 with \*\*\*\* in the individual graphs. Three or more biological replicates were included for all experiments. Overall survival was analyzed by using the Kaplan-Meier survival method with a log rank test to determine statistical differences.

## 3 Results

### 3.1 The impact of Serelaxin in pressure overload mouse models

Since the section 1.4.3 described preclinical studies and the clinical trials suggested a possible anti-fibrotic effect of Serelaxin, this project aimed to systematically investigate the impact of Serelaxin on cardiac fibrosis and further elucidate molecular mechanisms that Serelaxin may affect. For this purpose, the effect of Serelaxin was tested in two established, independent cardiac fibrosis mouse models, ascending aortic constriction and ATII treatment. Various parameters were obtained both during their lifetime and *postmortem*.

#### 3.1.1 Cardiac fibrosis and survival in AAC mouse model

Firstly, pressure overload was induced in twelve weeks old C57BL/6N mice of both sexes by ascending aortic constriction (AAC). In this model, either Serelaxin at three different dosages (50, 200 and 500  $\mu\text{g}/\text{kg}$  bodyweight) or a vehicle was administered via an osmotic minipump. Echocardiography was performed to verify constriction and to evaluate the cardiac performance. The mice were then sacrificed after four weeks, and their hearts were harvested and analyzed (**Figure 8**).

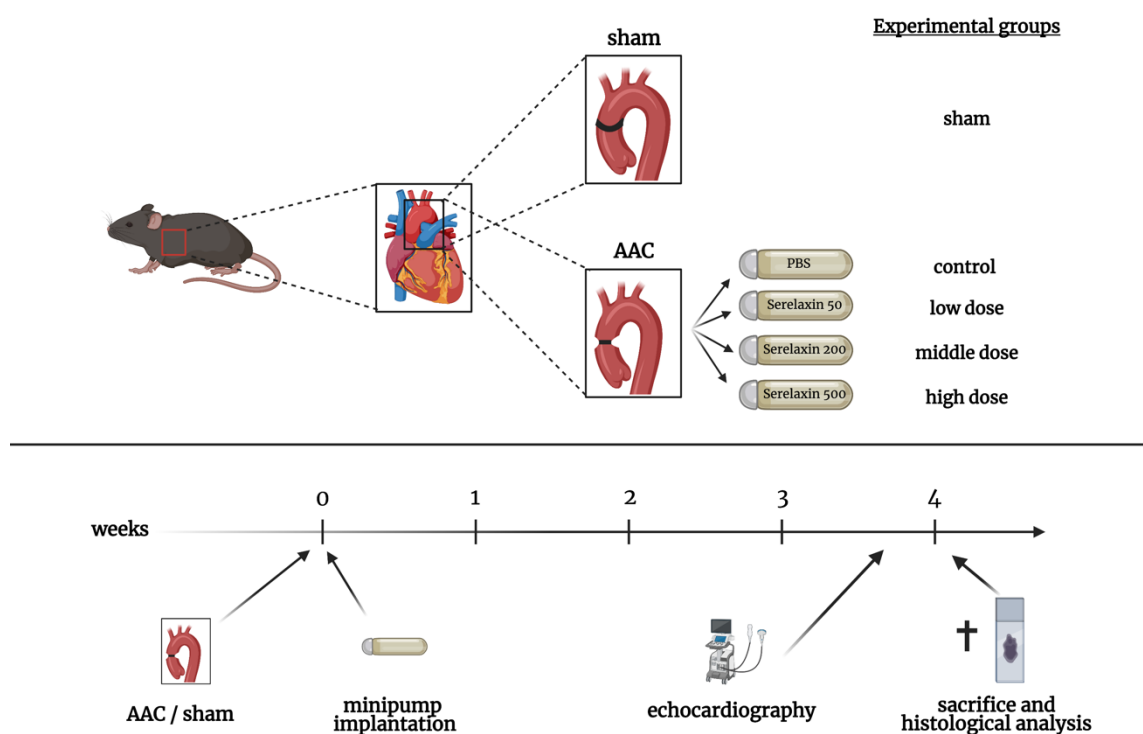


**Figure 8: Experimental design of an AAC mouse model** Schematic of AAC surgery, consecutive Serelaxin minipump implantation and experimental timeline.

The fibrotic area of the left ventricle was assessed by the quantification of Masson Trichrome staining. AAC constantly induced left ventricular fibrosis compared to the sham operation. The quantification revealed a dose-dependent anti-fibrotic effect of Serelaxin on the diseased heart. Overall fibrosis was reduced by approximately 30% in both low (50  $\mu\text{g}/\text{kg}$  bodyweight) and middle dose (200  $\mu\text{g}/\text{kg}$  bodyweight) Serelaxin groups compared to the vehicle group. A significant overall fibrosis reduction (by 50%) was exclusively observed in the high dose Serelaxin group (Figure 9A-B).

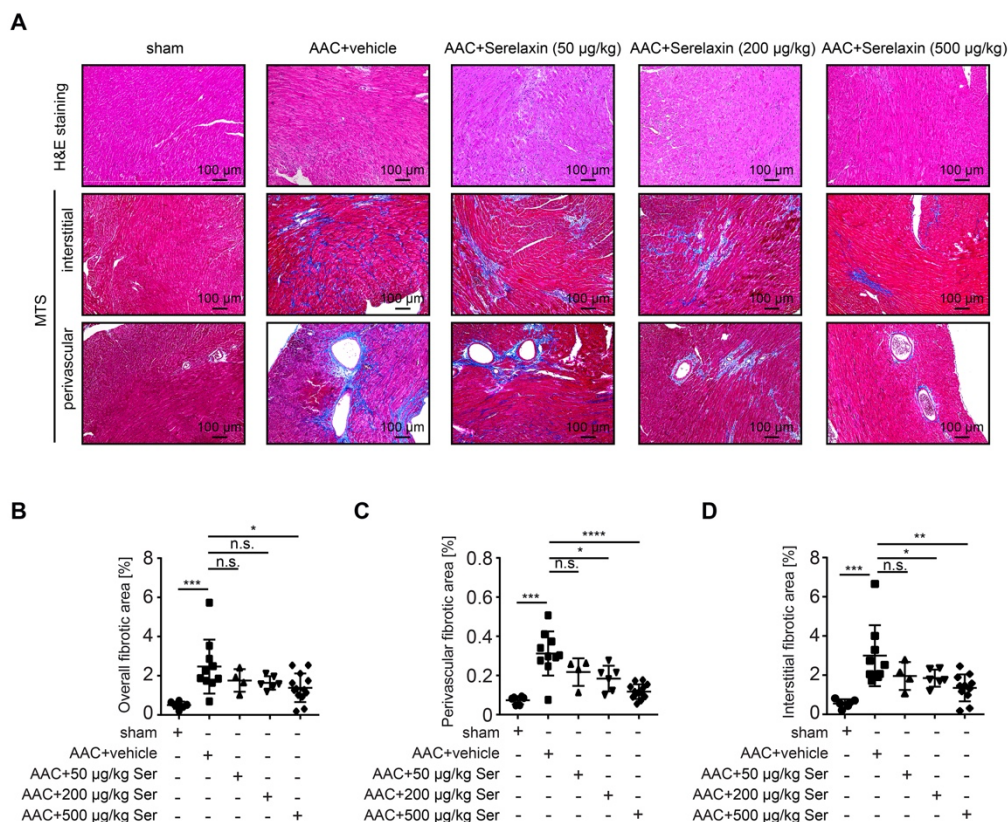


**Figure 9: Serelaxin ameliorates cardiac fibrosis in AAC mouse model** (A) HE and Masson's Trichrome Staining microphotography of sham and AAC-operated mouse heart depicting reduced interstitial and perivascular fibrosis in Serelaxin-treated (500  $\mu\text{g}/\text{kg}/\text{day}$ ) hearts compared to sham and vehicle-treated hearts. (B-D) Dot plots representing the percentage of overall, interstitial and perivascular fibrotic area in the sham ( $n = 6$ ), vehicle-treated ( $n = 10$ ) and low ( $n = 4$ ), middle ( $n = 6$ ) and high dose ( $n = 13$ ) Serelaxin-treated AAC mouse hearts, demonstrating a significant reduction of fibrosis in Serelaxin-treated hearts. Student's t-test was used for single comparison and one-way ANOVA with Bonferroni post-hoc analysis was used for multiple group comparisons. Error bars represent mean  $\pm$  SEM, n.s. no significance, \*  $p < 0.05$ , \*\*  $p < 0.01$ , \*\*\*  $p < 0.001$ , \*\*\*\*  $p < 0.0001$ . Adapted from Wilhelmi et al. 2020.

Further, a detailed sub-analysis for the distribution of cardiac fibrosis was performed. For this purpose, a distinction was made between perivascular fibrosis and interstitial fibrosis. For this study, perivascular fibrosis was defined as all fibrotic lesions surrounding vessels of more than 100  $\mu\text{m}$  in diameter. All other fibrotic lesions in the murine heart represented interstitial fibrosis. Low dose Serelaxin treatment failed to inhibit the development of fibrosis in either of these subgroups. Both, middle and high dose Serelaxin application reduced

perivascular as well as interstitial fibrosis in AAC-operated mice. The anti-fibrotic impact of Serelaxin was relatively higher for perivascular as compared to interstitial fibrosis (**Figure 9A, C-D**).

The attenuation of cardiac fibrosis was associated with a significantly reduced mortality in animals treated with high dose Serelaxin as compared to vehicle mice. Low and middle dose treatment failed to significantly affect survival of the mice (**Figure 10A**). A following sub analysis of both sexes revealed that the reduction of overall fibrosis as well as survival benefit upon high dose Serelaxin treatment was equally apparent in both sexes (**Figure 10B**).

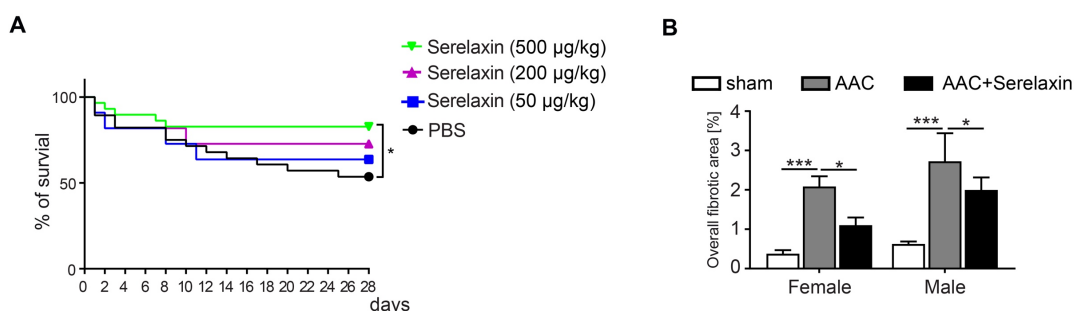


**Figure 10: Serelaxin ameliorates cardiac fibrosis** (A) Survival rates of mice from the date of AAC surgery until day 28 in vehicle-treated (n = 28), low (n = 13), middle (n = 13) and high dose Serelaxin-treated (n = 29) groups visualized by a Kaplan-Meier survival curve. Administration of high dose Serelaxin significantly increased survival. (B) Bar graphs showing the distribution of overall fibrosis within sexes in sham, AAC-operated and high dose Serelaxin-treated animals. Overall survival was analyzed by using a Kaplan-Meier survival method with a log rank test to determine statistical differences. Student's t-test was used for single comparison and one-way ANOVA with Bonferroni post-hoc analysis was used for multiple group comparisons. Error bars represent mean  $\pm$  SEM, n.s. no significance, \*  $p < 0.05$ , \*\*\*  $p < 0.001$ . Adapted from Wilhelmi et al. 2020.

**Table 33: AAC survival differences between both sexes.** Comparison between the two sexes did not reveal any significant survival differences in sham, AAC + vehicle or AAC + Serelaxin group. Student's t-test was used for single comparison.

	sham		AAC + vehicle		AAC + Serelaxin	
	Female	Male	Female	Male	Female	Male
Day 0	3	3	14	14	15	14
Day 28	3	3	8	7	12	11
Survival (%)	100	100	57.14	50	80	78.57
Significance	n.s. ( $p = 1$ )		n.s. ( $p = 0.82$ )		n.s. ( $p = 0.8$ )	

### 3.1.2 Cardiac phenotype and heart's performance in AAC mouse model

Analyzing the heart mass in relation to both body weight and tibia length revealed an increased heart weight in AAC-operated mice compared to sham mice. Treatment with high dose Serelaxin significantly limited the increase of heart weight (**Figure 11B-C**). Histological cross-sections of AAC-operated hearts showed an enlarged phenotype compared to sham operated animals suggesting a dilated left ventricle (**Figure 11A**). This was in line with the echocardiography parameters such as increased systolic and diastolic left ventricular internal

diameter (LVIDs and LVIDd), decreased systolic and diastolic volumes (Vols and Vold) and posterior wall thickness (PWTs and PWTd). These parameters significantly changed in AAC-operated compared to sham-operated animals. However, high dose Serelaxin administration did not significantly reverse the heart's performance (**Figure 11F-K**). Ejection fraction and fractional shortening were reduced in AAC-operated compared to sham-operated mice. Serelaxin failed to significantly counteract these heart performance parameters (**Figure 11D-E**).

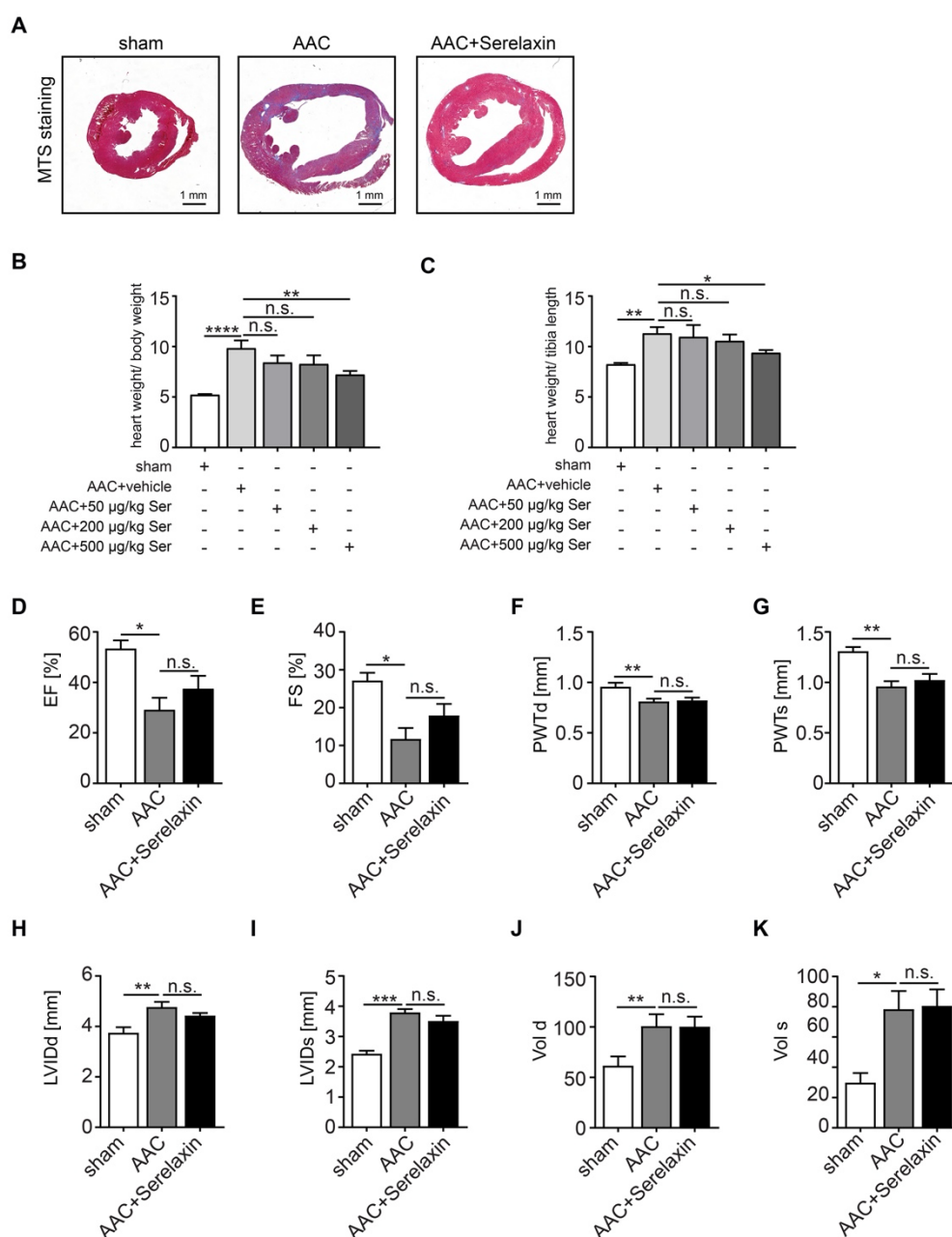


**Figure 11: AAC-operated mouse hearts showed an enlarged phenotype** (A) Images of Masson's trichrome stained sham, AAC-operated and AAC-operated + Serelaxin-treated mouse hearts. An enlarged phenotype and an increased area of fibrosis was demonstrated in AAC-treated hearts as compared to sham. The area of fibrosis was reduced, but the enlarged phenotype was not reversed by Serelaxin. (B-C) Bar graphs visualizing heart weight in relation to either bodyweight or tibia length. AAC-operation increased the mice heart weight while

Serelaxin treatment reduced it compared to vehicle treatment. (D-K) Echocardiographic parameters at 28 days after AAC operation are presented as bar graphs. EF, FS, PWTd and PWTs were significantly reduced upon AAC surgery and were not significantly reversed by administration of high dose Serelaxin. LVIDd, LVIDs, Vol d and Vol s were significantly increased upon AAC surgery but were not significantly reduced by application of high dose Serelaxin. EF: ejection fraction; FS: fractional shortening; PWTd: diastolic posterior wall thickness, PWTs: systolic posterior wall thickness; LVIDd: diastolic left ventricular inner diameter; LVIDs: systolic left ventricular inner diameter; Vol d: diastolic left ventricular volume; Vol s: systolic left ventricular volume. Student's t-test was used for single comparison and one-way ANOVA with Bonferroni post-hoc analysis was used for multiple group comparisons. Error bars represent mean  $\pm$  SEM, n.s. no significance, \*  $p < 0.05$ , \*\*  $p < 0.01$ , \*\*\*  $p < 0.001$ , \*\*\*\*  $p < 0.0001$ . Adapted from Wilhelmi et al. 2020.

### 3.1.3 Fibrosis in Angiotensin-2 mouse model

Alongside AAC animals, Serelaxin was tested in an additional, independent mouse model. Cardiac fibrosis was induced by ATII that was applied by osmotic minipumps and analyzed at two different time points. Blood pressure was measured to confirm the ATII-mediated increase of total peripheral resistance by a tail cuff method one week before the implantation of the minipump and shortly before the end of the experiment. After application of 1.5 mg/kg/day ATII and administration of either vehicle or high dose Serelaxin, the mice were sacrificed after two or four weeks and left ventricular fibrosis was quantified (**Figure 12**).

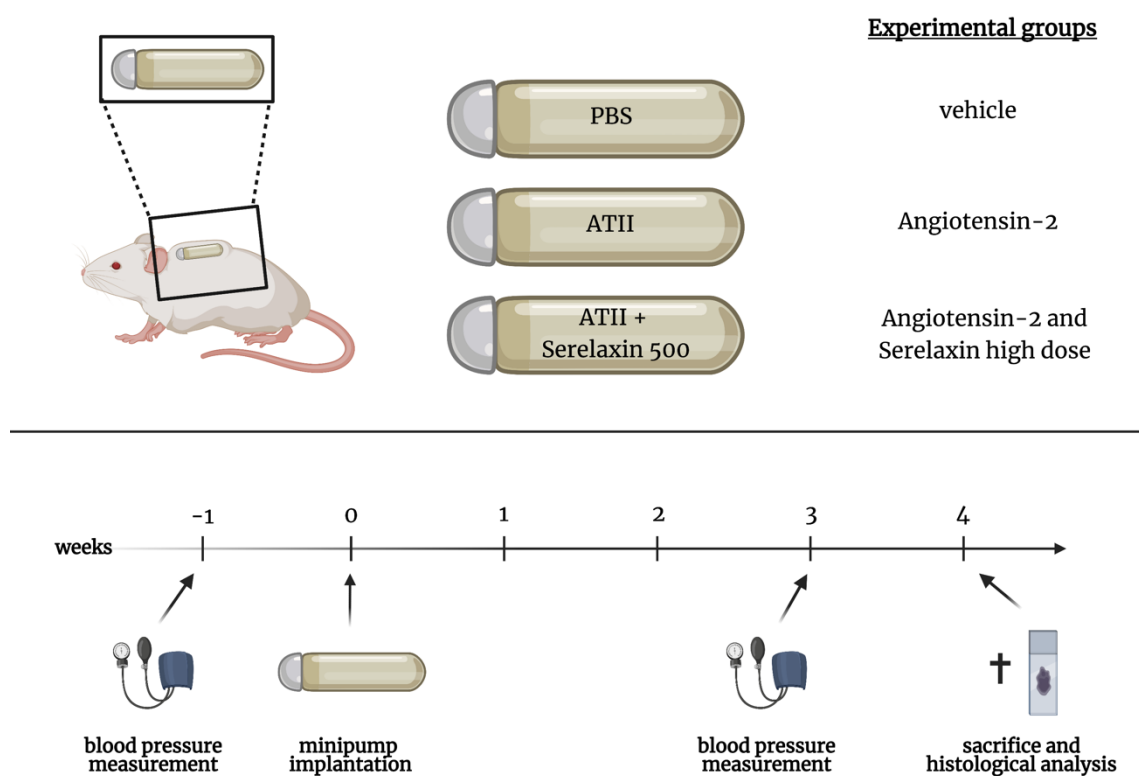


**Figure 12: Experimental design of ATII mouse model** Schematic of ATII surgery, consecutive Serelaxin minipump implantation and experimental timeline.

In mice treated with ATII for four weeks, perivascular and interstitial lesions were distinguished and separately quantified. Both were attenuated by Serelaxin, but the effect was



relatively higher on perivascular than on interstitial fibrosis (**Figure 13A,C**). Upon two weeks of ATII treatment the mice developed cardiac fibrosis, while after four weeks the amount of fibrosis was even more pronounced. Administration of Serelaxin significantly ameliorated overall left ventricular fibrosis in ATII hearts as compared to vehicle animals (**Figure 13B,C**).

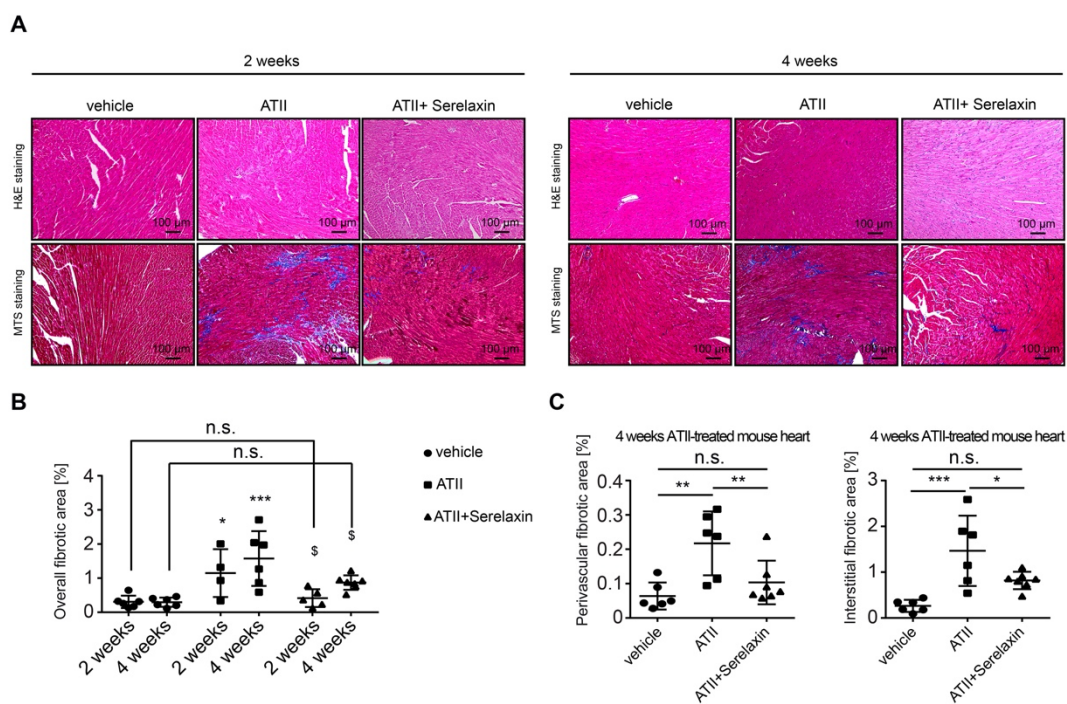


**Figure 13: Serelaxin ameliorates cardiac fibrosis in ATII mouse model** (A) HE and Masson's Trichrome Staining microphotography of sham and ATII-treated mouse heart depicting reduced fibrosis in Serelaxin-treated (500  $\mu\text{g}/\text{kg}/\text{day}$ ) hearts compared to ATII-treated and ATII + vehicle-treated hearts. (B) Dot plots representing the percentage of overall fibrotic area in the control (vehicle), ATII-treated and ATII + Serelaxin-treated mouse hearts after 2 weeks and 4 weeks. (C) Percentage of interstitial and perivascular fibrotic area in vehicle, ATII and ATII + Serelaxin-treated mouse hearts after 4 weeks shown as bar graphs. There is a significant reduction of interstitial and perivascular fibrosis in ATII and Serelaxin-treated (500  $\mu\text{g}/\text{kg}/\text{day}$ ) hearts compared to hearts treated with ATII alone. Student's t-test was used for single comparison and one-way ANOVA with Bonferroni post-hoc analysis was used for multiple group comparisons. Error bars represent mean  $\pm$  SEM, n.s. no significance, \*  $p < 0.05$ , \*\*  $p < 0.01$ , \*\*\*  $p < 0.001$ . Adapted from Wilhelmi et al. 2020.

## 3.2 Analysis of EndMT upon Serelaxin treatment

### 3.2.1 EndMT in two independent mouse models

Serelaxin has an anti-fibrotic effect which is particularly pronounced for the development of perivascular fibrosis. Since it is known that the hormonal effects of Relaxin primarily affect vascular cells, the next step was to address the influence of Serelaxin on EndMT and the preservation of endothelial cell properties (Jeyabalan et al. 2007). For this purpose, an immunofluorescence assay was performed that labelled the endothelial cell marker CD31 in combination with the mesenchymal markers  $\alpha$ -SMA and  $\alpha$ -1 type I collagen (Col1 $\alpha$ (I)), a component of type I collagen (**Figure 14A,C**). CD31-positive areas decreased and  $\alpha$ -SMA as well as Col1 $\alpha$ (I)-positive area increased in AAC-challenged hearts compared to sham. We then examined how many CD31-positive cells additionally showed a positive signal for  $\alpha$ -SMA ( $\frac{CD31^+ + \alpha-SMA^+}{CD31^+}$ ). The double-positive proportion increased from 2% to 12% in AAC-operated hearts compared to sham animals and indicated the presence of EndMT. This result is in line with previous studies (Zeisberg et al. 2007b; Xu et al. 2015a). In Serelaxin-treated mice the effects on CD31-,  $\alpha$ -SMA- and Col1 $\alpha$ (I)-positive areas were reversed, and the double-positive proportion was reduced from 12% to 7% as compared to vehicle-treated and AAC-operated mice, suggesting an EndMT-inhibiting effect of Serelaxin (**Figure 14B,D**).

Furthermore, we examined the mRNA expression level of CD31 as well as EndMT transcription factors Snail, Slug, and Twist in the hearts of the mice that underwent sham or AAC surgery and received either vehicle or Serelaxin. Once again, a suppressed expression of CD31 (by approximately 50%) in AAC-treated mice was determined compared to sham animals. The suppression was attenuated by administration of Serelaxin. Furthermore, the expression of EndMT transcription factors showed a significant increase in AAC-operated animals compared to sham mice, that could be partially blocked (by up to 50%) upon treatment with Serelaxin. Overall, these results suggest that Serelaxin is able to induce an inhibition of EndMT in AAC-challenged mice (**Figure 14E**). To test if these effects could be reproduced in the second, independent mouse model of cardiac fibrosis, the expression of CD31, Snail, Slug, and Twist was analyzed in ATII-treated animals. CD31 expression decreased, and expression of Snail, Slug, and Twist decreased upon ATII application but was partially blocked in Serelaxin-administered mice as compared to vehicle-treated mice (**Figure 14F**).

The observed loss of microvasculature is likely caused by EndMT. In order to rule out that apoptosis could play a decisive role in the loss of CD31-positive cells, an immunohistochemical staining of the cleaved Caspase 3 was carried out. Cleaved Caspase 3 is a critical executor of apoptosis. Antibodies directed against cleaved Caspase 3 are widely utilized in molecular biological and medical research as a marker for apoptotic cells (Porter and Jänicke 1999). The analysis of hearts stained with this antibody showed a 3.6 times higher



level of cleaved Caspase 3 in AAC-operated hearts compared to sham-operated. Administration of Serelaxin did not affect the level of Caspase 3.

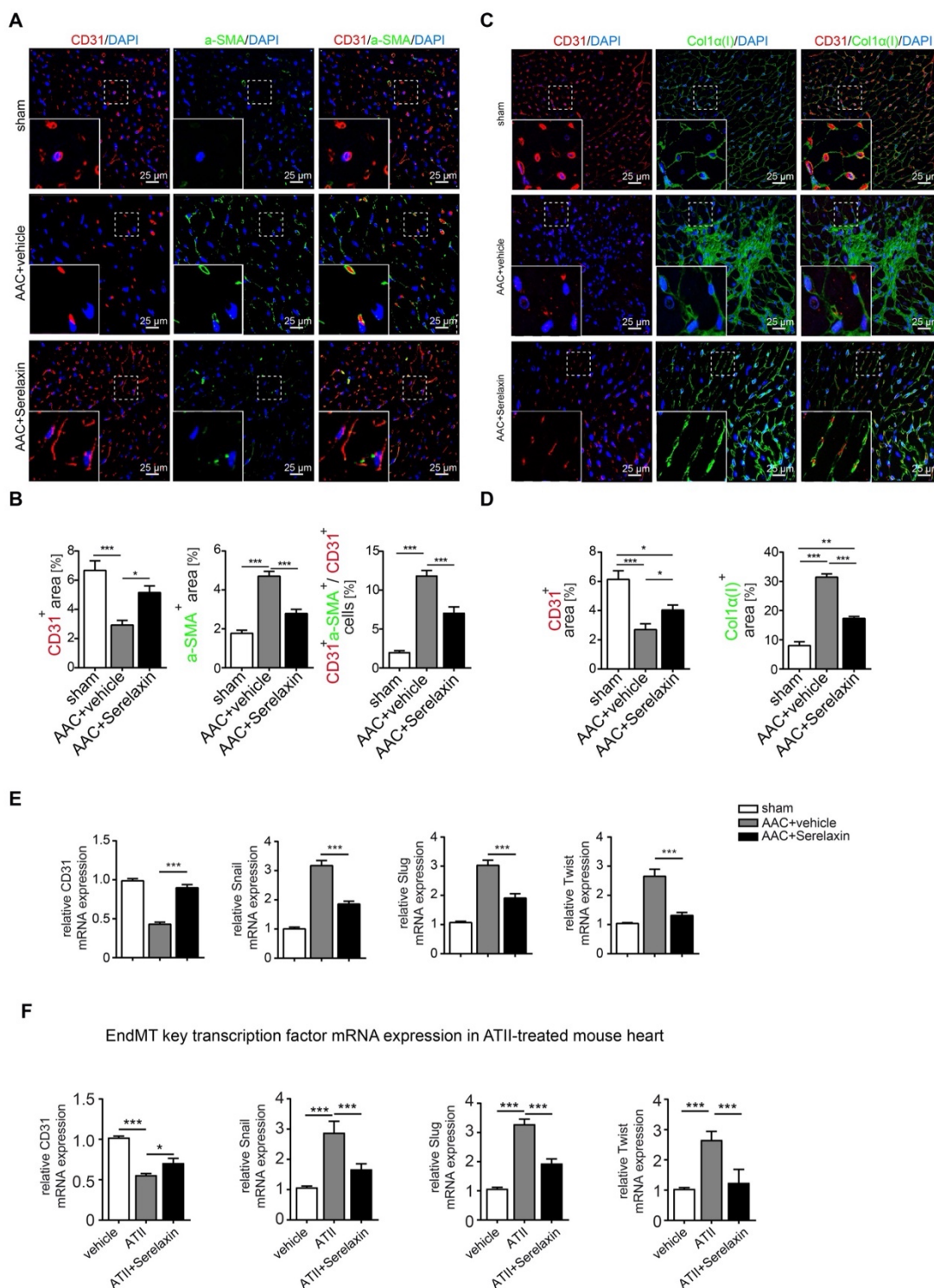


**Figure 14: Serelaxin attenuates EndMT in two different mouse models of cardiac fibrogenesis (A)** Immunofluorescence staining of endothelial cell marker CD31, mesenchymal marker  $\alpha$ -SMA and DAPI. (B) Bar graphs visualizing quantifications of CD31 and  $\alpha$ -SMA positive area as well as the ratio of CD31 positive and  $\alpha$ -SMA positive cells / CD31 positive cells. Compared to sham, Vehicle-treated hearts showed an increased expression of  $\alpha$ -SMA but a decreased protein expression of CD31 compared to sham hearts. Serelaxin treatment led to reduced  $\alpha$ -SMA and restored CD31 protein expression. In AAC-operated animals, double

positive cells significantly increased and were reduced by Serelaxin administration. (C) Immunofluorescence staining of endothelial cell marker CD31, fibrotic marker alpha-1 type I collagen (Col1 $\alpha$ (I)) and DAPI. (D) Bar graphs visualizing quantifications of CD31 and Col1 $\alpha$ (I) positive area. Col1 $\alpha$ (I) expression was upregulated in AAC hearts and inhibited by Serelaxin. Compared to sham, vehicle-treated hearts showed a decreased protein expression of CD31. Treatment with Serelaxin restored CD31 expression. (E) qPCR analysis showing the relative mRNA expression level of *CD31* and EndMT key regulators Snail, Slug, and Twist in AAC hearts treated with vehicle or Serelaxin. Vehicle-treated AAC-operated hearts showed an increased expression of Snail, Slug, and Twist but a decreased expression of *CD31*, while Serelaxin treatment reduced Snail, Slug, and Twist expression and restored *CD31* expression. (F) qPCR analysis showing the relative mRNA expression level of *CD31* and EndMT key regulators Snail, Slug, and Twist in vehicle, ATII and ATII + Serelaxin-treated mouse hearts. ATII-treated hearts showed an increased expression of Snail, Slug, and Twist but a decreased expression of *CD31* compared to vehicle-treated hearts, while ATII in combination with Serelaxin treatment reduced Snail, Slug, and Twist. Student's t-test was used for single comparison and one-way ANOVA with Bonferroni post-hoc analysis was used for multiple group comparisons. Gene expression and associated error bars represent mean  $\pm$  SEM,  $n \geq 3$ , n.s. no significance, \*  $p < 0.05$ , \*\*  $p < 0.01$ , \*\*\*  $p < 0.001$ . Adapted from Wilhelmi et al. 2020.

Together with the findings of Park et al. (2009) who showed that in the setting of HF, endothelial cells contribute to less than 19% of all apoptotic cells of the heart, our observations confirm the hypothesis that Serelaxin partially inhibits EndMT; independent of apoptosis (**Figure 15**).

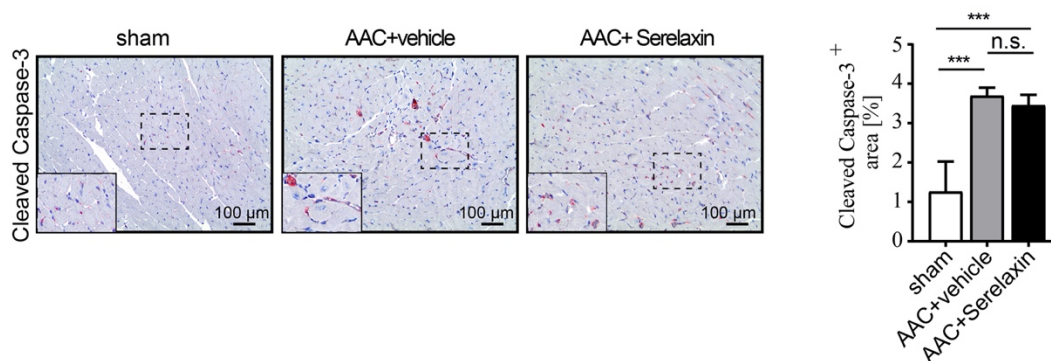


**Figure 15: Serelaxin does not affect apoptosis in AAC-operated mouse hearts** Immunohistochemistry staining of cleaved Caspase 3 and bar graphs visualizing quantifications. Both showed an increased level of cleaved Caspase 3 in AAC-operated hearts compared to sham operated hearts. Serelaxin could not significantly reduce cleaved Caspase 3 levels. Student's t-test was used for single comparison and one-way ANOVA with Bonferroni post-hoc analysis was used for multiple group comparisons. Error bars represent mean  $\pm$  SEM,  $n \geq 3$ , n.s. no significance, \*\*\*  $p < 0.001$ . Adapted from Wilhelmi et al. 2020.

### 3.2.2 TGF $\beta$ 1-induced EndMT *in vitro*

The next step was to gain mechanistic insights into the inhibition of EndMT induced by Serelaxin utilizing *in vitro* assays in both human and mouse endothelial cells. Firstly, EndMT was induced in HCAECs by TGF $\beta$ 1 (10 ng/ml) and subsequently Serelaxin was applied in four different concentrations (20, 50, 100 and 200 ng/ml). After two and four days, the mRNA expression level of endothelial cell marker CD31 and EndMT transcriptional factors SNAIL, SLUG, and TWIST were analyzed. Upon treatment with TGF $\beta$ 1, the expression of

CD31 was halved and that of the transcription factors tripled. Serelaxin was able to partially block these effects in a concentration of 200 ng/ml after two days (**Figure 16A**) and 100 ng/ml after four days (**Figure 16B**), indicating a dose- and time-dependent inhibition of EndMT. Considering the aim of obtaining insights into the observed anti-fibrotic effect in the mouse model, analog experiments were carried out in MCECs. Similar to the observations in HCAECs, the application of 100 ng/ml Serelaxin led to an inhibition of TGF $\beta$ 1-induced EndMT in MCECs as shown by mRNA expression level alterations of *CD31* and EndMT transcriptional factors Snail, Slug, and Twist. (**Figure 16C**).

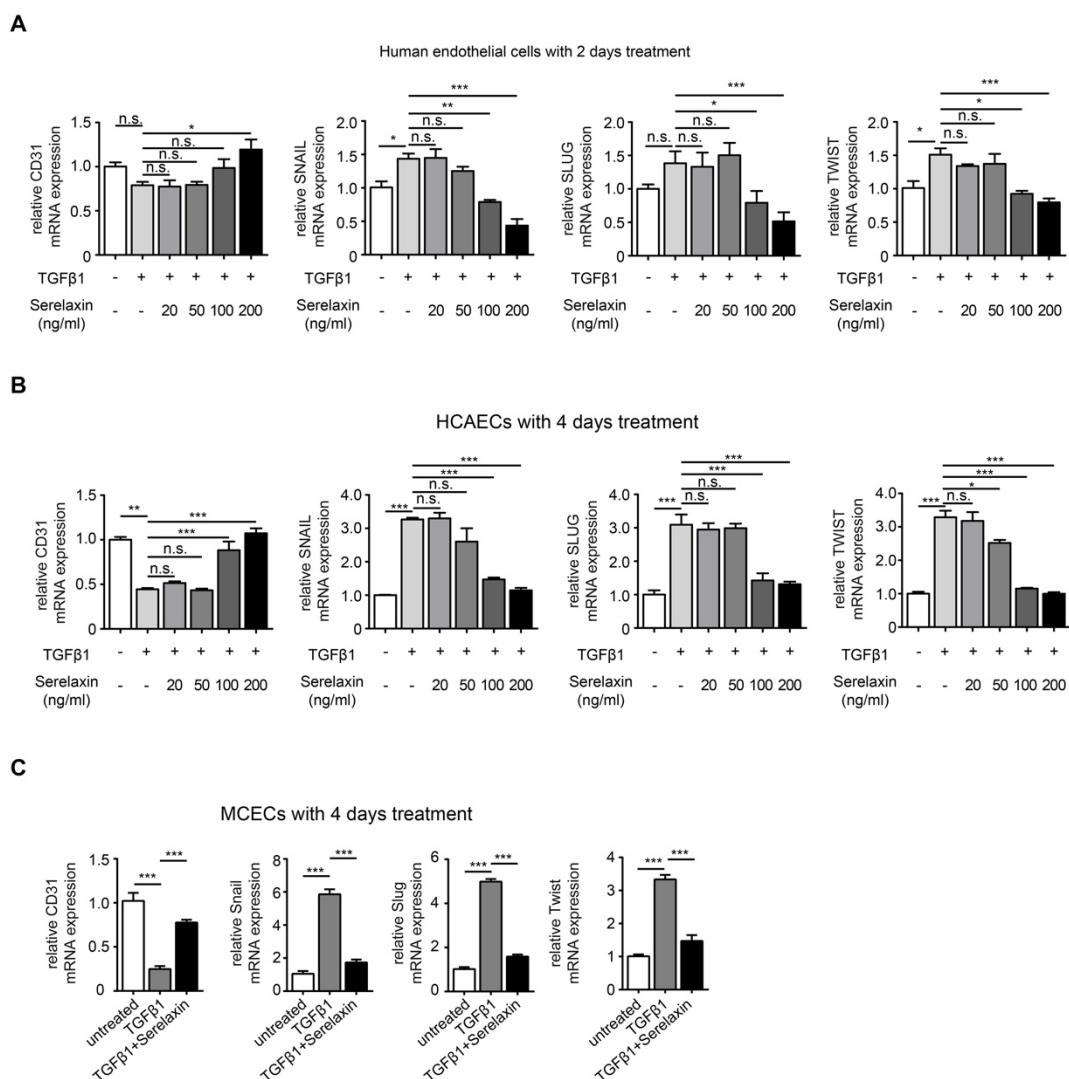


**Figure 16: Serelaxin partially inhibits TGF $\beta$ 1-induced EndMT in HCAECs and MCECs** (A) qPCR analysis showing the expression of endothelial cells marker *CD31* and expression of EndMT key regulators SNAIL, SLUG, and TWIST in TGF $\beta$ 1-treated HCAECs supplemented with different doses of Serelaxin after 4 days. Cells without any treatment were used as control. Serelaxin treatment significantly rescued expression of CD31 (100 and 200 ng/ml) and decreased expression of SNAIL, SLUG, and TWIST (100 and 200 ng/ml). (B) qPCR analysis showing the mRNA expression of EndMT transcriptional factors Snail, Slug, and Twist and of endothelial cell marker CD31 in TGF $\beta$ 1-treated MCECs. Upon TGF $\beta$ 1 treatment Snail, Slug, and Twist expression increased and *CD31* expression decreased. Treatment of Serelaxin showed a reduced expression of Snail, Slug, and Twist and a restored expression of CD31. (C) qPCR analysis showing the expression of EndMT key regulators Snail, Slug, and Twist in TGF $\beta$ 1 and Serelaxin-treated MCECs upon Rxfp1 knockdown. Cells

without any treatment were used as control. Serelaxin treatment showed a reversal effect on TGF $\beta$ 1-induced EndMT but not upon Rxfp1 knockdown. Student's t-test was used for single comparison and one-way ANOVA with Bonferroni post-hoc analysis was used for multiple group comparisons. Gene expression and associated error bars represent mean  $\pm$  SEM, n  $\geq$  3, n.s. no significance, \* p < 0.05, \*\* p < 0.01, \*\*\* p < 0.001. Adapted from Wilhelmi et al. 2020.

### 3.3 Role of RXFPs in Serelaxin-induced inhibitory effect on EndMT

#### 3.3.1 RXFPs in HCAECs

To understand how Serelaxin unfolds its effects, it was necessary to identify the receptor that mediates the inhibition of TGF $\beta$ 1-induced EndMT. Therefore, the mRNA expression level of each Relaxin family peptide receptor (RXFP 1-4) was analyzed by quantitative real-time PCR in HCAECs. Only RXFP1 and RXFP4 were detected to be expressed in these cells (**Figure 17A**). To confirm which receptor plays a crucial role in inhibiting EndMT, a knockdown assay of RXFP1 and RXFP4 was performed. HCAECs were transfected with small hairpin RNA (shRNA) mediating a knockdown of RXFP1 and RXFP4. An shRNA is an RNA molecule that forms a hairpin structure and can be used to artificially silence target genes with the help of RNA interference. In this case, the shRNA knockdown of RXFP1 and RXFP4 led to a transfection efficiency up to 40% causing a successfully decreased mRNA and protein expression of both receptors by approximately 80% (**Figure 17B-C**). HCAECs transfected with shRNA of either RXFP1 or RXFP4 were treated with TGF $\beta$ 1 to induce EndMT and subsequently administered by Serelaxin. After four days, the mRNA expressions of SNAIL, SLUG, and TWIST were analyzed. By knocking down RXFP4, the application of Serelaxin rescued TGF $\beta$ 1-induced upregulation of SNAIL, SLUG, and TWIST. However, the knockdown of RXFP1 abolished Serelaxin's impact on the expression of the EndMT transcriptional factors (**Figure 17D**). These results suggest that RXFP1 mediates the inhibitory effect of Serelaxin on EndMT.

#### 3.3.2 RXFPs in MCECs

To understand whether the observed anti-fibrotic effects of Serelaxin in AAC-treated mice are also mediated by RXFP1, a receptor screening analysis in MCECs (an analogous to the HCAECs) was performed. Quantitative real time PCR only detected *Rxfp1* to be expressed in MCECs (**Figure 18A**). Therefore, a silencing of *Rxfp1* by small interfering RNA was performed. Small interfering RNA (siRNA) are short ribonucleic acid components that do not encode proteins but rather bind to complementary single-stranded ribonucleic acid such as mRNA, thereby preventing their normal function and thus suppressing the expression of genes. Three different oligos were included into this experiment and they were either transfected individually or combined as a triple. Scrambled siRNA was used as a negative control to exclude unspecific effects. The most efficient result was achieved with the combination of all three oligos which led to 90% reduction of Rxfp1 (**Figure 18B**). EndMT

was then induced by TGF $\beta$ 1 followed by Serelaxin treatment. Upon *Rxfp1* knockdown, the inhibitory effect of Serelaxin on EndMT was abolished, as it was shown that neither the expression of CD31 nor that the key EndMT regulators were significantly altered by the administration of Serelaxin (**Figure 18C**). This finding was supported by the fact that overexpression of *Rxfp1* in MCECs significantly increased the inhibitory effects of Serelaxin on EndMT as shown by increased CD31 expression and decreased expression of EndMT transcriptional factors Snail, Slug, and Twist (**Figure 18D**).

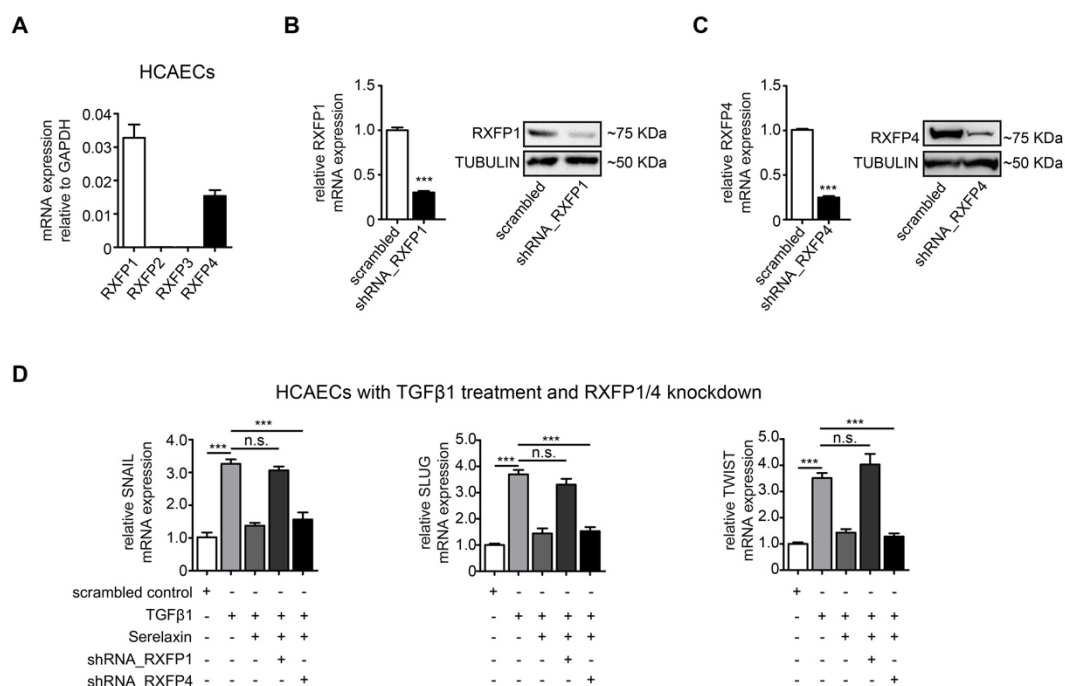


**Figure 17: Attenuation of TGF $\beta$ 1-induced EndMT by Serelaxin in HCAECs is mediated by RXFP1** (A) qPCR analysis showing relative mRNA expression levels of Relaxin family peptide receptors (RXFP) 1-4 in HCAEC. Only RXFP1 and RXFP4 expression was detectable. (B-C) Specificity validation of RXFP1- and RXFP4 shRNA knockdown by qPCR analysis and Western blot analysis showing the expression levels of RXFP1 and RXFP4 in shRNA-mediated knockdown of each compared to scrambled control in HCAECs. (D) qPCR analysis showing mRNA expression levels of SNAIL, SLUG, and TWIST in TGF $\beta$ 1- and Serelaxin-treated cells upon shRNA-mediated knockdown of RXFP1 and RXFP4. Serelaxin treatment reversed TGF $\beta$ 1-induced upregulation of SNAIL, SLUG, and TWIST but not in RXFP1 knockdown cells. Student's t-test was used for single comparison and one-way ANOVA with Bonferroni post-hoc analysis was used for multiple group comparisons. Gene expression and associated error bars, representing mean  $\pm$  SEM,  $n \geq 3$ , \*\*\*  $p < 0.001$ . Adapted from Wilhelmi et al. 2020.

### 3.3.3 RXFPs *in vivo*

To validate the acquired data *in vivo*, mouse heart sections were stained by immunofluorescence, using antibodies that label RXFP1 and wheat germ agglutinin (WGA), a lectin that binds to glycoconjugates, and thereby labeling cell membranes and fibrotic tissue (**Figure 19A**).



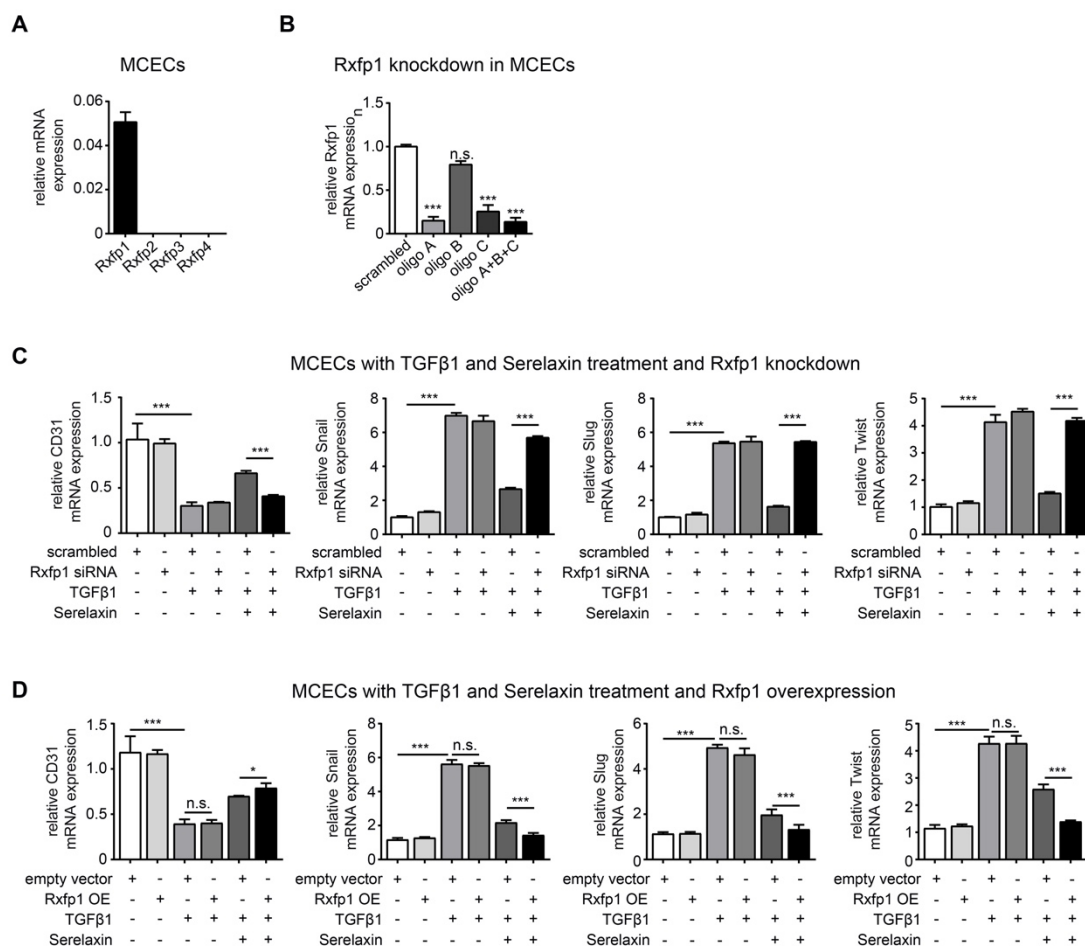


**Figure 18: Serelaxin partially inhibits TGFβ1-induced EndMT via Rxfp1 in MCEC** (A) qPCR analysis showing mRNA expression level of Rxfp1-4 in MCECs. Among all four genes, only Rxfp1 expression was detectable. (B) qPCR analysis showing a significant decrease of Rxfp1 mRNA expression level upon siRNA mediated Rxfp1 knockdown compared to scrambled controls. (C) qPCR analysis showing expression levels of CD31, Snail, Slug, and Twist in TGFβ1- and Serelaxin-treated MCECs upon siRNA mediated knockdown of Rxfp1 compared to cells without any treatment. Serelaxin reversed TGFβ1-induced EndMT but not upon Rxfp1 knockdown. (D) qPCR analysis showing the expression levels of EndMT transcriptional factors and CD31 in TGFβ1- and Serelaxin-treated MCECs upon Rxfp1 overexpression compared to cells transfected with empty vector. Under Rxfp1 overexpression, Serelaxin intensified its inhibitory effect on TGFβ1-induced EndMT. Student's t-test was used for single comparison and one-way ANOVA with Bonferroni post-hoc analysis was used for multiple group comparisons. Gene expression and associated error bars represent mean  $\pm$  SEM,  $n \geq 3$ , n.s. no significance, \*  $p < 0.05$ , \*\*\*  $p < 0.001$ . Adapted from Wilhelmi et al. 2020.

RXFP1 protein expression was significantly reduced in AAC-operated mice compared to sham animals and successfully restored by the administration of Serelaxin. The WGA-positive signal increased (by a factor of 1.5) in AAC-challenged mice indicating the development of cardiac fibrosis and could be reduced upon treatment with Serelaxin (**Figure 19B**). Next, RXFP1 was stained together with CD31 to indicate endothelial cells expressing RXFP1 by colocalization of both signals (**Figure 19C**). Interestingly, in sham hearts, 91% of CD31-positive signal was colocalized with a RXFP1-positive signal demonstrating that most endothelial cells express RXFP1 ( $\frac{CD31^+ + RXFP1^+}{CD31^+}$ ). Additionally, 71% of RXFP1-positive signal was colocalized with CD31-positive signals indicating that more than two

thirds of RXFP1 protein occurs in endothelial cells ( $\frac{RXFP1^+ + CD31^+}{RXFP1^+}$ ) (**Figure 19D**). Additionally, mRNA and protein expression of RXFP1 in sham and AAC-operated hearts under vehicle as well as Serelaxin treatment were quantified by qPCR and a Western blot. Both mRNA and protein expression levels were significantly reduced in AAC-operated mice as compared to sham mice. Serelaxin was able to restore a RXFP1 expression on the mRNA as well as on the protein level (**Figure 19E-F**).

Myocardial biopsies from patients without any heart disease showed that RXFP1 mRNA expression is the most abundant among all four receptors in human heart tissue (**Figure 19G**). In myocardial biopsies from patients suffering from end stage HF, the mRNA expression level of RXFP1 was significantly reduced as compared to healthy hearts (**Figure 19H**).

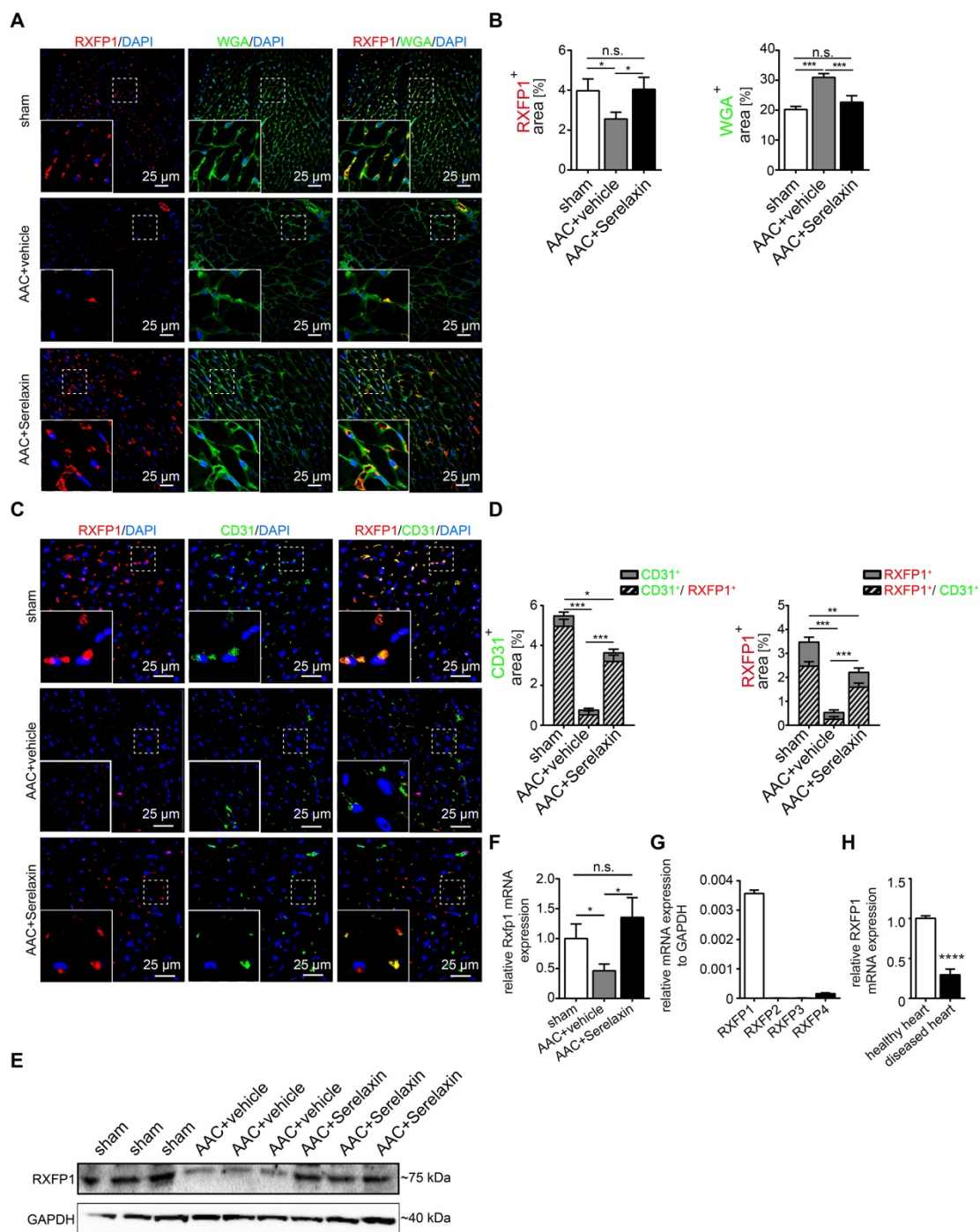


**Figure 19: Serelaxin attenuates EndMT via RXFP1 *in vitro* and *in vivo*** (A) Immunofluorescence staining of WGA, RXFP1 and DAPI in sham and AAC-treated mice hearts with vehicle or high dose Serelaxin treatment. (B) Quantification of RXFP1 and WGA positive area showing a reduced RXFP1 and increased WGA protein expression in AAC-operated compared to sham hearts that were restored upon Serelaxin treatment. (C) Immunofluorescence staining of CD31, RXFP1 and DAPI in sham and AAC-treated mice hearts with vehicle or high dose Serelaxin treatment. (D) Quantification of CD31 and WGA positive area showing a reduced CD31 and increased WGA protein expression in AAC-operated compared to sham hearts that were restored upon Serelaxin treatment. (E) Western blot analysis showing protein expression levels of RXFP1 in relation to GAPDH in sham and AAC-treated hearts with and without treatment with Serelaxin. Upon AAC RXFP1 protein level decreased and was restored upon Serelaxin treatment. (F) qPCR analysis showing relative Rxfp1 mRNA expression in sham, AAC- and vehicle-treated as well as AAC- and Serelaxin-treated hearts. Rxfp1 expression was reduced in AAC hearts and restored upon Serelaxin treatment. (G) qPCR analysis



showing relative mRNA expression levels of RXFP1-4 in human hearts. RXFP1 and RXFP4 were detected whereas RXFP2 was mainly represented. (H) qPCR analysis showing reduced mRNA expression levels of *RXFP1* in diseased human hearts as compared to healthy control hearts. Student's t-test was used for single comparison and one-way ANOVA with Bonferroni post-hoc analysis was used for multiple group comparisons. Gene expression and associated error bars, representing mean  $\pm$  SEM,  $n \geq 3$ , n.s. no significance, \*  $p < 0.05$ , \*\*  $p < 0.01$ , \*\*\*  $p < 0.001$ , \*\*\*\*  $p < 0.0001$ . Adapted from Wilhelmi et al. 2020.

### 3.4 Evaluation of signaling pathways affected by Serelaxin

#### 3.4.1 Gene candidates during EndMT

In order to further investigate the downstream signaling pathways that enable Serelaxin to execute the described effects, an EndMT qPCR array analysis was performed. This assay contains 84 EMT key genes that are analyzed by qPCR. These genes are either endothelial-related or mesenchymal- and EMT-related genes. All these genes are known to be either altered during EMT or to regulate this alteration (Lili et al. 2013). The underlying experiment was carried out in HCAECs consisting of four different samples: (1) control without any treatment, (2) TGF $\beta$ 1 treatment alone, (3) Serelaxin treatment alone and (4) TGF $\beta$ 1 and Serelaxin combined treatment. After four days the cells were harvested and analyzed. The heat map shows a relative, color-coded magnitude of gene expression (**Figure 20A**). A green color means a minimal, black color an average and red color a maximal gene expression. Genes related to endothelial cells are shown in the upper part of the heat map. These genes were downregulated under the influence of TGF $\beta$ 1 and could for the most part be rescued by a simultaneous administration of Serelaxin. Hence, in consistency with the previous results, it was shown that Serelaxin is able to preserve endothelial cell properties. The other genes shown in the heat map (mesenchymal- and EndMT-related) presented an upregulation under TGF $\beta$ 1 treatment alone, which could be ameliorated by the administration of Serelaxin (**Figure 20A**).

A comparison of altered mRNA levels in two treatment groups was visualized by scatter plots. TGF $\beta$ 1 treatment alone was on the one hand compared with the combined TGF $\beta$ 1/Serelaxin treatment (**Figure 20B**) and on the other hand with the Serelaxin treatment alone (**Figure 20C**). Both plots revealed a selective upregulation of four genes (*JAGGED1*, *NOTCH1*, *STEAP1*, *RAC1*) in the Serelaxin treatment alone as well as the combined TGF $\beta$ 1/Serelaxin treatment groups. However, five genes (*ERBB3*, *FZD7*, *GSC*, *GSK3B*, *TGFB2*) were upregulated in the TGF $\beta$ 1 treatment group. Regarding the latter genes, Serelaxin decreased a TGF $\beta$ 1-induced expression in HCAECs.

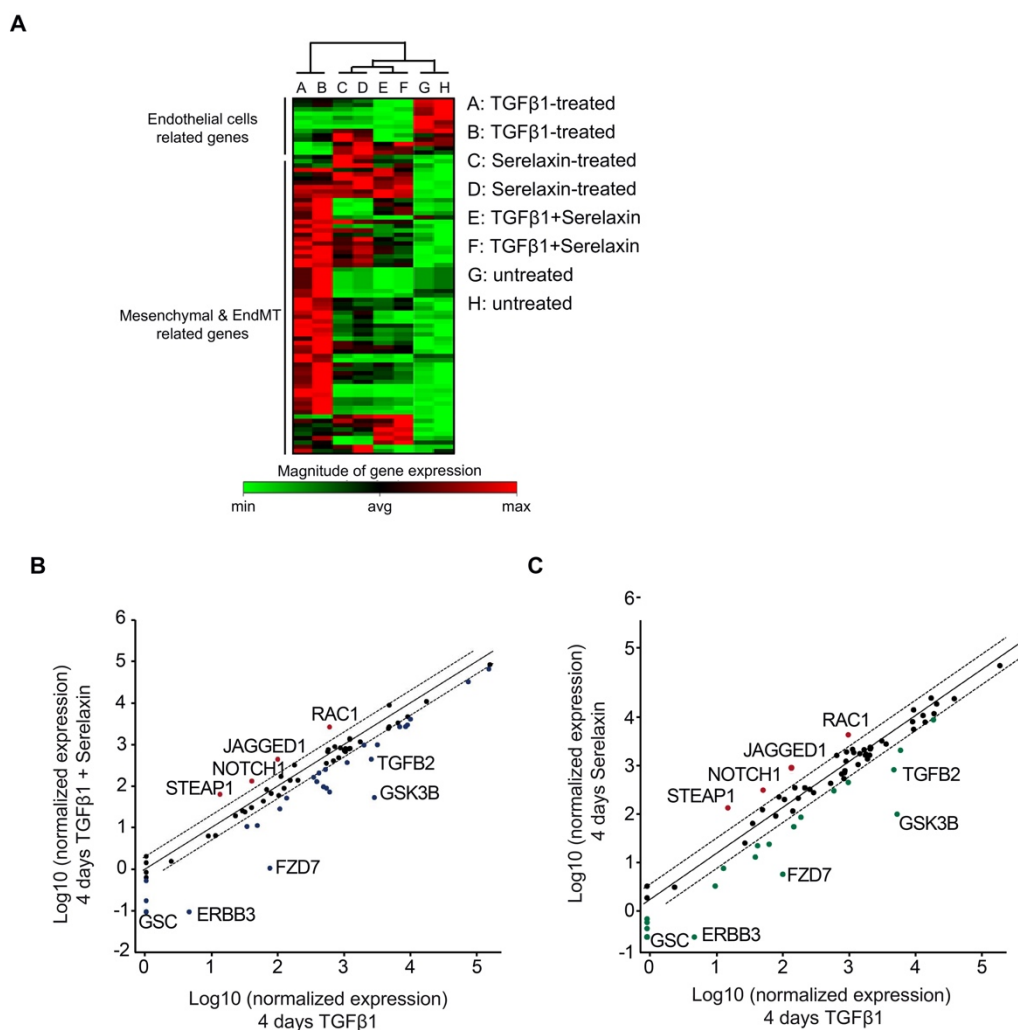


**Figure 20: Evaluation of EndMT gene candidates in TGF $\beta$ 1- and Serelaxin-treated HCAECs** (A) Heat map showing magnitude of EndMT array genes mRNA expression in untreated, only TGF $\beta$ 1-treated, only Serelaxin-treated and in both TGF $\beta$ 1- and Serelaxin-treated HCAECs. (B) Scatter plot showing genes with altered mRNA expression level in only TGF $\beta$ 1-treated (x-axis) or in both TGF $\beta$ 1- and Serelaxin-treated (y-axis) HCAECs. STEAP1, NOTCH1, JAGGED1, RAC1, DSP, GSC, ERBB3, FZD7, GSK3B and TGFB2 were significantly regulated by Serelaxin treatment, which is shown by separation from dot lines (cut-off by 4 folds). (C) Scatter plot showing genes with altered mRNA expression level in only TGF $\beta$ 1-treated (x-axis) or only Serelaxin-treated (y-axis) HCAECs. STEAP1, NOTCH1, JAGGED1, RAC1, DSP, GSC, ERBB3, FZD7, GSK3B and TGFB2 were also significantly regulated by Serelaxin treatment, which is shown by separation from dot lines (cut-off by 4 folds). Adapted from Wilhelmi et al. 2020.

### 3.4.2 Validation of EndMT gene candidates *in vitro* and *in vivo*

To transfer the obtained results to the AAC mouse model, the expression of the EndMT gene candidates was subsequently analyzed in MCECs and in mouse heart tissue. In Serelaxin administered TGF $\beta$ 1-treated MCECs, the expression of Jagged1, Notch1, Steap1 and Rac1 was significantly upregulated, which is in line with the findings in HCAECs. In addition, analogous to the EndMT array in HCAECs, Erbb3, Fzd7, Gsc, and Gsk3b were significantly decreased by Serelaxin compared to TGF $\beta$ 1 treatment alone. However, TGF $\beta$ 1 did not significantly affect Gsc expression compared to untreated control. In the case of Erbb3,

TGF $\beta$ 1, like Serelaxin, led to a decrease in expression compared to the untreated control group (**Figure 21A-B**).

Quantitative real time PCR analysis of all *in vivo* candidate genes was also performed. It showed that Serelaxin significantly rescued the downregulating effect of AAC on the expression levels of Jagged1, Notch1 and Rac1. Additionally, the beneficial effect of Serelaxin was shown by the reduction of AAC-induced upregulation of Erbb3, Fzd7 and Gsk3b; even though the alteration was not significant for Erbb3 (**Figure 21C**). Gsc expression was influenced neither by AAC nor by the application of Serelaxin. Interestingly, Steap1 was downregulated in both TGF $\beta$ 1-treated MCECs and in AAC hearts, but Serelaxin rescued its expression only *in vitro* but not *in vivo*. In Serelaxin-administered AAC-treated mice, the expression of Steap1 was even further decreased compared to AAC-treated animals. This discrepancy is likely due to cell type dependent gene regulation mechanisms.

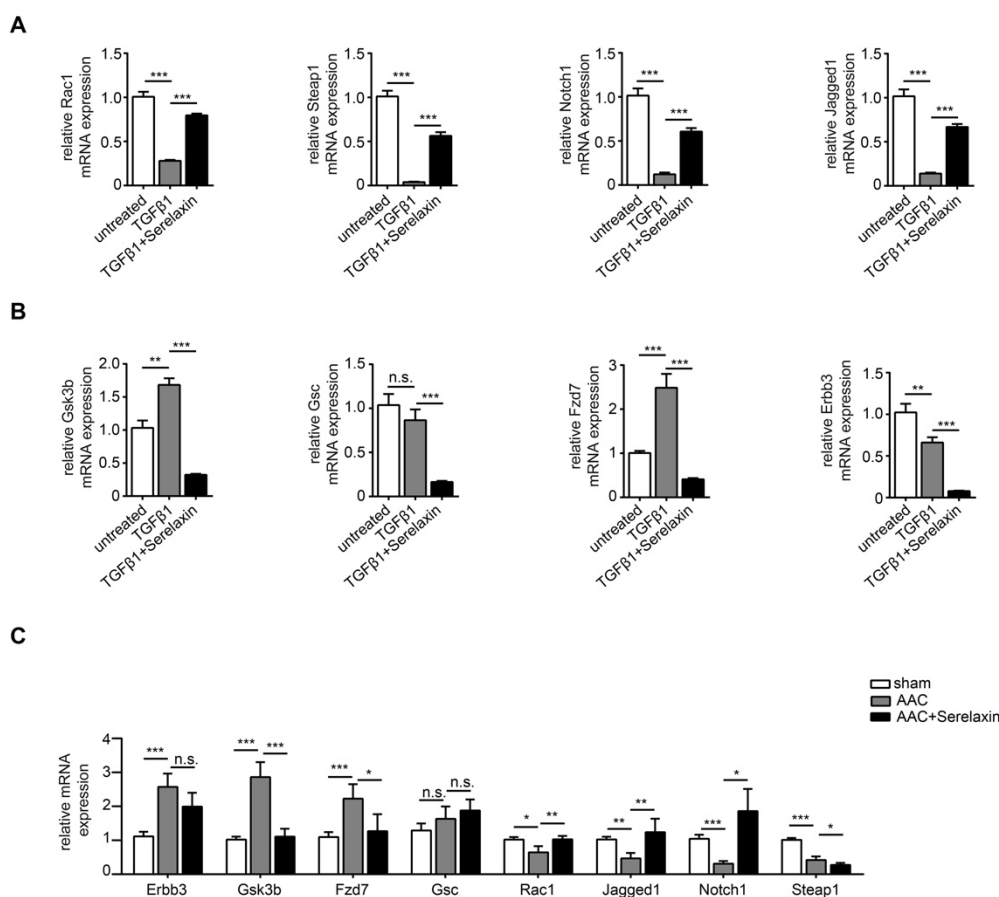


**Figure 21: Validation of EndMT gene candidates affected by Serelaxin *in vitro* and *in vivo*** (A-B) qPCR analysis showing mRNA expression of gene candidates in TGF $\beta$ 1- and Serelaxin-treated MCECs compared to untreated cells. (C) qPCR analysis showing mRNA expression of gene candidates in sham, AAC- and vehicle-treated as well as AAC- and Serelaxin-treated hearts. Serelaxin significantly rescued the effects of TGF $\beta$ 1 and AAC *in vitro* and *in vivo*. Except for Gsc, Erbb3 and Steap1. Student's t-test was used for single comparison and one-way ANOVA with Bonferroni post-hoc analysis was used for multiple group comparisons. Gene expression and associated error bars, representing mean  $\pm$  SEM,  $n \geq 3$ , n.s. no significance, \*  $p < 0.05$ , \*\*  $p < 0.01$ , \*\*\*  $p < 0.001$ . Adapted from Wilhelmi et al. 2020.

### 3.4.3 Expression of Notch pathway proteins *in vivo*

Among the identified candidate genes, this study further focused on Notch1 and its specific ligand Jagged1. There is already extensive knowledge about these genes, showing that they contribute to the maintenance of endothelial cell characteristics (Mack and Iruela-Arispe 2018). Immunofluorescence staining of NOTCH1, JAGGED1 and NICD revealed a significantly reduced expression of each protein in hearts of AAC-treated animals as compared to sham mice. This observation was confirmed especially within fibrotic areas as indicated by the green signal of WGA staining (**Figure 22A-C**). Upon treatment with Serelaxin the positive areas of NOTCH1, JAGGED1 and NICD were all significantly increased as compared to vehicle-treated mice (**Figure 22D-F**). The data confirmed that the observed effect of Serelaxin during EndMT *in vitro* occurs analogously *in vivo*. Notch1 activation is mediated by its ligand Jagged1 that is *inter alia* secreted. Here, JAGGED1 secretion was measured in medium, collected from TGF $\beta$ 1-treated and control MCECs. A significant decrease of JAGGED1 secretion upon treatment with TGF $\beta$ 1 as compared to untreated MCECs was confirmed by Ponceau stain and Western blot analysis (**Figure 23**). The data implies that Serelaxin is able to attenuate an AAC-induced partial inhibition of Notch pathway signaling.

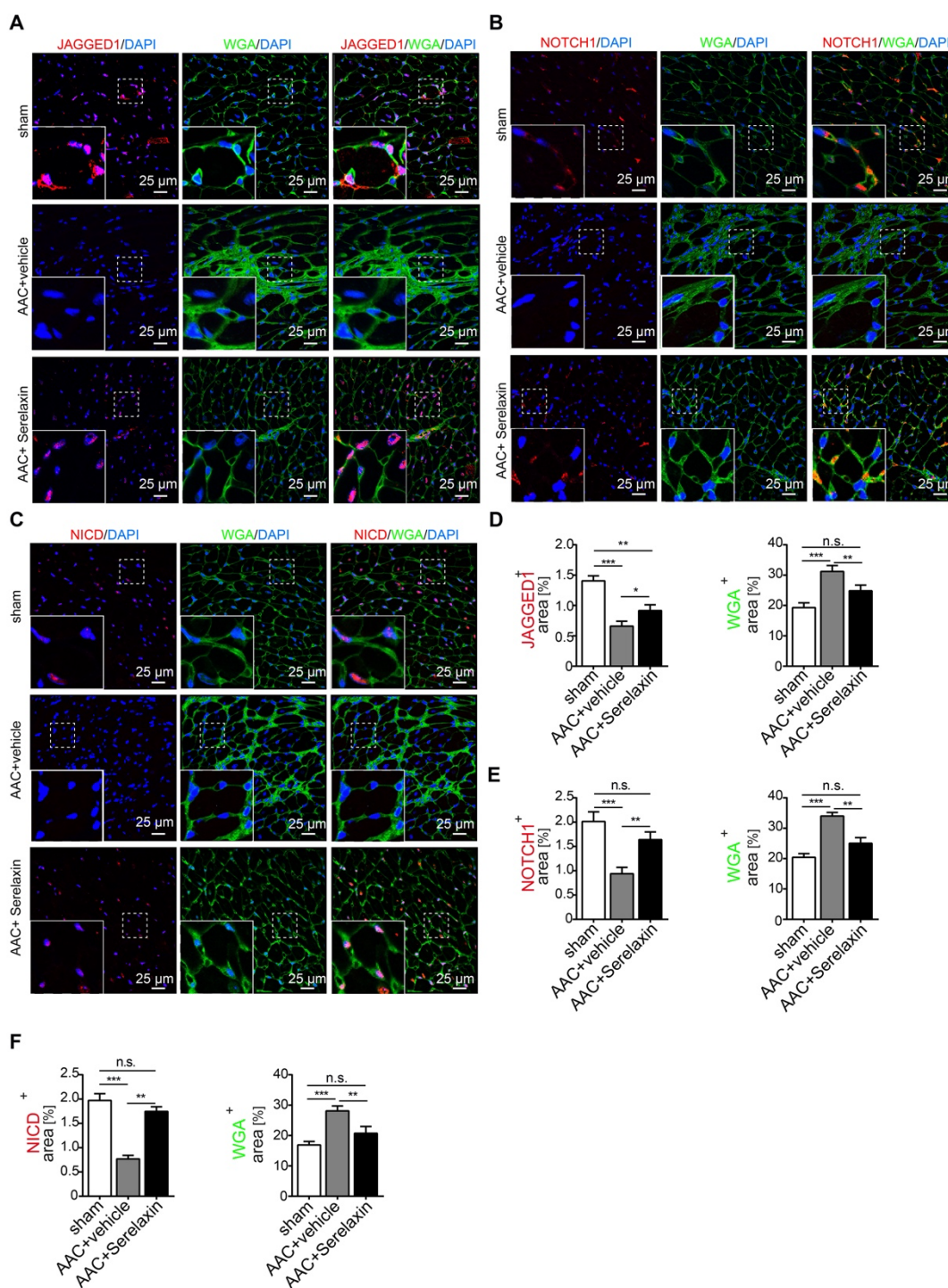


**Figure 22: Serelaxin restores expression of Notch1 pathway proteins in AAC-operated hearts** (A) Immunofluorescence staining of WGA, JAGGED-1 and DAPI in sham and AAC-treated mice hearts with vehicle or high dose Serelaxin treatment. (B) Immunofluorescence staining of WGA, NOTCH1 and DAPI in sham and AAC-treated mice hearts with vehicle or high dose Serelaxin treatment. (C) Immunofluorescence staining of WGA, NICD and DAPI in sham and AAC-treated mice hearts with vehicle or high dose Serelaxin treatment. (D) Quantification of JAGGED1 and WGA positive area showing a reduced JAGGED1 and increased WGA protein expression in AAC-operated compared to sham hearts that were restored upon Serelaxin treatment. (E) Quantification of NOTCH1 and WGA positive area showing a reduced NOTCH1 and increased WGA protein expression in AAC-operated compared to sham hearts that were restored upon Serelaxin treatment. (F) Quantification of NICD and WGA positive area showing a reduced NICD and increased WGA protein expression in AAC-operated compared to sham hearts that were restored upon

Serelaxin treatment. Student's t-test was used for single comparison and one-way ANOVA with Bonferroni post-hoc analysis was used for multiple group comparisons. Gene expression and associated error bars, representing mean  $\pm$  SEM,  $n \geq 3$ , n.s. no significance, \*  $p < 0.05$ , \*\*  $p < 0.01$ , \*\*\*  $p < 0.001$ . Adapted from Wilhelmi et al. 2020.

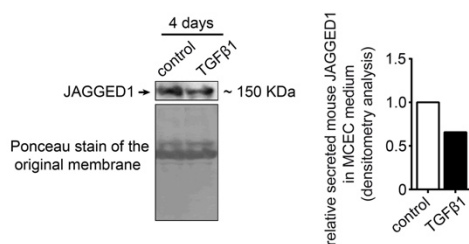


**Figure 23: Reduction of soluble Jagged1 upon TGFβ1 treatment in MCECs** (A) Western blot analysis shows the amount of the soluble form of JAGGED1 in the medium of TGFβ1-treated MCECs. Ponceau-S-stained membrane picture indicates that an equal amount of total precipitated protein was loaded for both the control and TGFβ1-treated MCECs. Soluble JAGGED1 was reduced in TGFβ1-treated MCECs as quantified by densitometry analysis (right panel). Adapted from Wilhelmi et al. 2020.

#### 3.4.4 Molecular activation of Notch signaling by Serelaxin

After studying the changes of expression of the Notch signaling components induced by Serelaxin, we now attempted to investigate the role of *Rxfp1* in this context. Consequently, EndMT was induced by TGFβ1 in MCECs with *Rxfp1* knock down by siRNA. The effect of Serelaxin supplementation was tested with respect to Notch1 and Jagged1 expressions. As demonstrated by quantitative real time PCR, the relative *Rxfp1* mRNA expression was reduced by approximately 70 % upon siRNA knockdown (**Figure 24A**). As expected, Serelaxin rescued mRNA expression of *Notch1* and *Jagged1* in TGFβ1-treated MCECs. However, this effect was not shown in the cells in which *Rxfp1* was knocked down (**Figure 24B-C**).

Next, a NICD overexpression was performed, to further elucidate the exact link between Serelaxin, *Rxfp1* and Notch signaling. By transfecting TGFβ1-treated MCECs with a NICD overexpression construct, we mimicked the Notch pathway activation. A TGFβ1-mediated reduction of CD31 was ameliorated upon simultaneous overexpression of NICD. Expression levels of EndMT key transcriptional factors Snail, Slug, and Twist were significantly less reduced by TGFβ1 treatment and the NICD overexpression together as compared to TGFβ1 treatment alone (**Figure 25A**). Additionally, TGFβ1-treated MCECs were applied with either DAPT, an inhibitor of Notch pathway activation, or DMSO as a control. Subsequently, these cells were treated with Serelaxin. The supplementation of Serelaxin to DAPT-treated MCECs led to a significantly decreased EndMT-inhibitory effect as compared to DMSO-treated MCECs (**Figure 25B**). To sum up, our results suggested that Serelaxin ameliorates TGFβ1-induced EndMT at least in part via reactivation of the Notch signaling pathway which is mediated by *Rxfp1*.



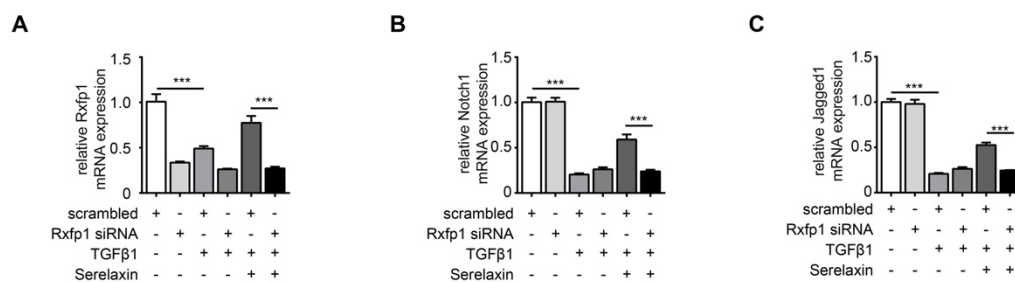


**Figure 24: Serelaxin rescues TGFβ1-induced inhibition of Notch pathway via Rxfp1 in MCECs (A-C)** qPCR analysis showing the expression of Rxfp1, Notch1 receptor and Jagged1 in TGFβ1- and Serelaxin-treated, MCECs, where Rxfp1 was knocked down via siRNA. Scrambled cells were used as control. The expression of all three genes was partly restored in Serelaxin-supplemented, TGFβ1-treated cells, but not in Rxfp1 knockdown cells. Student's t-test was used for single comparison and one-way ANOVA with Bonferroni post-hoc analysis was used for multiple group comparisons. Gene expression and associated error bars, representing mean  $\pm$  SEM,  $n \geq 3$ , n.s. no significance, \*\*\*  $p < 0.001$ . Adapted from Wilhelmi et al. 2020.

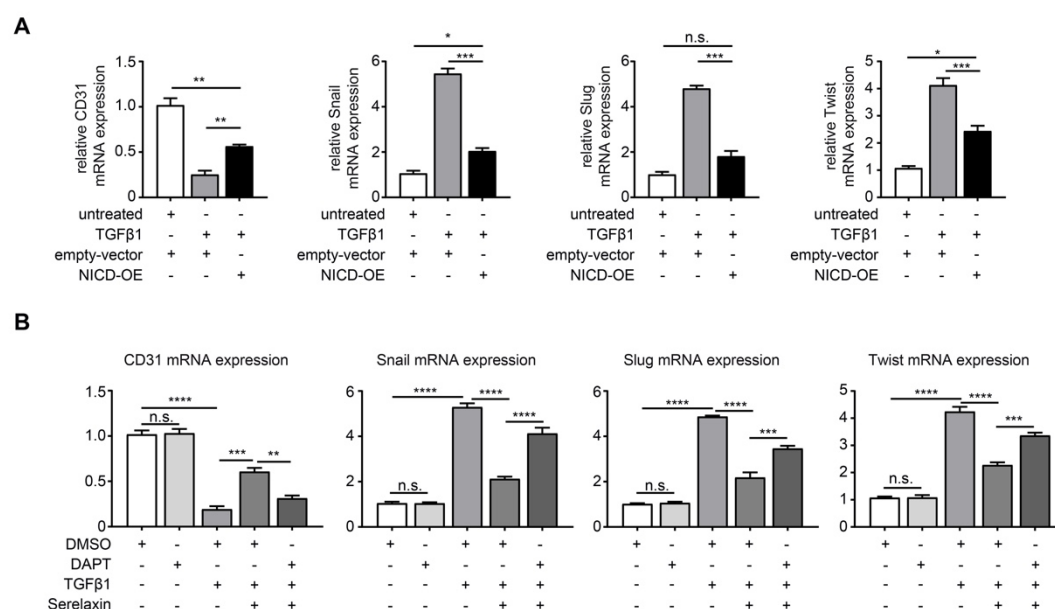


**Figure 25: Experimental validation of Serelaxin's ability to rescue Notch pathway *in vitro*** (A) qPCR analysis showing NICD overexpression partially blocking TGFβ1-induced EndMT as shown by increased expression of endothelial marker gene CD31 and decreased expression of EndMT transcriptional factors Snail, Slug, and Twist compared to cells transfected with an empty vector. (B) qPCR analysis showing increased mRNA expression of endothelial marker gene CD31 and decreased mRNA expression of EndMT transcriptional factors Snail, Slug, and Twist upon treatment with TGFβ1 and Serelaxin compared to TGFβ1 alone. Upon additional treatment with Notch-inhibitor DAPT this effect was abolished. Cells transfected with DMSO were used as control. Student's t-test was used for single comparison and one-way ANOVA with Bonferroni post-hoc analysis was used for multiple group comparisons. Gene expression and associated error bars, representing mean  $\pm$  SEM,  $n \geq 3$ , n.s. no significance, \*  $p < 0.05$ , \*\*  $p < 0.01$ , \*\*\*  $p < 0.001$ , \*\*\*\*  $p < 0.0001$ . Adapted from Wilhelmi et al. 2020.

### 3.5 Serelaxin rescues *Rxfp1* expression through histone modifications in *Rxfp1* promoter region

#### 3.5.1 Histone modifications upon Serelaxin treatment

So far, this study revealed that in human of HF diseased hearts, in AAC-treated mouse hearts as well as in TGF $\beta$ 1-treated endothelial cells, the expression of *Rxfp1* was significantly reduced as compared to healthy controls or untreated endothelial cells. However, in mouse hearts, the administration of Serelaxin led to a rescue of the receptor's downregulation. In this context, it has been reported that TGF $\beta$ 1 silences gene expression via epigenetic modifications during various diseases (Sun et al. 2010; Cardenas et al. 2014). These modifications essentially subsume methylation of CpG islands within the promoter region or chemical modifications to histone proteins.

The aim was to evaluate whether silencing of *Rxfp1* could be caused by one of these mechanisms and if Serelaxin is capable to impact such epigenetic changes. However, no CpG island was identified within the 5 kb upstream region of the transcription start site (TSS) of murine *Rxfp1*. Therefore, it can be concluded that another gene regulatory mechanism rather than methylation plays a role in the silencing of *Rxfp1*.

To identify the potential role of histone modifications, ChIP analysis of gene specific histone modification profiles at the promoter region of *Rxfp1* was performed in MCECs treated with TGF $\beta$ 1 and Serelaxin compared to TGF $\beta$ 1 treatment alone and untreated cells. Three primer amplicons targeting the *Rxfp1* promoter region 1 kb upstream of TSS and one targeting the intron 10 as a control were designed (**Figure 26A**). The analysis profile included activating markers H3K4me3 and H3K27ac as well as repressive markers H3K9me3 and H3K27me3. First, untreated cells were analyzed to assess the transcriptional activity of the chromatin within the *Rxfp1* promoter region. Quantitative real-time PCR revealed an enrichment of the activating modifications H3K4me3 and H3K27ac and a depletion of the repressive modifications H3K9me3 and H3K27me3 if performed with amplicons 1-3 but not with amplicon 4. Hence, in untreated cells, the chromatin within the *Rxfp1* promoter region was transcriptionally active. After supplementation with TGF $\beta$ 1 alone, H3K4me3 and H3K27ac were significantly depleted at amplicon 1 and 2 but not at amplicon 3 and 4, whereas H3K9me3 and H3K27me3 were significantly enriched at Amplicon 1-3 but not at Amplicon 4 as compared to untreated conditions. Upon treatment with TGF $\beta$ 1 and Serelaxin, the activating modification H3K4me3 was significantly increased and the repressive modifications H3K9me3 and H3K27me3 were significantly decreased as compared to TGF $\beta$ 1 treatment alone. However, H3K27ac enrichment was not significantly affected by Serelaxin. Analogous to untreated cells, qPCR analysis performed with amplicon 4 targeting the intron 10 did not show any significant changes of chromatin modification markers (**Figure 26B**).



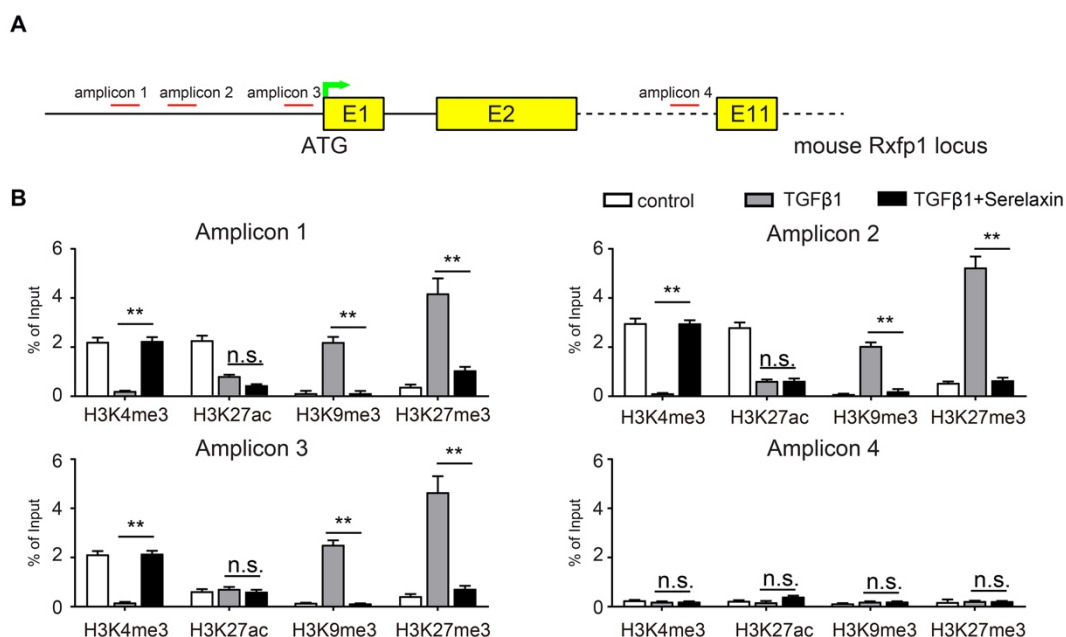


**Figure 26: Serelaxin reactivates *Rxfp1* expression via histone modifications** (A) Schematic visualizing the mouse *Rxfp1* locus with localization of ChIP-qPCR primers. (B) qPCR analysis showing the enrichment of H3K4me3, H3K27ac, H3K9me3 and H3K27me3 in the *Rxfp1* promoter region (Amplicon 1-3) and intron 10 as a control (Amplicon 4). The enrichment of TGFβ1-influenced H3K4me3, H3K9me3 and H3K27me3 marks were significantly compromised by Serelaxin if performed with amplicons 1-3 targeting the *Rxfp1* promoter region but not with amplicon 4 targeting intron10. Student's t-test was used for single comparison and one-way ANOVA with Bonferroni post-hoc analysis was used for multiple group comparisons. Gene expression and associated error bars, representing mean  $\pm$  SEM,  $n \geq 3$ , n.s. no significance, \*\*  $p < 0.01$ . Adapted from Wilhelmi et al. 2020.

### 3.5.2 Serelaxin's influence on histone modifications under *Rxfp1* knockdown

Since we could show that Serelaxin is able to epigenetically alter the expression of its own receptor through histone modification, the question is whether this effect is equally mediated via RXFP1. To find an adequate answer to this question, ChIP analysis was repeated in MCECs where *Rxfp1* had been knocked down with siRNA. Scrambled and knocked down MCECs were treated either with TGFβ1 alone or TGFβ1 and Serelaxin together. Quantitative real-time PCR revealed that upon knockdown of *Rxfp1*, Serelaxin could not significantly decrease repressive modification marks or increase activating modifications (**Figure 27**). To conclude, Serelaxin is able to induce the expression of its own receptor *Rxfp1* by binding to and activating the same. This mechanism is at least in part explained by regulatory histone modification.

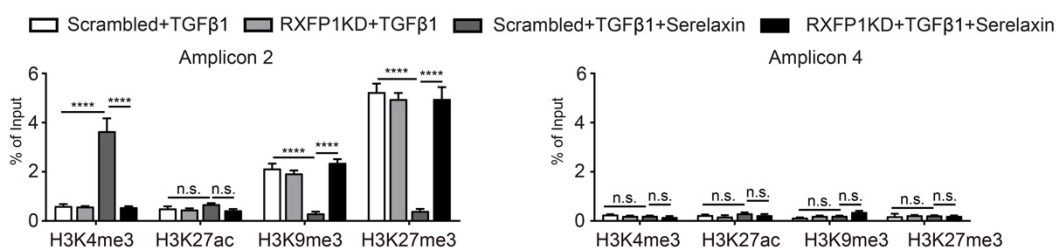


**Figure 27: Serelaxin induces cascade of histone modifications by binding to Rxfp1** ChIP-qPCR analysis showing the enrichment of histone modification marks in the *Rxfp1* promoter region after Rxfp1 knockdown. Upon Rxfp1 knockdown, treatment with Serelaxin did not significantly increase the activating modifications or decrease the repressive modification marks. Student's t-test was used for single comparison and one-way ANOVA with Bonferroni post-hoc analysis was used for multiple group comparisons. Gene expression and associated error bars, representing mean  $\pm$  SEM,  $n \geq 3$ , n.s. no significance, \*\*\*\*  $p < 0,0001$ . Adapted from Wilhelmi et al. 2020.

### 3.5.3 TGFβ/SMAD2/3 cascade affected by Serelaxin

Relaxin inhibits the TGFβ signaling pathway (Heeg et al. 2005; Mookerjee et al. 2009; Yuan et al. 2017). On the basis of these findings, we investigated whether and to what extent the activation of the expression of Rxfp1 caused by Serelaxin is due to an inhibition of the TGFβ signaling pathway. For this reason, we performed two additional experiments:

First, a Western blot analysis of pSMAD2 and pSMAD3 in sham, AAC-operated, vehicle-treated, and AAC-operated Serelaxin-treated mouse hearts was performed. Total SMAD2 and SMAD3 were used as protein loading controls. It revealed increased protein levels of pSMAD2 and pSMAD3 in AAC-operated animals compared to sham. The protein levels were decreased in AAC-operated mouse hearts that were treated with Serelaxin (**Figure 28A**). Since pSMAD2/3 are downstream transcription factors of the TGFβ pathway and well known to mediate histone marks, it was now of interest to further elucidate the mechanistic link between Serelaxin, pSMAD2/3 and the Rxfp1 expression.

To this end, a ChIP experiment was performed in MCECs with pSMAD2/3 antibodies. Subsequently, the enrichment at the *Rxfp1* promoter region was analyzed by qPCR. TGFβ1 treatment alone led to an enrichment of pSMAD2/3 at the promoter region of *Rxfp1* (Amplicon 2) but not in the region of the intron 10 (Amplicon 4). The enrichment was significantly compromised in cells treated with both TGFβ1 and Serelaxin compared to cells treated with TGFβ1 alone (**Figure 28B**).

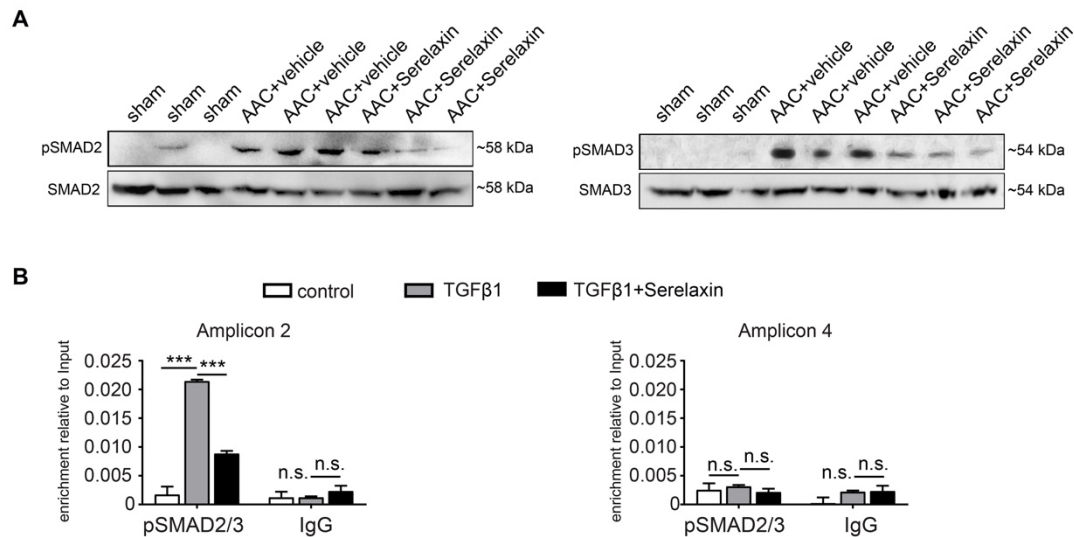


**Figure 28: Serelaxin impacts histone modifications by inhibiting TGFβ/ SMAD2/3 axis** (A) Western blot analysis showing protein levels of phosphorylated SMAD proteins (pSMAD2 and pSMAD3) in sham, AAC-operated and AAC- and Serelaxin-treated hearts. Total SMAD2 and SMAD3 were used as protein loading controls. (B) Immunoprecipitation of pSMAD2/3 at the *Rxfp1* promoter region in MCEC showing a significantly compromised enrichment of pSMAD2/3 in TGFβ1- and Serelaxin-treated cells compared to cells treated with TGFβ1 alone. Student's t-test was used for single comparison and one-way ANOVA with Bonferroni post-hoc analysis was used for multiple group comparisons. Gene expression and associated error bars, representing mean ± SEM, n ≥ 3, n.s. no significance, \*\*\* p < 0.001. Adapted from Wilhelmi et al. 2020.

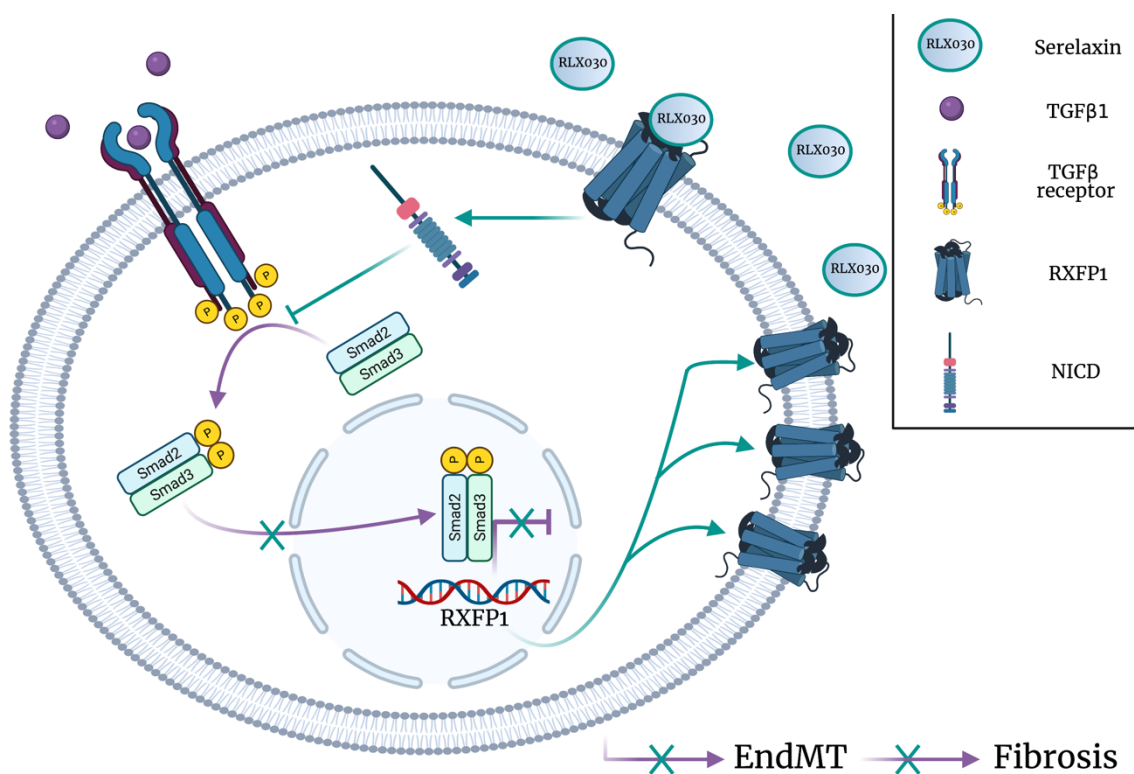


**Figure 29: Molecular mechanism Serelaxin drives to partially inhibit EndMT and cardiac fibrosis** Graphical abstract depicting Serelaxin binding to its specific receptor RXFP1, activating Notch signaling

---

pathway and consecutively inhibiting TGF $\beta$ -induced SMAD2/3 phosphorylation to restore RXFP1 expression via histone modifications (created with BioRender.com).

To sum up, our results suggested that Serelaxin promotes a positive feedback loop: By binding to a basal, low level of its specific receptor RXFP1 Serelaxin partially inhibits TGF $\beta$ 1-induced histone modifications at the *Rxfp1* promoter region and thereby induces *Rxfp1* expression (**Figure 29**).

## 4 Discussion

This study demonstrated an anti-fibrotic effect of Serelaxin in two independent pressure overload mouse models, AAC and the ATII infusion via osmotic minipumps. Furthermore, we demonstrated that the anti-fibrotic effect is associated with reduced mortality in mice and with inhibition of EndMT via the activation of Notch1 signaling. Next, this study provided evidence that this effect is mediated by the Relaxin receptor RXFP1. Finally, Serelaxin rescues low RXFP1 expression in diseased hearts by partially blocking the TGF $\beta$  pathway and consequently mediating *Rxfp1* gene histone modifications. In the subsequent section, the main results of this work will be reviewed and compared to the state-of-the-art literature. It will also discuss the limitations of this study.

### 4.1 Two independent disease models of pressure-overload

Various animal models of left ventricular pressure overload are commonly used to induce HF, e.g. ascending aortic constriction, transverse aortic constriction (TAC; constriction between the brachiocephalic trunk and the left common carotid artery), abdominal (suprarenal) aortic constriction and ATII infusion (Qi et al. 2011; Schwarzer 2016). In this study, two different pressure overload mouse models were used to induce cardiac fibrosis and analyze the impact of Serelaxin.

The first model we used was AAC, the constriction of the ascending aorta. AAC leads to a rapid and reliable development of cardiac fibrosis (Tarnavski et al. 2004). The relevance of EndMT occurring during aortic constriction has been controversially reported. For AAC, the involvement of EndMT in fibrogenesis was demonstrated previously (Zeisberg et al. 2007b). However, during the constriction of the transverse aorta (TAC), a milder model of cardiac fibrosis, EndMT has not been found (Moore-Morris et al. 2014). Notch1 signaling was shown to be downregulated 4 weeks after AAC, whereas 1 week after TAC Notch1 signaling has been demonstrated to be upregulated (Nemir et al. 2014). The fact that Notch signaling has been reported to mediate inhibition of TGF $\beta$  signaling and thereby might prevent EndMT could be a possible explanation for the different observations described above (Sassoli et al. 2013; Zhou et al. 2015; Rodriguez-Vita et al. 2017).

As a second model, infusion of ATII via osmotic minipumps, was performed in our study. This pressure overload mouse model is well-established and induces HF and cardiac fibrosis (Ichihara et al. 2001). However, it has been shown that ATII also exerts direct pro-fibrotic stimuli to the heart. By binding to Angiotensin II receptor type 1 (ATR1), abundantly present on cardiac fibroblasts, ATII activates TGF $\beta$ 1 and MAPK and thereby mediates fibroblast proliferation, their adhesion to matrices as well as increased production of ECM (Kawano et al. 2000). ATII negatively regulates TGF $\beta$ 1-induced fibrosis by acting on the Angiotensin II receptor type 2 (ATR2). Since it has been pointed out that – in the kidney – Relaxin requires

ATR2 and thereby abrogates kidney fibrosis, it is likely that there is an additional direct influence of Serelaxin on cardiac fibrogenesis in the ATII model (Chow et al. 2014).

## 4.2 Serelaxin attenuates cardiac fibrosis and improves overall survival

In both animal models, Serelaxin showed consistent anti-fibrotic effects. These findings are in line with several publications that reported an anti-fibrotic effect of Relaxin on the heart (Samuel et al. 2004; Lekgabe et al. 2005; Zhou et al. 2015). The severity of fibrosis in mice treated with the vehicle appears to be relatively mild with an average of ~2.5% (AAC). One might expect to have a higher fibrosis level after four weeks of AAC treatment as some studies report fibrosis levels up to 20% after 4 weeks of AAC (Goh et al. 2019). However, it appears that the strain of the mice, gauge size of the needle for constriction, and consecutive gradients influence the total amount of fibrosis. Nevertheless, we hypothesize that the method of quantification has the greatest impact on absolute numbers, as our images showing fibrosis by MTS staining are comparable to the ones published in the article of Goh et al. In our software, we used a stringent approach rather underestimating than overestimating fibrosis based on the intensity of blue color which require a pixel to be counted as fibrosis.

Furthermore, in both models we observed that the anti-fibrotic effect was relatively higher on perivascular regions as compared to interstitial areas. Interestingly, Maruyama et al. (2018) reported that a knockout of INSL6, another member of the relaxin/insulin-like peptide subfamily, did not show any spontaneous heart phenotype. However, upon infusion with ATII both knockout and wildtype mice developed cardiac fibrosis. Perivascular lesions were more than 50% higher in knockout mice as compared to wildtype. This indicates that Serelaxin has a disproportionate inhibitory effect on the development of perivascular fibrosis. Notably, perivascular fibrosis has been demonstrated to be a contributor to the reduction of myocardial and arterial compliance (Biernacka and Frangogiannis 2011). A vascular-protective effect of Serelaxin has recently been shown in an ATII mouse model (McCarthy et al. 2017). This is in line with the therapeutic effect of Serelaxin on perivascular fibrosis observed in this study.

Serelaxin has not only been shown to have an anti-fibrotic effect on the heart but also on various other organs. Patients suffering from HF regularly develop secondary renal dysfunction, which is called cardiorenal syndrome (CRS). Renal inflammation and fibrosis play a central role in the pathogenesis of CRS. In this context, Serelaxin attenuated renal tubulointerstitial and glomerular fibrosis in a mouse model of dilated cardiomyopathy (Giam et al. 2018). Since Relaxin treatment showed anti-fibrotic effects on hepatic stellate cells, which are the main collagen-producing cells in the liver, Serelaxin was subsequently tested to treat liver fibrosis in a combination with Rosiglitazone (an original anti-diabetic drug known to reduce liver fibrosis). Serelaxin enhanced the anti-fibrotic effect of Rosiglitazone in a model of hepatic fibrosis (Williams et al. 2001; Bennett et al. 2017). Furthermore, Pini et al.

(2016) chronically exposed guinea pigs to cigarette smoke to induce chronic obstructive pulmonary disease, which is characterized, among other hallmarks, by pulmonary fibrosis. The animals were treated with Serelaxin either delivered by osmotic pumps or aerosol. In both cases, Serelaxin was able to counteract the pathological pulmonary fibrosis. Interestingly, RXFP1-deficient mice showed an accumulation of collagen around the pulmonary blood vessels (perivascular fibrosis) at an age of 6 months. However, the lung parenchyma was not affected by fibrosis (Kamat et al. 2004). These data support our finding that Serelaxin appears to have a significantly mitigating effect on perivascular fibrosis.

In addition to the analysis of fibrosis, we examined the performance and the phenotype of the mouse hearts. The systolic function was not significantly reduced proving that AAC, in this context, induced HF of a diastolic subtype (HFpEF). It was shown that the hearts of the AAC-treated mice were extensively enlarged as compared to the sham hearts. Echocardiography examinations revealed a dilated hypertrophy of the hearts which is usually expected later than four weeks after AAC (Davidsohn et al. 2019). This may be due to a relatively strong constriction during the surgery which would also explain the high mortality of AAC-operated, untreated animals (46%) after four weeks. 46% is relatively high as compared to the literature e.g. Liao et al. (2002) where they described a mortality of 21% after 3 weeks. Unfortunately, the authors do not provide any details about the experimental mice (neither background nor the age of the animals). They may have used younger and therefore more resilient animals. Notably, in their study, the mortality increases to 40% after 8 weeks. Overall, only very little data was provided on the survival of AAC mice. In contrast, there is much more information on the mortality of TAC-operated animals as described by Rothermel et al. (2005). They showed a mortality of ~20% after 3 weeks. As previously described, AAC is a much more invasive model than TAC. Rothermel et al. also used a technique they call “severe transverse aortic binding”, which more closely resembles the conditions of AAC. Here, they showed a mortality of about 60% after 3 weeks. In both severe TAC and our AAC, C57Bl/6 mice were used, so the results are comparable. In general, the heart’s phenotype and performance were not altered by administration of Serelaxin.

Beside the attenuation of cardiac fibrosis, Serelaxin also improved the survival of the mice compared to vehicle-treated animals. This benefit on survival was dose dependent. However, only the high dose treatment was significant in reducing the mortality. The cause of death for the animals in the respective groups was not investigated. For future studies it might be important to examine whether the mice show arrhythmia or arrest and whether and how Serelaxin may affect it. Such assessment can be carried out by constant telemetric ECG monitoring of the mice, which is beyond the scope of this study. The survival results seem to contradict with the clinical second phase III trial (RELAX-AHF-2) that failed to reach its primary endpoint of reducing death at 180 days after Serelaxin or placebo administration in human patients (Metra et al. 2019). However, in the context of this animal experiment a constant four-week treatment with Serelaxin at a high dose of 500 µg/kg/d took place, as

opposed to a single infusion up to 48 hours at 30  $\mu\text{g}/\text{kg}/\text{d}$  in RELAX-AHF-2. The difference in mortality reduction can be seen as a first indication that Serelaxin develops its therapeutic potential mainly through the inhibition of fibrosis and is therefore more suitable as a high dose and long-term treatment for chronic HF.

### 4.3 Serelaxin impacts different signaling pathways to inhibit EndMT *in vitro* and *in vivo*

The observation that Serelaxin reduced perivascular fibrosis more significantly than interstitial fibrosis led us to focus on examining how Serelaxin affects fibrosis and whether EndMT plays a role. In a pressure overload mouse model, it was initially reported that EndMT contributed to cardiac fibrogenesis (Zeisberg et al. 2007b). Subsequent studies revealed a relevance of EndMT in different organ fibrosis including the kidney, the lung and the intestinal tract (Zeisberg et al. 2008; Rieder et al. 2011; Choi et al. 2016). EndMT also leads to the accumulation of carcinoma-specific fibroblasts and thereby not only promotes tumor growth but is also, similar to EMT, associated with the metastasis of the tumors (Zeisberg et al. 2007a). This leads to the hypothesis that Serelaxin can be used therapeutically in every fibrotic or malignant disease in all organs where EndMT plays a decisive role. Within the scope of this work, it was indeed shown that Serelaxin clearly inhibits EndMT and stabilizes microvasculature.

Through detailed EndMT pathway analysis, various candidate genes were detected *in vitro* and partially validated *in vivo*. An EndMT qPCR array analysis containing 84 EMT key genes that are either known to be endothelial-related or mesenchymal- and EMT-related was performed to detect gene candidates that might be targets for Serelaxin. This experiment was carried out *in vitro* in HCAECs. Notably, four genes (STEAP1, NOTCH1, JAGGED1, RAC1) were selectively upregulated in the Serelaxin treatment group and the TGF $\beta$ 1/Serelaxin combination group. Five genes (*ERBB3*, *FZD7*, *GSC*, *GSK3B*, *TGFB2*) were upregulated in the TGF $\beta$ 1 group and decreased upon administration of Serelaxin. An *in vivo* validation experiment revealed that Serelaxin significantly rescued the effects of AAC on all genes except for *ErbB3*, *Gsc* and *Steap1*.

The human *ERBB3* gene encodes a membrane bound protein called receptor tyrosine-protein kinase erbB-3, also known as HER3 (human epidermal growth factor receptor 3). *ERBB3* is expressed in various adult tissue but also plays a crucial role in organ development. During embryonic heart development, mesenchymal progenitors of the AV valves arrive from endothelial lining at the endocardial cushion. In this process, *ERBB3* plays a decisive role. The inactivation of the *ERBB3* pathway prevented cells undergoing EndMT and resulted in hypocellular cushions (Rivera-Feliciano et al. 2006). The significant upregulation of *ERBB3* in TGF $\beta$ 1-treated HCAECs is in line with its described importance during embryonic EndMT. However, in MCECs, TGF $\beta$ 1 treatment led to a downregulation of *ErbB3* that was enhanced upon administration of Serelaxin. Interestingly, the results in AAC



mouse hearts were again consistent with the data shown in HCAECs; even though Serelaxin's amelioration of AAC-induced upregulation of *ErbB3* was not significant. This effect might be explained by different signaling patterns in different species. In addition, it has already been shown that the ERBB3 signaling pathway stimulates cardiac fibroblasts and leads to their proliferation, survival and paracrine signaling (Kirabo et al. 2017). This suggests that during AAC-induced cardiac fibrosis, *ErbB3* expression is upregulated in the entire heart and may be absent in the murine endothelial cells.

*FZD7* encodes a 7-transmembrane domain protein (Frizzled-7) that is a receptor for Wnt signaling proteins. Its pathway has emerged as an important regulator of developmental and a wide range of disease processes. Among others, it could be shown that the WNT/FZD signal transduction enables EndMT and leads to cardiac fibrosis (Aisagbonhi et al. 2011). These findings are in line with our results proving an upregulation of *FZD7* *in vitro* and *in vivo* by TGF $\beta$ 1 and AAC respectively. In both cases, the upregulation of *FZD7* was ameliorated by the administration of Serelaxin. However, *FZD7* has recently been reported to maintain endothelial cell function by accumulating at the points of cell-cell contact, associating with VE-cadherin and  $\beta$ -catenin and thereby minimizing the endothelium's paracellular permeability (Ferreira Tojais et al. 2014). Since these cell contacts are naturally lost during EndMT, the upregulation of *Fzd7* could be understood as a compensatory regulation of the endothelium to preserve its integrity.

The next gene that showed a noticeable expression pattern in HCAECs was *GSC* encoding Gooseoid protein, a homeobox transcriptional factor. It was upregulated upon TGF $\beta$ 1 treatment and downregulated upon Serelaxin administration. *GSC* is well known to promote breast cancer metastasis by inducing EMT suggesting a possible, similar effect on EndMT (Hartwell et al. 2006). However, since the HCAEC data generated in the qPCR array could not be consistently replicated neither in MCECs nor in the *in vivo* mouse model, *GSC* was no longer pursued as a possible molecular mediator of Serelaxin.

A significant upregulation could be observed for *GSK3B* gene in HCAECs and MCECs after administration of TGF $\beta$ 1, as well as in AAC-operated hearts. It encodes the beta isoform of glycogen synthase kinase 3 and is an enzyme that not only regulates glucose homeostasis but is also involved in various diseases such as bipolar disorder, Alzheimer's disease, diabetes and HF (Lal et al. 2015). In a mouse model of Bleomycin-induced idiopathic pulmonary fibrosis it has recently been shown that activation of the AKT/GSK3 $\beta$ / $\beta$ -Catenin signaling pathway promotes EndMT and thereby causes pulmonary fibrosis (Jia et al. 2021). The explicit importance of GSK3 $\beta$  for endothelial cells in the context of EndMT and the development of cardiac fibrosis is reinforced by the study from Lal et al. (2014). They examined the function of GSK3 $\beta$  in cardiac fibroblasts. A specific deletion of *Gsk3b* in cardiac fibroblasts led to left ventricular dysfunction and an excessive deposition of collagen in a model of myocardial infarction. This shows that GSK3B has a pro-fibrotic role in endothelial cells and an anti-fibrotic role in fibroblasts. Since Serelaxin was able to attenuate

the upregulation of GSK3B in HCAECs, MCECs and *in vivo*, this gene is an interesting candidate, that is possibly decisively involved in the anti-EndMT and anti-fibrotic effect of Serelaxin. Moreover, several tumor studies revealed that Relaxin promotes matrix invasion by affecting the WNT/ $\beta$ -Catenin and GSK3 $\beta$  pathway (Thompson et al. 2006; Astuti et al. 2015; Fue et al. 2018). Interestingly, in these studies, the Relaxin treatment led to an increase of phosphorylated GSK3 $\beta$  but not total GSK3 $\beta$ . Here, we have studied mRNA of total GSK3 $\beta$  and found decreased expression of Gsk3b in whole heart tissue and cardiac endothelial cells. At first glance, our findings may appear to contradict previous studies but they are in line with the findings of Thanasupawat et al. (2019) who summarized that the respective effect of Relaxin depends on the exposure time, Relaxin concentration as well as on the cell model.

In this study, RAC1 was downregulated after the TGF $\beta$ 1 treatment as well as in AAC-operated hearts. Serelaxin was able to ameliorate the change in expression in each case. However, RAC1 probably does not play a decisive role in the development of the antifibrotic effect of Serelaxin since previous works describe a more profibrotic role to RAC1 (Patel et al. 2019). RAC1, also known as Ras-related C3 botulinum toxin substrate 1, encodes a small signaling G protein which is a member of the RAC subfamily of the RHO family of GTPases. RAC1B, an alternatively spliced isoform of this gene, has been shown to be involved in cytoskeleton organization, membrane trafficking and cell proliferation. Stallings-Mann et al. showed in 2012 that the expression of mouse Rac1b stimulated EMT in lung epithelial cells and thereby promoted lung tumor progression and metastasis. A similar effect on EndMT can therefore be assumed. Furthermore, RAC1 GTPase regulates mineralocorticoid receptor-mediated, pro-fibrotic remodeling in mouse heart (Lavall et al. 2017).

In both AAC-treated hearts and TGF $\beta$ 1-applied endothelial cells, STEAP1 was downregulated to a high degree. Serelaxin was only able to reverse expression *in vitro* but not *in vivo* where Serelaxin even further decreased Steap1 expression. STEAP1, six Transmembrane Epithelial Antigen of Prostate member 1, has so far been found in various cancerous tissues, in particular prostate cancer, and is thought to play a pro-carcinogenic role. In lung adenocarcinoma, STEAP1 was shown to facilitate metastasis and EMT (Huo et al. 2020). Until now, there is only rare data on STEAP1 in cardiac tissue as well as in cardiac endothelial cells. Based on the available literature, the effect of Relaxin on the expression of Steap1 is completely unknown today.

The Notch1 signaling pathway was reactivated by the Serelaxin supplement both *in vitro* and *in vivo*. It seems to be a promising candidate pathway or at least partially respond to the Serelaxin treatment on EndMT and fibrosis. Depending on the context, Notch1 signaling can induce or inhibit EndMT. To mimic a strong Notch1 signaling activation, NICD overexpression was performed. Thereby it was possible to observe that NOTCH1 preserves the endothelial phenotype in the context of adult coronary artery endothelial cells. These findings are in line with a study in a rat model of HF, where Relaxin and Notch1 signaling

were confirmed to be clearly linked to each other (Zhou et al. 2015). The effect of a TGF $\beta$ 1 treatment on the Notch signaling pathway is also dependent on the context. In other cells than endothelial, a positive regulatory role of TGF $\beta$ 1 through activating Notch signaling has been reported. Notch1 and TGF $\beta$  signaling pathways crosstalk in mouse neural stem cells and mouse myoblasts (Blokzijl et al. 2003). Here, the expression of the target for the Notch pathway, Hes1, was increased upon treatment of TGF $\beta$ 1 which is in line with Hajdu et al. (2010) who showed increased levels of HES1 and TIEG expression in human non-Hodgkin B-cell lymphoma cell lines. Notably, both projects focused on the effect of TGF $\beta$ 1 treatment on Notch1 target gene expression rather than on Notch1 expression itself. Contrary to these data, a reduced Notch1 target gene expression was observed in adult Mueller stem cells upon treatment with TGF $\beta$ 1 which is in line with the results of our work (Wu et al. 2014).

In conclusion, this study revealed that Serelaxin impacts different signaling pathways to inhibit EndMT and thereby attenuates cardiac fibrosis. However, several other studies have proven an influence of Relaxin on cardiac fibroblasts. Sassoli et al. (2013) demonstrated that Relaxin prevents cardiac fibroblast-to-myofibroblast transition. This effect was mediated via an upregulation of the Notch1 pathway and consecutive inhibition of TGF $\beta$ /SMAD3 signaling, which is an analogue mechanism to the inhibition of EndMT shown by us. Furthermore, Wu et al. (2018) showed that Serelaxin suppressed the expression of ALK5 in TGF $\beta$ 1-treated cardiac fibroblasts and thereby inhibited the TGF $\beta$ 1/SMAD2/3 signaling pathway. Based on these studies, it can be stated that inhibition of both fibroblast-to-myofibroblast activation and EndMT likely affect fibrosis synergistically.

#### 4.4 Epigenetic regulation of *Rxfp1* by Serelaxin in endothelial cells

Our study is the first to identify RXFP1 as the receptor mediating the EndMT-inhibiting effect of Serelaxin. We not only identified this receptor in *in vitro* studies of EndMT, but also observed Rxfp1 to be downregulated in diseased hearts as compared to healthy hearts *in vivo*. Potentially, one of the most important and novel findings of this study is that Serelaxin rescued expression of Rxfp1 in mice hearts which had undergone AAC to the level of sham operated animals. This study is the first to report that Serelaxin affects histone modifications by an anti-TGF $\beta$ -SMAD2/3 cascade and thus rescues Rxfp1 expression that is downregulated in diseased hearts. The identified mechanism can be described as self-reinforcing feedback: a high dose application of Serelaxin leads to an increased supply of its complementary receptor via the epigenetic mechanism described and thus causes a more pronounced effect despite an initially low expression of the RXFP1 receptor.

In detail, Serelaxin influences histone modifications of the *Rxfp1* promoter by blocking the TGF $\beta$ /SMAD2/3 signaling pathway. These modifications include activating marker H3K4me3 as well as repressive markers subsuming H3K9me3 and H3K27me3, which are all four prominent representatives of histone modification marks.

Methylation is an effective, stable modification of histones. It plays a crucial role during fibrosis and other diseases (Shrishrimal et al. 2019). Trimethylation on the 4<sup>th</sup> and 9<sup>th</sup> lysine residue of the histone H3 protein, H3K4me3 and H3K9me3, respectively, are chromatin modifications that have been associated with transcription in terms of fibrosis and mesenchymal transition. Zhuang et al. (2019) demonstrated that a diminishment of H3K9me3 at the promoter region of the transcription factor ZEB1 led to an inhibition of EMT in epithelial cells. This effect was driven by an application of Schisandrin B, a bioactive chemical compound found in *Schisandra chinensis*, an Asian vine plant. Notably, Schisandrin B led to preservation of epithelial phenotype and inhibited the expression of  $\alpha$ -SMA during EMT induced by TGF $\beta$ 1. The effect on the promoter diminishment of H3K9me3 could be mediated – analogously to that of Serelaxin shown in our study - by an inhibition of the TGF $\beta$ /SMAD2/3 axis. However, the authors did not carry out any experiments to prove this hypothesis. Wang et al. (2018) observed that long non-coding RNA of ZEB1 antisense RNA 1 (lnc ZEB1-AS1) bound directly to HSK4 methyltransferase and thereby promoted H3K4me3 histone modification on ZEB1 promoter region. In their murine model, a tumor suppressor gene (p53) was reported to reduce expression of lnc ZEB1-AS1 and subsequently ameliorated renal dysfunction and fibrosis. However, histone modification affects mesenchymal transition in other organs as well. In a mouse model that was treated with radiation H3K9me3 enrichment in E-Cadherin promoter induced EMT in the lung (Sunnaghatta Nagaraja et al. 2020).

Another prominent repressive mark that was diminished in the promoter region of *Rxfp1* by Serelaxin treatment is H3K27me3, protein H3 being trimethylated at the 27<sup>th</sup> lysine residue. The expression of a catalytic subunit of the enzyme that methylates lysine 27 on histone 3 has recently been shown to be decreased by MAPK7 and thereby inhibits EndMT (Vanchin et al. 2021). Interestingly, Relaxin is known to activate MAPK via Rxfp1 and thereby, as shown in our study, equally inhibits EndMT. For future studies, it would be of great interest to investigate whether Serelaxin induces the expression of its receptor RXFP1 by exhibiting a direct influence on the trimethylation of H3K27 – apart from the TGF $\beta$ /SMAD-associated, decreased accumulation of H3K27me3 on the *Rxfp1* promoter – demonstrated by us, for example via an activation of the MAPK signaling pathway.

H3K27ac indicates acetylation of the lysine residue at N-terminal position 27 of the histone H3 protein. Even though H3K27ac was diminished at the promoter region of *Rxfp1* upon TGF $\beta$ 1 treatment, Serelaxin was not able to enrich the presence of H3K27ac at the observed sites of the *Rxfp1* promoter region. Nevertheless, it cannot be ruled out that Serelaxin has an influence on this histone marker as well and thereby indeed allows for an inhibiting effect on EndMT and cardiac fibrosis. It is possible that the selection of the amplicons merely missed the crucial region of the *Rxfp1* promoter occupied by H3K27ac. During myocardial remodeling (where cardiac fibrosis plays a fundamental role), H3K27ac is widely utilized as a key predictive marker for pathological, epigenetic gene programming (Pei et al. 2020). Acetylation of H3K27 is governed by acetyltransferases whereas histone deacetylases

(HDACs) remove the acetyl group from histone proteins. In the last decade, HDACs were found to play a decisive role in the pathogenesis of cardiac fibrosis as summarized by Lyu et al. (2019). Additionally, they introduce the application of HDAC-inhibitors (which are already approved for clinical use in hematologic tumors and investigated in clinical trials for a variety of other tumors) and discuss their potential applications and limitations in cardiac fibrosis. This is an interesting approach insofar as in our study, Serelaxin was only able to develop the desired anti-fibrotic and consecutively mortality-reducing effect in high doses. Our results suggest that this is probably due to the reduced expression of Rxfp1 under fibrosis. Before the effect of Serelaxin can occur, the expression of the receptor must be rescued which requires a certain concentration of the drug. It can therefore be hypothesized that a combination therapy of an HDAC-inhibitor and a low dose of Serelaxin has a similar antifibrotic effect as a high dose of Serelaxin would have. Considering possible serious side effects of a high dose of Serelaxin, an investigation of HDAC-inhibitor and low dose of Serelaxin treatment would be of exceptional interest and should be approached in further studies.

To summarize, we were the first to show that Serelaxin affects histone modification in terms of EndMT and cardiac fibrosis. Martin et al. (2018) investigated that Relaxin reversed inflammatory and immune signals in aged hearts. They showed evidence that multiple pro-inflammatory molecules are transcriptionally controlled through histone modification or phosphorylation. Finally, they observed that Relaxin regulates phosphorylation of proteins and consequently summarized that “future studies should look into [Relaxin’s] ability to regulate histone modification”. We made the first step to demonstrate that Serelaxin indeed affects histone modification and thereby at least partially enhances its antifibrotic effects. Now, further studies are needed to investigate if not only Serelaxin’s anti-fibrotic but also its anti-inflammatory and pro-hemodynamic potential might be caused by epigenetic regulation such as histone modification.

#### 4.5 Future perspectives and potential applications

The recent phase III trial (RELAX-AHF 2) examined short-term intravenous Serelaxin administration for acute decompensated HF. It did neither show a reduced cardiovascular mortality after 6 months nor did it reduce the worsening of HF after 5 days and therefore failed. Serelaxin is a recombinant form of a hormone. As the name of the hormone is Relaxin, it already suggests, that Serelaxin confers a potential benefit in patients with acute HF first and foremost by a vasodilating (“relaxing”) and thus a systemic blood pressure lowering function. Surprisingly, no greater effect of Serelaxin was found in patients with elevated systolic blood pressure at baseline (Grand et al. 2021). Nevertheless, study-level meta-analyses considered a follow-up, which occurred at an average of 4.5 months (1-6 months), and showed that treatment of Serelaxin was associated with a significant reduction in all-cause mortality with an estimated HR of 0.87 (95% CI, 0.77–0.98,  $p = 0.0261$ ) (Teerlink et

al. 2020). It should therefore be noted that in an overview of all clinical trials Serelaxin did rather exert long-term than short-term effects.

In RELAX-AHF2, Serelaxin was administered intravenously to the patients over 48 hours and the endpoints were defined as the effects on the clinical picture of acute HF. However, since we were able to show that the potential of Serelaxin does not lie in acute recompensating mechanisms, but in the histone modification-mediated, antifibrotic ability, which must be assessed in long-term, we hypothesize that Serelaxin may have a more beneficial effect for chronic rather than acute HF. It would have been of great interest to implement measurement of cardiac fibrosis in both the treatment and placebo groups of RELAX-AHF2. A subgroup analysis could then have assessed whether reduction in fibrosis correlates with the achievement of certain endpoints. Of course, this could also be analyzed in future randomized, placebo-controlled studies. However, a multicenter implementation is likely to be difficult given costly and not widely available clinical diagnostic tools for fibrosis assessment.

Current data show that our approach of high dose Serelaxin therapy to induce the positive feedback loop described above should be pursued and investigated further: Sasipong et al. (2021) exposed mice to pressure overload by transverse aortic constriction and treated them with adeno-associated viral vectors (AAV) harboring rat-derived Rxfp1 cDNA (rRXFP1). Subsequently, mice were treated with Relaxin or saline. The authors observed improved calcium handlings in cardiomyocytes, induction of positive inotropy and amelioration of cardiac dysfunction in AAV and Relaxin treated compared to control groups. Finally, the combined treatment consisting of AAV-mediated expression of rRXFP1 and continuous Relaxin administration attenuated cardiac fibrosis assessed by reduced fibrotic area and declined expression of fibrotic marker genes such as Collagen-1, Collagen-3 and Periostin (Sasipong et al. 2021). Although Serelaxin showed few side effects in all clinical trials, the approach of an ectopic Rxfp1 expression seems to be an interesting opportunity to apply Serelaxin in lower doses and over a shorter period.

Given its biochemical properties and pharmacokinetics, Serelaxin can currently only be administered intravenously and, due to its short half-life, continuously. The need for long-acting agents has been attempted to address using aminoacid mutations on the A chain of Relaxin. These mutations were covalently modified with half-life-extending moieties such as lipids or polyethylene glycol. Notably, the mRNA therapeutic encoding for long-lasting Relaxin and designed for treating cardiac fibrosis and cardiovascular disease was reported to have advanced in clinical development. Based on the knowledge that RXFP1 is primarily activated through the interaction with Relaxin's B chain, it has recently been reported that modifications of the B chain as well as introduction of suitable spacers and fatty acids created a single chain lipidated peptide agonist of RXFP1. This agonist showed high subcutaneous bioavailability, extended half-lives, and *in vivo* efficacy leading to a strong chronotropic effect in pithed rats (Muppidi et al. 2019; Mallart et al. 2021).

These new developments probably enable Serelaxin to be utilized apart from continuous i.v. treatment but rather short-lasting, multiple drug intakes to improve chronic HF and, in particular, cardiac fibrosis. Not only in the heart but also in the lung, it was recently attempted to address the problem of short half-life of Serelaxin. Therefore, Serelaxin was conjugated to biodegradable and non-inflammatory nanoparticles to alleviate its limitation of a short half-life and intranasally delivered to a rodent model of chronic allergic airways disease. Serelaxin thereby attenuated airway inflammation and ameliorated the pro-fibrotic TGF- $\beta$ 1-mediated airway remodeling. The role of the receptor RXFP1 or EndMT was unfortunately not examined here (Chakraborty et al. 2021).

Since Serelaxin has not only shown promising results for the treatment of HF, the novel findings of our work can also be transferred to other fields of medicine. Serelaxin has been tested as an anti-fibrotic agent in systemic sclerosis, a rare but severe rheumatologic disease characterized by progressive fibrosis of the skin and internal organs. The results of clinical trials were controversial. The clinical inefficacy of Serelaxin could be partially explained by the fact that cells from affected skin of systemic sclerosis patients do not express the wildtype form of RXFP1 (Giordano et al. 2012). More recently, the sequencing of the *RXFP1* gene in fibroblasts of systemic sclerosis patients did not reveal any relevant mutations. Analysis of mRNA transcripts showed different mRNA isoforms of *RXFP1* upregulated in diseased samples but not in healthy ones (Corallo et al. 2019). This finding could explain the inefficacy of the anti-fibrotic treatment attempt with Serelaxin. Rescued expression of *RXFP1* in the affected cells would allow Serelaxin to treat systemic sclerosis. Since we are the first to prove that histone modifications affect Rxfp1 expression in terms of fibrotic mechanisms, our data might serve as a relevant trail to follow with the aim to treat systemic sclerosis.

The fact that Serelaxin should by no means be shelved after the failed phase III trial RELAX-AHF2 is shown – in addition to the new results we have collected – from data on the greatest medical and health policy challenge of our time: the Covid-19 pandemic. Relaxin is known to play a crucial role in relaxing bronchi, decreasing lung inflammation, as well as maintaining the lung's perfusion and overall functionality (Alexiou et al. 2013). It was recently shown that different proteins of the SARS-CoV-2 virus bind and inhibit Relaxin receptors and downstream targets (Khan and Islam 2020). In addition to that an increased supply of Serelaxin might competitively inhibit the binding of SARS-CoV-2 to the Relaxin receptor. The positive feedback loop identified in this study could therefore lead to a stabilization of lung function through increased expression of Rxfp1.

To summarize, our results have led us to further understand the beneficial effects of Serelaxin on diseased HF hearts. In particular, the influence on EndMT, the Notch signaling pathway and the epigenetic regulation of its own receptor offer interesting approaches for further research on Serelaxin as a promising drug for the treatment of not only the heart but also various other organ diseases.

## 5 Summary

This study is based on the finding that Relaxin was identified in *Rln1* gene knockout mice as a naturally occurring regulator of collagen turnover in the heart (Du et al. 2003). Additionally, in a model of spontaneously hypertensive rats, Relaxin was able to prevent the fibrogenesis of multiple organs (Lekgabe et al. 2005). However, these studies could not provide any insight into the pathomechanisms or molecular pathways involved. Since an anti-TGF $\beta$ /SMAD3-mediated preventive effect of Relaxin on the activation of fibroblasts was revealed, this suggested an inhibitory influence of Serelaxin on equally SMAD3-mediated profibrotic mechanisms and EndMT (Sassoli et al. 2013). Clinical trials on the administration of Serelaxin in patients suffering from acute HF showed a significant improvement in dyspnea and reduction of early worsening of HF but could not significantly affect systolic parameters such as cardiac output and thereby reinforced the suspicion of a possible influence of Serelaxin on wall tension and cardiac fibrosis (Metra et al. 2019).

Consequently, the aim of this work was to evaluate and assess the precise influence of Serelaxin on the development of cardiac fibrosis. For this purpose, we quantified the dose-dependent, anti-fibrotic effect on interstitial and perivascular fibrosis. As per literature, we hypothesized that Serelaxin could influence EndMT. To examine this hypothesis and to evaluate possible regulatory effects of Serelaxin, EndMT was induced both *in vivo* and *in vitro*. Further, we investigated receptor subtypes through which Serelaxin may potentially mediate its effects in the heart and in endothelial cells. The focus was on the cellular distribution of the receptors and their regulation. However, the most central question was how Serelaxin mediates a possible anti-fibrotic effect. To elucidate on how signaling pathways play a role, and on mechanisms the recombinant form of Relaxin steers for, extensive downstream experiments were performed.

By carrying out this broad-based study, detailed and novel knowledge about the impact of Serelaxin on the diseased heart could be gained: The anti-fibrotic effect of Serelaxin was demonstrated in two independent pressure overload mouse models, AAC and ATII infusion, and was even more pronounced in perivascular than in interstitial fibrotic lesions. The anti-fibrotic effect was associated with lower mortality in mice, but not with an improvement in cardiac performance, which is in line with clinical studies. Furthermore, Serelaxin developed its anti-fibrotic impact at least partially due to an inhibition of EndMT. This influence on EndMT was led through activation of Notch signaling, which was mediated via RXFP1. Finally, this study was able to show for the first time that Serelaxin can prevent histone modifications of the *Rxfp1* promoter by blocking the TGF $\beta$ /SMAD2/3 signaling pathway. As a result, the expression of initially low-expressed *Rxfp1* was upregulated in the sense of a positive feedback loop, whereby the effect of Serelaxin can in principle be potentiated.



## 6 References

- Aisagbonhi O, Rai M, Ryzhov S, Atria N, Feoktistov I, Hatzopoulos AK (2011): Experimental myocardial infarction triggers canonical Wnt signaling and endothelial-to-mesenchymal transition. *Dis Model Mech* 4, 469–483
- Alexiou K, Wilbring M, Matschke K, Dschietzig T (2013): Relaxin protects rat lungs from ischemia-reperfusion injury via inducible NO synthase: role of ERK-1/2, PI3K, and forkhead transcription factor FKHRL1. *PloS One* 8, e75592
- Al-Gobari M, Khatib CE, Pillon F, Gueyffier F (2013): Beta-blockers for the prevention of sudden cardiac death in heart failure patients: a meta-analysis of randomized controlled trials. *BMC Cardiovasc Disord* 13, 52
- Ambale-Venkatesh B, Lima JAC (2015): Cardiac MRI: a central prognostic tool in myocardial fibrosis. *Nat Rev Cardiol* 12, 18–29
- Ammirati E, Cipriani M, Moro C, Raineri C, Pini D, Sormani P, Mantovani R, Varrenti M, Pedrotti P, Conca C, et al. (2018): Clinical Presentation and Outcome in a Contemporary Cohort of Patients With Acute Myocarditis: Multicenter Lombardy Registry. *Circulation* 138, 1088–1099
- Anderson KR, Sutton MGSJ, Lie JT (1979): Histopathological types of cardiac fibrosis in myocardial disease. *J Pathol* 128, 79–85
- Anker SD, Butler J, Filippatos G, Ferreira JP, Bocchi E, Böhm M, Brunner–La Rocca HP, Choi DJ, Chopra V, Chuquiure-Valenzuela E, et al. (2021): Empagliflozin in Heart Failure with a Preserved Ejection Fraction. *N Engl J Med* 385, 1451–1461
- Arciniegas E, Sutton AB, Allen TD, Schor AM (1992): Transforming growth factor beta 1 promotes the differentiation of endothelial cells into smooth muscle-like cells in vitro. *J Cell Sci* 103 ( Pt 2), 521–529
- Arciniegas E, Frid MG, Douglas IS, Stenmark KR (2007): Perspectives on endothelial-to-mesenchymal transition: potential contribution to vascular remodeling in chronic pulmonary hypertension. *Am J Physiol Lung Cell Mol Physiol* 293, L1-8
- Astuti Y, Nakabayashi K, Deguchi M, Ebina Y, Yamada H (2015): Human recombinant H2 relaxin induces AKT and GSK3 $\beta$  phosphorylation and HTR-8/SVneo cell proliferation. *Kobe J Med Sci* 61, 1–8
- Azhar M, Runyan RB, Gard C, Sanford LP, Miller ML, Andringa A, Pawlowski S, Rajan S, Doetschman T (2009): Ligand-Specific Function of Transforming Growth Factor Beta in Epithelial-Mesenchymal Transition in Heart Development. *Dev Dyn Off Publ Am Assoc Anat* 238, 431–442

- Bani D (1997): Relaxin: a pleiotropic hormone. *Gen Pharmacol* 28, 13–22
- Bashey RI, Martinez-Hernandez A, Jimenez SA (1992): Isolation, characterization, and localization of cardiac collagen type VI. Associations with other extracellular matrix components. *Circ Res* 70, 1006–1017
- Bathgate RA, Ivell R, Sanborn BM, Sherwood OD, Summers RJ (2006): International Union of Pharmacology LVII: recommendations for the nomenclature of receptors for relaxin family peptides. *Pharmacol Rev* 58, 7–31
- Bathgate RAD, Samuel CS, Burazin TCD, Layfield S, Claasz AA, Reytomas IGT, Dawson NF, Zhao C, Bond C, Summers RJ, et al. (2002): Human relaxin gene 3 (H3) and the equivalent mouse relaxin (M3) gene. Novel members of the relaxin peptide family. *J Biol Chem* 277, 1148–1157
- Bathgate RAD, Halls ML, van der Westhuizen ET, Callander GE, Kocan M, Summers RJ (2013): Relaxin family peptides and their receptors. *Physiol Rev* 93, 405–80
- Baxter SC, Morales MO, Goldsmith EC (2008): Adaptive Changes in Cardiac Fibroblast Morphology and Collagen Organization as a Result of Mechanical Environment. *Cell Biochem Biophys* 51, 33–44
- Bennett RG, Simpson RL, Hamel FG (2017): Serelaxin increases the antifibrotic action of rosiglitazone in a model of hepatic fibrosis. *World J Gastroenterol* 23, 3999–4006
- Bernaba BN, Chan JB, Lai CK, Fishbein MC (2010): Pathology of late-onset anthracycline cardiomyopathy. *Cardiovasc Pathol* 19, 308–311
- Biernacka A, Frangogiannis NG (2011): Aging and Cardiac Fibrosis. *Aging Dis* 2, 158–173
- Bleumink G, Knetsch A, Sturkenboom M, Straus S, Hofman A, Deckers J, Witteman J, Stricker B (2004): Quantifying the heart failure epidemic: prevalence, incidence rate, lifetime risk and prognosis of heart failure The Rotterdam Study. *Eur Heart J* 25, 1614–1619
- Blokzijl A, Dahlqvist C, Reissmann E, Falk A, Moliner A, Lendahl U, Ibáñez CF (2003): Cross-talk between the Notch and TGF-beta signaling pathways mediated by interaction of the Notch intracellular domain with Smad3. *J Cell Biol* 163, 723–8
- Boström KI, Yao J, Guihard PJ, Blazquez-Medela AM, Yao Y (2016): Endothelial-mesenchymal transition in atherosclerotic lesion calcification. *Atherosclerosis* 253, 124–127
- Boudoulas KD, Hatzopoulos AK (2009): Cardiac repair and regeneration: the Rubik's cube of cell therapy for heart disease. *Dis Model Mech* 2, 344–358
- Brown RD, Ambler SK, Mitchell MD, Long CS (2005): THE CARDIAC FIBROBLAST:

- Therapeutic Target in Myocardial Remodeling and Failure. *Annu Rev Pharmacol Toxicol* 45, 657–687
- Bryant-Greenwood GD, Schwabe C (1994): Human relaxins: chemistry and biology. *Endocr Rev* 15, 5–26
- Büllesbach EE, Schwabe C (1988): On the receptor binding site of relaxins. *Int J Pept Protein Res* 32, 361–367
- Büllesbach EE, Yang S, Schwabe C (1992): The receptor-binding site of human relaxin II. A dual prong-binding mechanism. *J Biol Chem* 267, 22957–22960
- Burchell HB (1960): Unusual Causes of Heart Failure. *Circulation* 21, 436–443
- Burt JR, Zimmerman SL, Kamel IR, Halushka M, Bluemke DA (2014): Myocardial T1 Mapping: Techniques and Potential Applications. *RadioGraphics* 34, 377–395
- Cao Y, Feng B, Chen S, Chu Y, Chakrabarti S (2014): Mechanisms of endothelial to mesenchymal transition in the retina in diabetes. *Invest Ophthalmol Vis Sci* 55, 7321–7331
- Caraballo C, Desai NR, Mulder H, Alhanti B, Wilson FP, Fiuzat M, Felker GM, Piña IL, O'Connor CM, Lindenfeld J, et al. (2019): Clinical Implications of the New York Heart Association Classification. *J Am Heart Assoc* 8, e014240
- Cardenas H, Vieth E, Lee J, Segar M, Liu Y, Nephew KP, Matei D (2014): TGF- $\beta$  induces global changes in DNA methylation during the epithelial-to-mesenchymal transition in ovarian cancer cells. *Epigenetics* 9, 1461–1472
- Chakraborty A, Pinar AA, Lam M, Bourke JE, Royce SG, Selomulya C, Samuel CS (2021): Pulmonary myeloid cell uptake of biodegradable nanoparticles conjugated with an anti-fibrotic agent provides a novel strategy for treating chronic allergic airways disease. *Biomaterials* 273, 120796
- Chang ACY, Fu Y, Garside VC, Niessen K, Chang L, Fuller M, Setiadi A, Smrz J, Kyle A, Minchinton A, et al. (2011): Notch initiates the endothelial-to-mesenchymal transition in the atrioventricular canal through autocrine activation of soluble guanylyl cyclase. *Dev Cell* 21, 288–300
- Chen M, Sinha M, Luxon BA, Bresnick AR, O'Connor KL (2009): Integrin  $\alpha 6\beta 4$  Controls the Expression of Genes Associated with Cell Motility, Invasion, and Metastasis, Including *S100A4* /Metastasin. *J Biol Chem* 284, 1484–1494
- Cheng W, Li X, Liu D, Cui C, Wang X (2021): Endothelial-to-Mesenchymal Transition: Role in Cardiac Fibrosis. *J Cardiovasc Pharmacol Ther* 26, 3–11
- Chigurupati S, Arumugam TV, Son TG, Lathia JD, Jameel S, Mughal MR, Tang SC, Jo DG, Camandola S, Giunta M, et al. (2007): Involvement of notch signaling in wound

healing. *PLoS One* 2, e1167

Choi SH, Nam JK, Kim BY, Jang J, Jin YB, Lee HJ, Park S, Ji YH, Cho J, Lee YJ (2016): HSPB1 Inhibits the Endothelial-to-Mesenchymal Transition to Suppress Pulmonary Fibrosis and Lung Tumorigenesis. *Cancer Res* 76, 1019–30

Chow BSM, Kocan M, Bosnyak S, Sarwar M, Wigg B, Jones ES, Widdop RE, Summers RJ, Bathgate RAD, Hewitson TD, Samuel CS (2014): Relaxin requires the angiotensin II type 2 receptor to abrogate renal interstitial fibrosis. *Kidney Int* 86, 75–85

Cleland JGF, Daubert JC, Erdmann E, Freemantle N, Gras D, Kappenberger L, Tavazzi L, on behalf of The CARE-HF Study Investigators (2006): Longer-term effects of cardiac resynchronization therapy on mortality in heart failure [the CARDiac RESynchronization-Heart Failure (CARE-HF) trial extension phase]. *Eur Heart J* 27, 1928–1932

Cohn JN, Ferrari R, Sharpe N (2000): Cardiac remodeling—concepts and clinical implications: a consensus paper from an international forum on cardiac remodeling. *J Am Coll Cardiol* 35, 569–582

Conrad KP, Novak J (2004): Emerging role of relaxin in renal and cardiovascular function. *Am J Physiol Regul Integr Comp Physiol* 287, R250-261

Conrad KP, Debrah DO, Novak J, Danielson LA, Shroff SG (2004): Relaxin modifies systemic arterial resistance and compliance in conscious, nonpregnant rats. *Endocrinology* 145, 3289–3296

Corallo C, Pinto AM, Renieri A, Chelieschi S, Fioravanti A, Cutolo M, Soldano S, Nuti R, Giordano N (2019): Altered expression of RXFP1 receptor contributes to the inefficacy of relaxin-based anti-fibrotic treatments in systemic sclerosis. *Clin Exp Rheumatol* 37 Suppl 119, 69–75

Creemers EE, Pinto YM (2011): Molecular mechanisms that control interstitial fibrosis in the pressure-overloaded heart. *Cardiovasc Res* 89, 265–272

Dave JM, Bayless KJ (2014): Vimentin as an Integral Regulator of Cell Adhesion and Endothelial Sprouting. *Microcirculation* 21, 333–344

Davidsohn N, Pezone M, Vernet A, Graveline A, Oliver D, Slomovic S, Punthambaker S, Sun X, Liao R, Bonventre JV, Church GM (2019): A single combination gene therapy treats multiple age-related diseases. *Proc Natl Acad Sci U S A* 116, 23505–23511

DeLisser HM, Baldwin HS, Albelda SM (1997): Platelet Endothelial Cell Adhesion Molecule 1 (PECAM-1/CD31): A Multifunctional Vascular Cell Adhesion Molecule. *Trends Cardiovasc Med* 7, 203–210

Du XJ, Samuel CS, Gao XM, Zhao L, Parry LJ, Tregear GW (2003): Increased myocardial collagen and ventricular diastolic dysfunction in relaxin deficient mice: a gender-specific phenotype. *Cardiovasc Res* 57, 395–404

- Duan Q, McMahon S, Anand P, Shah H, Thomas S, Salunga HT, Huang Y, Zhang R, Sahadevan A, Lemieux ME, et al. (2017): BET bromodomain inhibition suppresses innate inflammatory and profibrotic transcriptional networks in heart failure. *Sci Transl Med* 9, eaah5084
- Eisenberg LM, Markwald RR (1995): Molecular regulation of atrioventricular valvuloseptal morphogenesis. *Circ Res* 77, 1–6
- Elliott DA, Kirk EP, Yeoh T, Chandar S, McKenzie F, Taylor P, Grossfeld P, Fatkin D, Jones O, Hayes P, et al. (2003): Cardiac homeobox gene NKX2-5 mutations and congenital heart disease: associations with atrial septal defect and hypoplastic left heart syndrome. *J Am Coll Cardiol* 41, 2072–2076
- Ertl G, Frantz S (2005): Healing after myocardial infarction. *Cardiovasc Res* 66, 22–32
- European Medicines Agency (2014): Assessment report EMA/303748/2014.
- Everett RJ, Stirrat CG, Semple SIR, Newby DE, Dweck MR, Mirsadraee S (2016): Assessment of myocardial fibrosis with T1 mapping MRI. *Clin Radiol* 71, 768–778
- Felisbino MB, McKinsey TA (2018): Epigenetics in Cardiac Fibrosis. *JACC Basic Transl Sci* 3, 704–715
- Ferlin A, Menegazzo M, Giancesello L, Selice R, Foresta C (2012): Effect of relaxin on human sperm functions. *J Androl* 33, 474–482
- Ferreira Tojais N, Peghaire C, Franzl N, Larrieu-Lahargue F, Jaspard B, Reynaud A, Moreau C, Couffignal T, Dupl a C, Dufourcq P (2014): Frizzled7 controls vascular permeability through the Wnt-canonical pathway and cross-talk with endothelial cell junction complexes. *Cardiovasc Res* 103, 291–303
- Festing MF (1979): Properties of inbred strains and outbred stocks, with special reference to toxicity testing. *J Toxicol Environ Health* 5, 53–68
- Fevold HL, Hisaw FL, Meyer RK (1930): The Relaxative Hormone Of The Corpus Luteum. Its Purification And Concentration. *J Am Chem Soc* 52, 3340–3348
- Flack EC, Lindsey ML, Squires CE, Kaplan BS, Stroud RE, Clark LL, Escobar PG, Yarbrough WM, Spinale FG (2006): Alterations in cultured myocardial fibroblast function following the development of left ventricular failure. *J Mol Cell Cardiol* 40, 474–483
- Frantz C, Stewart KM, Weaver VM (2010): The extracellular matrix at a glance. *J Cell Sci* 123, 4195–4200
- Frid MG, Kale VA, Stenmark KR (2002): Mature Vascular Endothelium Can Give Rise to Smooth Muscle Cells via Endothelial-Mesenchymal Transdifferentiation: In Vitro Analysis. *Circ Res* 90, 1189–1196

- Fue M, Miki Y, Takagi K, Hashimoto C, Yaegashi N, Suzuki T, Ito K (2018): Relaxin 2/RXFP1 Signaling Induces Cell Invasion via the  $\beta$ -Catenin Pathway in Endometrial Cancer. *Int J Mol Sci* 19
- Gast MJ (1983): Characterization of preprorelaxin by tryptic digestion and inhibition of its conversion to prorelaxin by amino acid analogs. *J Biol Chem* 258, 9001–9004
- Gerd Herold: *Innere Medizin* 2021. 2020
- Giam B, Chu PY, Kuruppu S, Smith AI, Horlock D, Murali A, Kiriazis H, Du XJ, Kaye DM, Rajapakse NW (2018): Serelaxin attenuates renal inflammation and fibrosis in a mouse model of dilated cardiomyopathy. *Exp Physiol* 103, 1593–1602
- Giordano N, Volpi N, Franci D, Corallo C, Fioravanti A, Papakostas P, Montella A, Biagioli M, Fimiani M, Grasso G, et al. (2012): Expression of RXFP1 in skin of scleroderma patients and control subjects. *Scand J Rheumatol* 41, 391–395
- Goh KY, He L, Song J, Jinno M, Rogers AJ, Sethu P, Halade GV, Rajasekaran NS, Liu X, Prabhu SD, et al. (2019): Mitoquinone ameliorates pressure overload-induced cardiac fibrosis and left ventricular dysfunction in mice. *Redox Biol* 21, 101100
- Gong H, Lyu X, Wang Q, Hu M, Zhang X (2017): Endothelial to mesenchymal transition in the cardiovascular system. *Life Sci* 184, 95–102
- Goumans MJ, Valdimarsdottir G, Itoh S, Lebrin F, Larsson J, Mummery C, Karlsson S, ten Dijke P (2003): Activin receptor-like kinase (ALK)1 is an antagonistic mediator of lateral TGF $\beta$ /ALK5 signaling. *Mol Cell* 12, 817–828
- Graham-Brown MPM, Patel AS, Stensel DJ, March DS, Marsh A-M, McAdam J, McCann GP, Burton JO (2017): Imaging of Myocardial Fibrosis in Patients with End-Stage Renal Disease: Current Limitations and Future Possibilities. *BioMed Res Int* 2017, 1–14
- Grand J, Miger K, Sajadieh A, Køber L, Torp-Pedersen C, Ertl G, López-Sendón J, Pietro Maggioni A, Teerlink JR, Sato N, et al. (2021): Systolic Blood Pressure and Outcome in Patients Admitted With Acute Heart Failure: An Analysis of Individual Patient Data From 4 Randomized Clinical Trials. *J Am Heart Assoc* 10
- Gunnarsen JM, Fu P, Roche PJ, Tregear GW (1996): Expression of human relaxin genes: characterization of a novel alternatively-spliced human relaxin mRNA species. *Mol Cell Endocrinol* 118, 85–94
- Hajdu M, Kopper L, Sebestyén A (2010): Notch-regulation upon Dll4-stimulation of TGF $\beta$ -induced apoptosis and gene expression in human B-cell non-Hodgkin lymphomas. *Scand J Immunol* 71, 29–37
- Harper JA, Yuan JS, Tan JB, Visan I, Guidos CJ (2003): Notch signaling in development and disease. *Clin Genet* 64, 461–472

- Hartwell KA, Muir B, Reinhardt F, Carpenter AE, Sgroi DC, Weinberg RA (2006): The Spemann organizer gene, Goosecoid, promotes tumor metastasis. *Proc Natl Acad Sci U S A* 103, 18969–18974
- Hashimura H, Kimura F, Ishibashi-Ueda H, Morita Y, Higashi M, Nakano S, Iguchi A, Uotani K, Sugimura K, Naito H (2017): Radiologic-Pathologic Correlation of Primary and Secondary Cardiomyopathies: MR Imaging and Histopathologic Findings in Hearts from Autopsy and Transplantation. *RadioGraphics* 37, 719–736
- Heeg MHJ, Koziolk MJ, Vasko R, Schaefer L, Sharma K, Müller GA, Strutz F (2005): The antifibrotic effects of relaxin in human renal fibroblasts are mediated in part by inhibition of the Smad2 pathway. *Kidney Int* 68, 96–109
- Heinke J, Wehofsits L, Zhou Q, Zoeller C, Baar KM, Helbing T, Laib A, Augustin H, Bode C, Patterson C, Moser M (2008): BMPER is an endothelial cell regulator and controls bone morphogenetic protein-4-dependent angiogenesis. *Circ Res* 103, 804–812
- High FA, Epstein JA (2008): The multifaceted role of Notch in cardiac development and disease. *Nat Rev Genet* 9, 49–61
- Hisaw FL (1926): Experimental relaxation of the pubic ligament of the guinea pig. *Exp Biol Med* 23, 661–663
- Ho JE, Liu C, Lyass A, Courchesne P, Pencina MJ, Vasan RS, Larson MG, Levy D (2012): Galectin-3, a Marker of Cardiac Fibrosis, Predicts Incident Heart Failure in the Community. *J Am Coll Cardiol* 60, 1249–1256
- Hombach-Klonisch S, Bialek J, Trojanowicz B, Weber E, Holzhausen H-J, Silvertown JD, Summerlee AJ, Dralle H, Hoang-Vu C, Klonisch T (2006): Relaxin enhances the oncogenic potential of human thyroid carcinoma cells. *Am J Pathol* 169, 617–632
- Hsu SY, Nakabayashi K, Nishi S, Kumagai J, Kudo M, Sherwood OD, Hsueh AJW (2002): Activation of orphan receptors by the hormone relaxin. *Science* 295, 671–674
- Huang Y, Qi Y, Du JQ, Zhang D (2014): MicroRNA-34a regulates cardiac fibrosis after myocardial infarction by targeting Smad4. *Expert Opin Ther Targets* 1–11
- Hudson P, Haley J, John M, Cronk M, Crawford R, Haralambidis J, Tregear G, Shine J, Niall H (1983): Structure of a genomic clone encoding biologically active human relaxin. *Nature* 301, 628–631
- Humbel RE (1990): Insulin-like growth factors I and II. *Eur J Biochem* 190, 445–462
- Huo SF, Shang WL, Yu M, Ren XP, Wen HX, Chai CY, Sun L, Hui K, Liu LH, Wei SH, et al. (2020): STEAP1 facilitates metastasis and epithelial-mesenchymal transition of lung adenocarcinoma via the JAK2/STAT3 signaling pathway. *Biosci Rep* 40, BSR20193169

- Ichihara S, Senbonmatsu T, Price E, Ichiki T, Gaffney FA, Inagami T (2001): Angiotensin II Type 2 Receptor Is Essential for Left Ventricular Hypertrophy and Cardiac Fibrosis in Chronic Angiotensin II-Induced Hypertension. *Circulation* 104, 346–351
- Inagawa K, Miyamoto K, Yamakawa H, Muraoka N, Sadahiro T, Umei T, Wada R, Katsumata Y, Kaneda R, Nakade K, et al. (2012): Induction of Cardiomyocyte-Like Cells in Infarct Hearts by Gene Transfer of Gata4, Mef2c, and Tbx5. *Circ Res* 111, 1147–1156
- Inamdar Arati, Inamdar Ajinkya (2016): Heart Failure: Diagnosis, Management and Utilization. *J Clin Med* 5, 62
- Isoyama S, Nitta-Komatsubara Y (2002): Acute and chronic adaptation to hemodynamic overload and ischemia in the aged heart. *Heart Fail Rev* 7, 63–69
- Iyengar R (1993): Molecular and functional diversity of mammalian Gs-stimulated adenylyl cyclases. *FASEB J Off Publ Fed Am Soc Exp Biol* 7, 768–775
- Iyer A, Fenning A, Lim J, Le GT, Reid RC, Halili MA, Fairlie DP, Brown L (2010): Antifibrotic activity of an inhibitor of histone deacetylases in DOCA-salt hypertensive rats. *Br J Pharmacol* 159, 1408–1417
- Jellis C, Martin J, Narula J, Marwick TH (2010): Assessment of Nonischemic Myocardial Fibrosis. *J Am Coll Cardiol* 56, 89–97
- Jeyabalan A, Shroff SG, Novak J, Conrad KP (2007): The vascular actions of relaxin. *Adv Exp Med Biol* 612, 65–87
- Jia W, Wang Z, Gao C, Wu J, Wu Q (2021): Trajectory modeling of endothelial-to-mesenchymal transition reveals galectin-3 as a mediator in pulmonary fibrosis. *Cell Death Dis* 12, 327
- Jiang Y, Reynolds C, Xiao C, Feng W, Zhou Z, Rodriguez W, Tyagi SC, Eaton JW, Saari JT, Kang YJ (2007): Dietary copper supplementation reverses hypertrophic cardiomyopathy induced by chronic pressure overload in mice. *J Exp Med* 204, 657–666
- Kamat AA, Feng S, Bogatcheva NV, Truong A, Bishop CE, AgoulNIK AI (2004): Genetic targeting of relaxin and insulin-like factor 3 receptors in mice. *Endocrinology* 145, 4712–4720
- Kamat AA, Feng S, AgoulNIK IU, Kheradmand F, Bogatcheva NV, Coffey D, Sood AK, AgoulNIK AI (2006): The role of relaxin in endometrial cancer. *Cancer Biol Ther* 5, 71–77
- Kantharia BK (2010): Cardiac arrhythmias in congestive heart failure. *Expert Rev Cardiovasc Ther* 8, 137–140
- Karow T: Allgemeine und Spezielle Pharmakologie und Toxikologie 2020. 2019
- Kass DA, Bronzwaer JGF, Paulus WJ (2004): What mechanisms underlie diastolic



- dysfunction in heart failure? *Circ Res* 94, 1533–1542
- Katz SD (2018): Pathophysiology of Chronic Systolic Heart Failure. A View from the Periphery. *Ann Am Thorac Soc* 15, S38–S41
- Kawano H, Do YS, Kawano Y, Starnes V, Barr M, Law RE, Hsueh WA (2000): Angiotensin II has multiple profibrotic effects in human cardiac fibroblasts. *Circulation* 101, 1130–1137
- Khan MAAK, Islam ABMMK (2020): SARS-CoV-2 Proteins Exploit Host's Genetic and Epigenetic Mediators for the Annexation of Key Host Signaling Pathways. *Front Mol Biosci* 7, 598583
- Khanna D, Clements PJ, Furst DE, Korn JH, Ellman M, Rothfield N, Wigley FM, Moreland LW, Silver R, Kim YH, et al. (2009): Recombinant human relaxin in the treatment of systemic sclerosis with diffuse cutaneous involvement: a randomized, double-blind, placebo-controlled trial. *Arthritis Rheum* 60, 1102–1111
- Kimura H (2013): Histone modifications for human epigenome analysis. *J Hum Genet* 58, 439–445
- Kirabo A, Ryzhov S, Gupte M, Sengsayadeth S, Gumina RJ, Sawyer DB, Galindo CL (2017): Neuregulin-1 $\beta$  induces proliferation, survival and paracrine signaling in normal human cardiac ventricular fibroblasts. *J Mol Cell Cardiol* 105, 59–69
- Kong P, Christia P, Frangogiannis NG (2014): The pathogenesis of cardiac fibrosis. *Cell Mol Life Sci* 71, 549–574
- Konstam MA, Kiernan MS, Bernstein D, Bozkurt B, Jacob M, Kapur NK, Kociol RD, Lewis EF, Mehra MR, Pagani FD, et al. (2018): Evaluation and Management of Right-Sided Heart Failure: A Scientific Statement From the American Heart Association. *Circulation* 137
- Kramann R, Schneider RK, DiRocco DP, Machado F, Fleig S, Bondzie PA, Henderson JM, Ebert BL, Humphreys BD (2015): Perivascular Gli1+ Progenitors Are Key Contributors to Injury-Induced Organ Fibrosis. *Cell Stem Cell* 16, 51–66
- Kumagai J, Hsu SY, Matsumi H, Roh JS, Fu P, Wade JD, Bathgate RAD, Hsueh AJW (2002): INSL3/Leydig insulin-like peptide activates the LGR8 receptor important in testis descent. *J Biol Chem* 277, 31283–31286
- Lal H, Ahmad F, Zhou J, Yu JE, Vagnozzi RJ, Guo Y, Yu D, Tsai EJ, Woodgett J, Gao E, Force T (2014): Cardiac fibroblast glycogen synthase kinase-3 $\beta$  regulates ventricular remodeling and dysfunction in ischemic heart. *Circulation* 130, 419–430
- Lal H, Ahmad F, Woodgett J, Force T (2015): The GSK-3 family as therapeutic target for myocardial diseases. *Circ Res* 116, 138–149

- Lam M, Royce SG, Samuel CS, Bourke JE (2018): Serelaxin as a novel therapeutic opposing fibrosis and contraction in lung diseases. *Pharmacol Ther* 187, 61–70
- Lapinskas T, Kelle S, Grune J, Foryst-Ludwig A, Meyborg H, Jeuthe S, Wellnhofer E, Elsanhoury A, Pieske B, Gebker R, et al. (2020): Serelaxin Improves Regional Myocardial Function in Experimental Heart Failure: An In Vivo Cardiac Magnetic Resonance Study. *J Am Heart Assoc* 9, e013702
- Lavall D, Schuster P, Jacobs N, Kazakov A, Böhm M, Laufs U (2017): Rac1 GTPase regulates 11 $\beta$  hydroxysteroid dehydrogenase type 2 and fibrotic remodeling. *J Biol Chem* 292, 7542–7553
- Lee WJ, Park JH, Shin JU, Noh H, Lew DH, Yang WI, Yun CO, Lee KH, Lee JH (2015): Endothelial-to-mesenchymal transition induced by Wnt 3a in keloid pathogenesis. *Wound Repair Regen Off Publ Wound Heal Soc Eur Tissue Repair Soc* 23, 435–442
- Lekgabe ED, Kiriazis H, Zhao C, Xu Q, Moore XL, Su Y, Bathgate RAD, Du XJ, Samuel CS (2005): Relaxin reverses cardiac and renal fibrosis in spontaneously hypertensive rats. *Hypertens Dallas Tex* 1979 46, 412–8
- Levet S, Ouarné M, Ciais D, Coutton C, Subileau M, Mallet C, Ricard N, Bidart M, Debillon T, Faravelli F, et al. (2015): BMP9 and BMP10 are necessary for proper closure of the ductus arteriosus. *Proc Natl Acad Sci U S A* 112, E3207-3215
- Li J, Qu X, Bertram JF (2009): Endothelial-myofibroblast transition contributes to the early development of diabetic renal interstitial fibrosis in streptozotocin-induced diabetic mice. *Am J Pathol* 175, 1380–1388
- Liao R, Jain M, Cui L, D’Agostino J, Aiello F, Luptak I, Ngoy S, Mortensen RM, Tian R (2002): Cardiac-specific overexpression of GLUT1 prevents the development of heart failure attributable to pressure overload in mice. *Circulation* 106, 2125–2131
- Lili LN, Matyunina LV, Walker LD, Wells SL, Benigno BB, McDonald JF (2013): Molecular profiling supports the role of epithelial-to-mesenchymal transition (EMT) in ovarian cancer metastasis. *J Ovarian Res* 6, 49
- Lin F, Wang N, Zhang TC (2012): The role of endothelial–mesenchymal transition in development and pathological process. *IUBMB Life* 64, 717–723
- Lindner D, Li J, Savvatis K, Klingel K, Blankenberg S, Tschöpe C, Westermann D (2014): Cardiac fibroblasts aggravate viral myocarditis: cell specific coxsackievirus B3 replication. *Mediators Inflamm* 2014, 519528
- Lip GY, Gibbs CR, Beevers DG (2000): ABC of heart failure: aetiology. *BMJ* 320, 104–107
- Liu LCY, Voors AA, Teerlink JR, Cotter G, Davison BA, Felker GM, Filippatos G, Chen Y, Greenberg BH, Ponikowski P, et al. (2016): Effects of serelaxin in acute heart failure

patients with renal impairment: results from RELAX-AHF. *Clin Res Cardiol Off J Ger Card Soc* 105, 727–737

Liu T, Song D, Dong J, Zhu P, Liu J, Liu W, Ma X, Zhao L, Ling S (2017): Current Understanding of the Pathophysiology of Myocardial Fibrosis and Its Quantitative Assessment in Heart Failure. *Front Physiol* 8, 238

López B, González A, Beaumont J, Querejeta R, Larman M, Díez J (2007): Identification of a Potential Cardiac Antifibrotic Mechanism of Torasemide in Patients With Chronic Heart Failure. *J Am Coll Cardiol* 50, 859–867

López B, Querejeta R, González A, Beaumont J, Larman M, Díez J (2009): Impact of treatment on myocardial lysyl oxidase expression and collagen cross-linking in patients with heart failure. *Hypertens Dallas Tex 1979* 53, 236–242

López B, González A, Ravassa S, Beaumont J, Moreno MU, San José G, Querejeta R, Díez J (2015): Circulating Biomarkers of Myocardial Fibrosis. *J Am Coll Cardiol* 65, 2449–2456

Lopez D, Niu G, Huber P, Carter WB (2009): Tumor-induced upregulation of Twist, Snail, and Slug represses the activity of the human VE-cadherin promoter. *Arch Biochem Biophys* 482, 77–82

Loring Z, Zareba W, McNitt S, Strauss DG, Wagner GS, Daubert JP (2013): ECG Quantification of Myocardial Scar and Risk Stratification in MADIT-II: ECG Scar Quantification in MADIT-II. *Ann Noninvasive Electrocardiol* 18, 427–435

Louvi A, Artavanis-Tsakonas S (2012): Notch and disease: a growing field. *Semin Cell Dev Biol* 23, 473–480

Lyu X, Hu M, Peng J, Zhang X, Sanders YY (2019): HDAC inhibitors as antifibrotic drugs in cardiac and pulmonary fibrosis. *Ther Adv Chronic Dis* 10, 2040622319862697

Mack JJ, Iruela-Arispe ML (2018): NOTCH regulation of the endothelial cell phenotype. *Curr Opin Hematol* 25, 212–218

Madias JE (2007): The resting electrocardiogram in the management of patients with congestive heart failure: established applications and new insights. *Pacing Clin Electrophysiol PACE* 30, 123–128

Mahler GJ, Frenzl CM, Cao Q, Butcher JT (2014): Effects of shear stress pattern and magnitude on mesenchymal transformation and invasion of aortic valve endothelial cells. *Biotechnol Bioeng* 111, 2326–2337

Mallart S, Ingenito R, Bianchi E, Bresciani A, Esposito S, Gallo M, Magotti P, Monteagudo E, Orsatti L, Roversi D, et al. (2021): Identification of Potent and Long-Acting Single-Chain Peptide Mimetics of Human Relaxin-2 for Cardiovascular Diseases. *J Med Chem* 64, 2139–2150

- Mandinov L (2000): Diastolic heart failure. *Cardiovasc Res* 45, 813–825
- Martin B, Gabris-Weber BA, Reddy R, Romero G, Chattopadhyay A, Salama G (2018): Relaxin reverses inflammatory and immune signals in aged hearts. *PloS One* 13, e0190935
- Maruyama S, Wu CL, Yoshida S, Zhang D, Li PH, Wu F, Parker Duffen J, Yao R, Jardin B, Adham IM, et al. (2018): Relaxin Family Member Insulin-Like Peptide 6 Ameliorates Cardiac Fibrosis and Prevents Cardiac Remodeling in Murine Heart Failure Models. *J Am Heart Assoc* 7
- McCarthy JC, Aronovitz M, DuPont JJ, Calamaras TD, Jaffe IZ, Blanton RM (2017): Short-Term Administration of Serelaxin Produces Predominantly Vascular Benefits in the Angiotensin II/L-NAME Chronic Heart Failure Model. *JACC Basic Transl Sci* 2, 285–296
- McCullough PA, Nowak RM, McCord J, Hollander JE, Herrmann HC, Steg PG, Duc P, Westheim A, Omland T, Knudsen CW, et al. (2002): B-type natriuretic peptide and clinical judgment in emergency diagnosis of heart failure: analysis from Breathing Not Properly (BNP) Multinational Study. *Circulation* 106, 416–422
- McDonagh TA, Metra M, Adamo M, Gardner RS, Baumbach A, Böhm M, Burri H, Butler J, Čelutkienė J, Chioncel O, et al. (2021): 2021 ESC Guidelines for the diagnosis and treatment of acute and chronic heart failure. *Eur Heart J* 42, 3599–3726
- Medici D, Kalluri R (2012): Endothelial-mesenchymal transition and its contribution to the emergence of stem cell phenotype. *Semin Cancer Biol* 22, 379–384
- Mehra MR, Kobashigawa J, Starling R, Russell S, Uber PA, Parameshwar J, Mohacsi P, Augustine S, Aaronson K, Barr M (2006): Listing criteria for heart transplantation: International Society for Heart and Lung Transplantation guidelines for the care of cardiac transplant candidates--2006. *J Heart Lung Transplant Off Publ Int Soc Heart Transplant* 25, 1024–1042
- Metra M, Teerlink JR, Cotter G, Davison BA, Felker GM, Filippatos G, Greenberg BH, Pang PS, Ponikowski P, Voors AA, et al. (2019): Effects of Serelaxin in Patients with Acute Heart Failure. *N Engl J Med* 381, 716–726
- Michael Seganish W, Lynch JJ, Sorota S: Treatments for Heart Failure. In: *Comprehensive Medicinal Chemistry III*. Elsevier 2017, 628–662
- Micheletti R, Plaisance I, Abraham BJ, Sarre A, Ting CC, Alexanian M, Maric D, Maison D, Nemir M, Young RA, et al. (2017): The long noncoding RNA *Wisper* controls cardiac fibrosis and remodeling. *Sci Transl Med* 9, eaai9118
- Miyamoto K, Akiyama M, Tamura F, Isomi M, Yamakawa H, Sadahiro T, Muraoka N, Kojima H, Haginiwa S, Kurotsu S, et al. (2018): Direct In Vivo Reprogramming with

- Sendai Virus Vectors Improves Cardiac Function after Myocardial Infarction. *Cell Stem Cell* 22, 91-103.e5
- Miyares MA, Davis KA (2013): Serelaxin, a „breakthrough“ investigational intravenous agent for acute heart failure. *P T Peer-Rev J Formul Manag* 38, 606–611
- Mookerjee I, Hewitson TD, Halls ML, Summers RJ, Mathai ML, Bathgate RAD, Tregear GW, Samuel CS (2009): Relaxin inhibits renal myofibroblast differentiation via RXFP1, the nitric oxide pathway, and Smad2. *FASEB J Off Publ Fed Am Soc Exp Biol* 23, 1219–29
- Moore LD, Le T, Fan G (2013): DNA methylation and its basic function. *Neuropsychopharmacol Off Publ Am Coll Neuropsychopharmacol* 38, 23–38
- Moore-Morris T, Guimarães-Camboa N, Banerjee I, Zambon AC, Kisseleva T, Velayoudon A, Stallcup WB, Gu Y, Dalton ND, Cedenilla M, et al. (2014): Resident fibroblast lineages mediate pressure overload–induced cardiac fibrosis. *J Clin Invest* 124, 2921–2934
- Mosterd A, Hoes AW (2007): Clinical epidemiology of heart failure. *Heart* 93, 1137–1146
- Mukherjee D, Sen S (1991): Alteration of collagen phenotypes in ischemic cardiomyopathy. *J Clin Invest* 88, 1141–1146
- Mukherjee D, Sen S (1993): Alteration of Cardiac Collagen Phenotypes in Hypertensive Hypertrophy: Role of Blood Pressure. *J Mol Cell Cardiol* 25, 185–196
- Muñoz-Chápuli R, Pérez-Pomares JM, Macías D, García-Garrido L, Carmona R, González-Iriarte M (2001): The epicardium as a source of mesenchyme for the developing heart. *Ital J Anat Embryol Arch Ital Anat Ed Embriologia* 106, 187–196
- Muppidi A, Lee SJ, Hsu CH, Zou H, Lee C, Pflimlin E, Mahankali M, Yang P, Chao E, Ahmad I, et al. (2019): Design and Synthesis of Potent, Long-Acting Lipidated Relaxin-2 Analogs. *Bioconjug Chem* 30, 83–89
- Nagarajan S, Benito E, Fischer A, Johnsen SA (2015): H4K12ac is regulated by estrogen receptor-alpha and is associated with BRD4 function and inducible transcription. *Oncotarget* 6, 7305–17
- Nakajima H, Nakajima HO, Salcher O, Dittiè AS, Dembowsky K, Jing S, Field LJ (2000): Atrial but not ventricular fibrosis in mice expressing a mutant transforming growth factor-beta(1) transgene in the heart. *Circ Res* 86, 571–579
- Nakano J, Marui A, Muranaka H, Masumoto H, Noma H, Tabata Y, Ido A, Tsubouchi H, Ikeda T, Sakata R (2014): Effects of hepatocyte growth factor in myocarditis rats induced by immunization with porcine cardiac myosin. *Interact Cardiovasc Thorac Surg* 18, 300–307

- Neefs J, van den Berg NWE, Limpens J, Berger WR, Boekholdt SM, Sanders P, de Groot JR (2017): Aldosterone Pathway Blockade to Prevent Atrial Fibrillation: A Systematic Review and Meta-Analysis. *Int J Cardiol* 231, 155–161
- Neill JD, Knobil E (Hrsg.): Knobil and Neill's physiology of reproduction. 3. ed. ff.; Elsevier/Academic Press, Amsterdam 2006
- Nemir M, Metrich M, Plaisance I, Lepore M, Cruchet S, Berthonneche C, Sarre A, Radtke F, Pedrazzini T (2014): The Notch pathway controls fibrotic and regenerative repair in the adult heart. *Eur Heart J* 35, 2174–2185
- Nistri S, Bani D (2003): Relaxin receptors and nitric oxide synthases: search for the missing link. *Reprod Biol Endocrinol RBE* 1, 5
- Nistri S, Sassoli C, Bani D (2017): Notch Signaling in Ischemic Damage and Fibrosis: Evidence and Clues from the Heart. *Front Pharmacol* 8, 187
- Nural-Guvener HF, Zakharova L, Nimlos J, Popovic S, Mastroeni D, Gaballa MA (2014): HDAC class I inhibitor, Mocetinostat, reverses cardiac fibrosis in heart failure and diminishes CD90+ cardiac myofibroblast activation. *Fibrogenesis Tissue Repair* 7, 10
- O'Byrne EM, Carriere BT, Sorensen L, Segaloff A, Schwabe C, Steinetz BG (1978): Plasma immunoreactive relaxin levels in pregnant and nonpregnant women. *J Clin Endocrinol Metab* 47, 1106–1110
- Osheroff PL, Ho WH (1993): Expression of relaxin mRNA and relaxin receptors in postnatal and adult rat brains and hearts. Localization and developmental patterns. *J Biol Chem* 268, 15193–15199
- Overbeek PA, Gorlov IP, Sutherland RW, Houston JB, Harrison WR, Boettger-Tong HL, Bishop CE, AgoulNIK AI (2001): A transgenic insertion causing cryptorchidism in mice. *Genes N Y N* 2000 30, 26–35
- Palazzuoli A, Gallotta M, Quatrini I, Nuti R (2010): Natriuretic peptides (BNP and NT-proBNP): measurement and relevance in heart failure. *Vasc Health Risk Manag* 6, 411–418
- Palejwala S, Stein D, Wojtczuk A, Weiss G, Goldsmith LT (1998): Demonstration of a relaxin receptor and relaxin-stimulated tyrosine phosphorylation in human lower uterine segment fibroblasts. *Endocrinology* 139, 1208–1212
- Park M, Shen YT, Gaussin V, Heyndrickx GR, Bartunek J, Resuello RRG, Natividad FF, Kitsis RN, Vatner DE, Vatner SF (2009): Apoptosis predominates in nonmyocytes in heart failure. *Am J Physiol Heart Circ Physiol* 297, 785–91
- Passino C, Barison A, Vergaro G, Gabutti A, Borrelli C, Emdin M, Clerico A (2015): Markers of fibrosis, inflammation, and remodeling pathways in heart failure. *Clin Chim Acta* 443, 29–38

- Patel S, Tang J, Overstreet JM, Anorga S, Lian F, Arnouk A, Goldschmeding R, Higgins PJ, Samarakoon R (2019): Rac-GTPase promotes fibrotic TGF- $\beta$ 1 signaling and chronic kidney disease *via* EGFR, p53, and Hippo/YAP/TAZ pathways. *FASEB J* 33, 9797–9810
- Pattanayak P, Bleumke DA (2015): Tissue Characterization of the Myocardium. *Radiol Clin North Am* 53, 413–423
- Paulus WJ, Tschöpe C, Sanderson JE, Rusconi C, Flachskampf FA, Rademakers FE, Marino P, Smiseth OA, De Keulenaer G, Leite-Moreira AF, et al. (2007): How to diagnose diastolic heart failure: a consensus statement on the diagnosis of heart failure with normal left ventricular ejection fraction by the Heart Failure and Echocardiography Associations of the European Society of Cardiology. *Eur Heart J* 28, 2539–2550
- Pei J, Harakalova M, Treibel TA, Lumbers RT, Boukens BJ, Efimov IR, van Dinter JT, González A, López B, El Azzouzi H, et al. (2020): H3K27ac acetylome signatures reveal the epigenomic reorganization in remodeled non-failing human hearts. *Clin Epigenetics* 12, 106
- Peinado H, Portillo F, Cano A (2004): Transcriptional regulation of cadherins during development and carcinogenesis. *Int J Dev Biol* 48, 365–375
- Peng H, Li Y, Wang C, Zhang J, Chen Y, Chen W, Cao J, Wang Y, Hu Z, Lou T (2016): ROCK1 Induces Endothelial-to-Mesenchymal Transition in Glomeruli to Aggravate Albuminuria in Diabetic Nephropathy. *Sci Rep* 6, 20304
- Peterzan MA, Rider OJ, Anderson LJ (2016): The Role of Cardiovascular Magnetic Resonance Imaging in Heart Failure. *Card Fail Rev* 2, 115–122
- Piera-Velazquez S, Jimenez SA (2012): Molecular mechanisms of endothelial to mesenchymal cell transition (EndoMT) in experimentally induced fibrotic diseases. *Fibrogenesis Tissue Repair* 5, S7
- Piera-Velazquez S, Jimenez SA (2019): Endothelial to Mesenchymal Transition: Role in Physiology and in the Pathogenesis of Human Diseases. *Physiol Rev* 99, 1281–1324
- Pini A, Boccalini G, Lucarini L, Catarinichia S, Guasti D, Masini E, Bani D, Nistri S (2016): Protection from Cigarette Smoke-Induced Lung Dysfunction and Damage by H2 Relaxin (Serelaxin). *J Pharmacol Exp Ther* 357, 451–458
- Ponikowski P, Voors AA, Anker SD, Bueno H, Cleland JGF, Coats AJS, Falk V, González-Juanatey JR, Harjola VP, Jankowska EA, et al. (2016): 2016 ESC Guidelines for the diagnosis and treatment of acute and chronic heart failure: The Task Force for the diagnosis and treatment of acute and chronic heart failure of the European Society of Cardiology (ESC) Developed with the special contribution of the Heart Failure Association (HFA) of the ESC. *Eur Heart J* 37, 2129–2200
- Porter AG, Jänicke RU (1999): Emerging roles of caspase-3 in apoptosis. *Cell Death*

Differ 6, 99–104

Prockop DJ, Kivirikko KI (1995): Collagens: Molecular Biology, Diseases, and Potentials for Therapy. *Annu Rev Biochem* 64, 403–434

Qi G, Jia L, Li Y, Bian Y, Cheng J, Li H, Xiao C, Du J (2011): Angiotensin II infusion-induced inflammation, monocytic fibroblast precursor infiltration, and cardiac fibrosis are pressure dependent. *Cardiovasc Toxicol* 11, 157–167

Qian L, Huang Y, Spencer CI, Foley A, Vedantham V, Liu L, Conway SJ, Fu J, Srivastava D (2012): In vivo reprogramming of murine cardiac fibroblasts into induced cardiomyocytes. *Nature* 485, 593–598

Qu X, Du Y, Shu Y, Gao M, Sun F, Luo S, Yang T, Zhan L, Yuan Y, Chu W, et al. (2017): MIAT Is a Pro-fibrotic Long Non-coding RNA Governing Cardiac Fibrosis in Post-infarct Myocardium. *Sci Rep* 7, 42657

Ranchoux B, Antigny F, Rucker-Martin C, Hautefort A, Péchoux C, Bogaard HJ, Dorfmueller P, Remy S, Lecerf F, Planté S, et al. (2015): Endothelial-to-Mesenchymal Transition in Pulmonary Hypertension. *Circulation* 131, 1006–1018

Ribera J, Pauta M, Melgar-Lesmes P, Córdoba B, Bosch A, Calvo M, Rodrigo-Torres D, Sancho-Bru P, Mira A, Jiménez W, Morales-Ruiz M (2017): A small population of liver endothelial cells undergoes endothelial-to-mesenchymal transition in response to chronic liver injury. *Am J Physiol Gastrointest Liver Physiol* 313, G492–G504

Rieder F, Kessler SP, West GA, Bhilocha S, de la Motte C, Sadler TM, Gopalan B, Stylianou E, Fiocchi C (2011): Inflammation-induced endothelial-to-mesenchymal transition: a novel mechanism of intestinal fibrosis. *Am J Pathol* 179, 2660–2673

Rivera-Feliciano J, Lee KH, Kong SW, Rajagopal S, Ma Q, Springer Z, Izumo S, Tabin CJ, Pu WT (2006): Development of heart valves requires Gata4 expression in endothelial-derived cells. *Dev Camb Engl* 133, 3607–3618

Rodriguez-Vita J, Tetzlaff F, Fischer A (2017): Notch controls endothelial cells. *Oncoscience* 4, 45–46

Rogler G, Gelbmann CM, Vogl D, Brunner M, Schölmerich J, Falk W, Andus T, Brand K (2001): Differential Activation of Cytokine Secretion in Primary Human Colonic Fibroblast/Myofibroblast Cultures. *Scand J Gastroenterol* 36, 389–398

Rog-Zielinska EA, Norris RA, Kohl P, Markwald R (2016): The Living Scar – Cardiac Fibroblasts and the Injured Heart. *Trends Mol Med* 22, 99–114

Rothermel BA, Berenji K, Tannous P, Kutschke W, Dey A, Nolan B, Yoo KD, Demetroulis E, Gimbel M, Cabuay B, et al. (2005): Differential activation of stress-response signaling in load-induced cardiac hypertrophy and failure. *Physiol Genomics* 23, 18–27



- Roy O, Leclerc VB, Bourget JM, Thériault M, Proulx S (2015): Understanding the process of corneal endothelial morphological change in vitro. *Invest Ophthalmol Vis Sci* 56, 1228–37
- Sabbah HN, Sharov VG, Lesch M, Goldstein S (1995): Progression of heart failure: A role for interstitial fibrosis. *Mol Cell Biochem* 147, 29–34
- Samuel CS, Unemori EN, Mookerjee I, Bathgate RAD, Layfield SL, Mak J, Tregear GW, Du X-J (2004): Relaxin modulates cardiac fibroblast proliferation, differentiation, and collagen production and reverses cardiac fibrosis in vivo. *Endocrinology* 145, 4125–4133
- Samuel CS, Hewitson TD, Zhang Y, Kelly DJ (2008): Relaxin ameliorates fibrosis in experimental diabetic cardiomyopathy. *Endocrinology* 149, 3286–3293
- Samuel CS, Bodaragama H, Chew JY, Widdop RE, Royce SG, Hewitson TD (2014): Serelaxin is a more efficacious antifibrotic than enalapril in an experimental model of heart disease. *Hypertens Dallas Tex* 1979 64, 315–322
- Sartini S, Frizzi J, Borselli M, Sarcoli E, Granai C, Gialli V, Cevenini G, Guazzi G, Bruni F, Gonnelli S, Pastorelli M (2017): Which method is best for an early accurate diagnosis of acute heart failure? Comparison between lung ultrasound, chest X-ray and NT pro-BNP performance: a prospective study. *Intern Emerg Med* 12, 861–869
- Sasipong N, Schlegel P, Wingert J, Lederer C, Meinhardt E, Ziefer A, Schmidt C, Rapti K, Thöni C, Frey N, et al. (2021): Ligand-activated RXFP1 gene therapy ameliorates pressure overload-induced cardiac dysfunction. *Mol Ther* 29, 2499–2513
- Sassoli C, Chellini F, Pini A, Tani A, Nistri S, Nosi D, Zecchi-Orlandini S, Bani D, Formigli L (2013): Relaxin prevents cardiac fibroblast-myofibroblast transition via notch-1-mediated inhibition of TGF- $\beta$ /Smad3 signaling. *PloS One* 8, 63896
- Saxonov S, Berg P, Brutlag DL (2006): A genome-wide analysis of CpG dinucleotides in the human genome distinguishes two distinct classes of promoters. *Proc Natl Acad Sci U S A* 103, 1412–1417
- Schaer BA, Kühne MS, Blatter D, Osswald S, Sticherling C (2014): Application of a mortality risk score in a general population of patients with an implantable cardioverter defibrillator (ICD). *Heart Br Card Soc* 100, 487–491
- Schotten U, de Haan S, Neuberger HR, Eijsbouts S, Blaauw Y, Tieleman R, Allessie M (2004): Loss of atrial contractility is primary cause of atrial dilatation during first days of atrial fibrillation. *Am J Physiol-Heart Circ Physiol* 287, H2324–H2331
- Schroer AK, Merryman WD (2015): Mechanobiology of myofibroblast adhesion in fibrotic cardiac disease. *J Cell Sci* 128, 1865–1875
- Schwarzer M: Models to Investigate Cardiac Metabolism. In: *The Scientist's Guide to Cardiac Metabolism*. Elsevier 2016, 103–122

- Seibold JR, Korn JH, Simms R, Clements PJ, Moreland LW, Mayes MD, Furst DE, Rothfield N, Steen V, Weisman M, et al. (2000): Recombinant human relaxin in the treatment of scleroderma. A randomized, double-blind, placebo-controlled trial. *Ann Intern Med* 132, 871–879
- Shinde AV, Frangogiannis NG (2014): Fibroblasts in myocardial infarction: A role in inflammation and repair. *J Mol Cell Cardiol* 70, 74–82
- Shi-Wen X, Chen Y, Denton CP, Eastwood M, Renzoni EA, Bou-Gharios G, Pearson JD, Dashwood M, du Bois RM, Black CM, et al. (2004): Endothelin-1 Promotes Myofibroblast Induction through the ETA Receptor via a rac/Phosphoinositide 3-Kinase/Akt-dependent Pathway and Is Essential for the Enhanced Contractile Phenotype of Fibrotic Fibroblasts. *Mol Biol Cell* 15, 2707–2719
- Shortt J, Ott CJ, Johnstone RW, Bradner JE (2017): A chemical probe toolbox for dissecting the cancer epigenome. *Nat Rev Cancer* 17, 268
- Shrishrimal S, Kosmacek EA, Oberley-Deegan RE (2019): Reactive Oxygen Species Drive Epigenetic Changes in Radiation-Induced Fibrosis. *Oxid Med Cell Longev* 2019, 1–27
- Sime PJ, Xing Z, Graham FL, Csaky KG, Gauldie J (1997): Adenovector-mediated gene transfer of active transforming growth factor-beta1 induces prolonged severe fibrosis in rat lung. *J Clin Invest* 100, 768–776
- Sokol RZ, Wang XS, Lechago J, Johnston PD, Swerdloff RS (1989): Immunohistochemical localization of relaxin in human prostate. *J Histochem Cytochem Off J Histochem Soc* 37, 1253–1255
- Squires C, Escobar G, Payne J, Leonardi R, Goshorn D, Sheats N, Mains I, Mingoia J, Flack E, Lindsey M (2005): Altered fibroblast function following myocardial infarction. *J Mol Cell Cardiol* 39, 699–707
- Stallings-Mann ML, Waldmann J, Zhang Y, Miller E, Gauthier ML, Visscher DW, Downey GP, Radisky ES, Fields AP, Radisky DC (2012): Matrix metalloproteinase induction of Rac1b, a key effector of lung cancer progression. *Sci Transl Med* 4, 142ra95
- Starling MR, Kirsh MM, Montgomery DG, Gross MD (1991): Mechanisms for left ventricular systolic dysfunction in aortic regurgitation: importance for predicting the functional response to aortic valve replacement. *J Am Coll Cardiol* 17, 887–897
- Sun G, Reddy MA, Yuan H, Lanting L, Kato M, Natarajan R (2010): Epigenetic histone methylation modulates fibrotic gene expression. *J Am Soc Nephrol JASN* 21, 2069–2080
- Sun Y (1998): Angiotensin II, Transforming Growth Factor- $\beta$ 1 and Repair in the Infarcted Heart. *J Mol Cell Cardiol* 30, 1559–1569
- Sunnaghatta Nagaraja S, Raviraj R, Selvakumar I, Dharmalingam D, Ramadas N,

- Chellappan DR, Ponnachipudhur Chinnaswamy P, Nagarajan D (2020): Radiation-induced H3K9 tri-methylation in E-cadherin promoter during lung EMT: *in vitro* and *in vivo* approaches using vanillin. *Free Radic Res* 54, 540–555
- Swedberg K, Komajda M, Böhm M, Borer JS, Ford I, Dubost-Brama A, Lerebours G, Tavazzi L, SHIFT Investigators (2010): Ivabradine and outcomes in chronic heart failure (SHIFT): a randomised placebo-controlled study. *Lancet Lond Engl* 376, 875–885
- Sweeney M, Corden B, Cook SA (2020): Targeting cardiac fibrosis in heart failure with preserved ejection fraction: mirage or miracle? *EMBO Mol Med* 12
- Takahashi R, Asai T, Murakami H, Murakami R, Tsuzuki M, Numaguchi Y, Matsui H, Murohara T, Okumura K (2007): Pressure overload-induced cardiomyopathy in heterozygous carrier mice of carnitine transporter gene mutation. *Hypertens Dallas Tex* 1979 50, 497–502
- Tampe B, Tampe D, Müller CA, Sugimoto H, LeBleu V, Xu X, Müller GA, Zeisberg EM, Kalluri R, Zeisberg M (2014): Tet3-mediated hydroxymethylation of epigenetically silenced genes contributes to bone morphogenic protein 7-induced reversal of kidney fibrosis. *J Am Soc Nephrol JASN* 25, 905–912
- Tarnavski O, McMullen JR, Schinke M, Nie Q, Kong S, Izumo S (2004): Mouse cardiac surgery: comprehensive techniques for the generation of mouse models of human diseases and their application for genomic studies. *Physiol Genomics* 16, 349–360
- Tashima LS, Mazoujian G, Bryant-Greenwood GD (1994): Human relaxins in normal, benign and neoplastic breast tissue. *J Mol Endocrinol* 12, 351–364
- Teerlink JR, Metra M, Felker GM, Ponikowski P, Voors AA, Weatherley BD, Marmor A, Katz A, Grzybowski J, Unemori E, et al. (2009): Relaxin for the treatment of patients with acute heart failure (Pre-RELAX-AHF): a multicentre, randomised, placebo-controlled, parallel-group, dose-finding phase IIb study. *Lancet Lond Engl* 373, 1429–1439
- Teerlink JR, Cotter G, Davison BA, Felker GM, Filippatos G, Greenberg BH, Ponikowski P, Unemori E, Voors AA, Adams KF, et al. (2013): Serelaxin, recombinant human relaxin-2, for treatment of acute heart failure (RELAX-AHF): A randomised, placebo-controlled trial. *The Lancet* 381, 29–39
- Teerlink JR, Davison BA, Cotter G, Maggioni AP, Sato N, Chioncel O, Ertl G, Felker GM, Filippatos G, Greenberg BH, et al. (2020): Effects of serelaxin in patients admitted for acute heart failure: a meta-analysis. *Eur J Heart Fail* 22, 315–329
- Teichert-Kuliszewska K, Kutryk MJB, Kuliszewski MA, Karoubi G, Courtman DW, Zucco L, Granton J, Stewart DJ (2006): Bone morphogenetic protein receptor-2 signaling promotes pulmonary arterial endothelial cell survival: implications for loss-of-function

mutations in the pathogenesis of pulmonary hypertension. *Circ Res* 98, 209–217

Thanasupawat T, Glogowska A, Nivedita-Krishnan S, Wilson B, Klonisch T, Hombach-Klonisch S (2019): Emerging roles for the relaxin/RXFP1 system in cancer therapy. *Mol Cell Endocrinol* 487, 85–93

Thompson VC, Morris TGW, Cochrane DR, Cavanagh J, Wafa LA, Hamilton T, Wang S, Fazli L, Gleave ME, Nelson CC (2006): Relaxin becomes upregulated during prostate cancer progression to androgen independence and is negatively regulated by androgens. *The Prostate* 66, 1698–1709

Thum T (2014): Noncoding RNAs and myocardial fibrosis. *Nat Rev Cardiol* 11, 655–663

Thum T, Gross C, Fiedler J, Fischer T, Kissler S, Bussen M, Galuppo P, Just S, Rottbauer W, Frantz S, et al. (2008): MicroRNA-21 contributes to myocardial disease by stimulating MAP kinase signalling in fibroblasts. *Nature* 456, 980–984

Timmerman LA, Grego-Bessa J, Raya A, Bertrán E, Pérez-Pomares JM, Díez J, Aranda S, Palomo S, McCormick F, Izpisua-Belmonte JC, de la Pompa JL (2004): Notch promotes epithelial-mesenchymal transition during cardiac development and oncogenic transformation. *Genes Dev* 18, 99–115

Valdimarsdottir G, Goumans MJ, Rosendahl A, Brugman M, Itoh S, Lebrin F, Sideras P, ten Dijke P (2002): Stimulation of Id1 expression by bone morphogenetic protein is sufficient and necessary for bone morphogenetic protein-induced activation of endothelial cells. *Circulation* 106, 2263–2270

van Meeteren LA, ten Dijke P (2012): Regulation of endothelial cell plasticity by TGF- $\beta$ . *Cell Tissue Res* 347, 177–186

van Rooij E, Sutherland LB, Thatcher JE, DiMaio JM, Naseem RH, Marshall WS, Hill JA, Olson EN (2008): Dysregulation of microRNAs after myocardial infarction reveals a role of miR-29 in cardiac fibrosis. *Proc Natl Acad Sci* 105, 13027–13032

Vanchin B, Sol M, Gjaltema RAF, Brinker M, Kiers B, Pereira AC, Harmsen MC, Moonen JRAJ, Krenning G (2021): Reciprocal regulation of endothelial-mesenchymal transition by MAPK7 and EZH2 in intimal hyperplasia and coronary artery disease. *Sci Rep* 11, 17764

Vikhorev P, Vikhoreva N (2018): Cardiomyopathies and Related Changes in Contractility of Human Heart Muscle. *Int J Mol Sci* 19, 2234

Vinall RL, Tepper CG, Shi XB, Xue LA, Gandour-Edwards R, de Vere White RW (2006): The R273H p53 mutation can facilitate the androgen-independent growth of LNCaP by a mechanism that involves H2 relaxin and its cognate receptor LGR7. *Oncogene* 25, 2082–2093

Waddington CH (1968): Towards a theoretical biology. *Nature* 218, 525–527

- Wang J, Pan J, Li H, Long J, Fang F, Chen J, Zhu X, Xiang X, Zhang D (2018): lncRNA ZEB1-AS1 Was Suppressed by p53 for Renal Fibrosis in Diabetic Nephropathy. *Mol Ther Nucleic Acids* 12, 741–750
- Watson RD, Gibbs CR, Lip GY (2000): ABC of heart failure. Clinical features and complications. *BMJ* 320, 236–239
- Wawro ME, Chojnacka K, Wieczorek-Szukała K, Sobierajska K, Niewiarowska J (2018): Invasive Colon Cancer Cells Induce Transdifferentiation of Endothelium to Cancer-Associated Fibroblasts through Microtubules Enriched in Tubulin- $\beta$ 3. *Int J Mol Sci* 20
- Weber KT, Janicki JS, Shroff SG, Pick R, Chen RM, Bashey RI (1988): Collagen remodeling of the pressure-overloaded, hypertrophied nonhuman primate myocardium. *Circ Res* 62, 757–765
- Wei WY, Zhang N, Li LL, Ma ZG, Xu M, Yuan YP, Deng W, Tang QZ (2018): Pioglitazone Alleviates Cardiac Fibrosis and Inhibits Endothelial to Mesenchymal Transition Induced by Pressure Overload. *Cell Physiol Biochem* 45, 26–36
- Weinhold B (2006): Epigenetics: the science of change. *Environ Health Perspect* 114, A160-167
- Weiss A, Attisano L (2013): The TGF $\beta$  superfamily signaling pathway. *Wiley Interdiscip Rev Dev Biol* 2, 47–63
- Wilhelmi T, Xu X, Tan X, Hulshoff MS, Maamari S, Sossalla S, Zeisberg M, Zeisberg EM (2020): Serelaxin alleviates cardiac fibrosis through inhibiting endothelial-to-mesenchymal transition via RXFP1. *Theranostics* 10, 3905
- Wilkinson TN, Speed TP, Tregear GW, Bathgate RAD (2005): Evolution of the relaxin-like peptide family. *BMC Evol Biol* 5, 14
- Williams EJ, Benyon RC, Trim N, Hadwin R, Grove BH, Arthur MJ, Unemori EN, Iredale JP (2001): Relaxin inhibits effective collagen deposition by cultured hepatic stellate cells and decreases rat liver fibrosis in vivo. *Gut* 49, 577–583
- Wirtz HS, Sheer R, Honarpour N, Casebeer AW, Simmons JD, Kurtz CE, Pasquale MK, Globe G (2020): Real-World Analysis of Guideline-Based Therapy After Hospitalization for Heart Failure. *J Am Heart Assoc* 9
- Wong SH, Hamel L, Chevalier S, Philip A (2000): Endoglin expression on human microvascular endothelial cells association with betaglycan and formation of higher order complexes with TGF- $\beta$  signalling receptors. *Eur J Biochem* 267, 5550–5560
- Woodfin A, Voisin MB, Nourshargh S (2007): PECAM-1: A Multi-Functional Molecule in Inflammation and Vascular Biology. *Arterioscler Thromb Vasc Biol* 27, 2514–2523
- Wu NA, Wiseman J, Lei Y, Eastlake K, Sun X, Limb GA (2014): Modulation of the

Notch and Wnt signalling by TGF-  $\beta$  in adult human Müller stem cells. *Invest Ophthalmol Vis Sci* **1373**

Wu XP, Wang HJ, Wang YL, Shen HR, Tan YZ (2018): Serelaxin inhibits differentiation and fibrotic behaviors of cardiac fibroblasts by suppressing ALK-5/Smad2/3 signaling pathway. *Exp Cell Res* **362**, 17–27

Wynn TA, Ramalingam TR (2012): Mechanisms of fibrosis: therapeutic translation for fibrotic disease. *Nat Med* **18**, 1028–1040

Xiong J, Kawagishi H, Yan Y, Liu J, Wells QS, Edmunds LR, Fergusson MM, Yu ZX, Rovira II, Brittain EL, et al. (2018): A Metabolic Basis for Endothelial-to-Mesenchymal Transition. *Mol Cell* **69**, 689-698.e7

Xu X, Friehs I, Zhong Hu T, Melnychenko I, Tampe B, Alnour F, Iascone M, Kalluri R, Zeisberg M, Del Nido PJ, Zeisberg EM (2015a): Endocardial fibroelastosis is caused by aberrant endothelial to mesenchymal transition. *Circ Res* **116**, 857–66

Xu X, Tan X, Tampe B, Nyamsuren G, Liu X, Maier LS, Sossalla S, Kalluri R, Zeisberg M, Hasenfuss G, Zeisberg EM (2015b): Epigenetic balance of aberrant Rasal1 promoter methylation and hydroxymethylation regulates cardiac fibrosis. *Cardiovasc Res* **105**, 279–91

Xu X, Tan X, Tampe B, Sanchez E, Zeisberg M, Zeisberg EM (2015c): Snail Is a Direct Target of Hypoxia-inducible Factor 1 $\alpha$  (HIF1 $\alpha$ ) in Hypoxia-induced Endothelial to Mesenchymal Transition of Human Coronary Endothelial Cells. *J Biol Chem* **290**, 16653–64

Yamaguchi A, Sakamoto K, Minamizato T, Katsube K, Nakanishi S (2008): Regulation of osteoblast differentiation mediated by BMP, Notch, and CCN3/NOV. *Jpn Dent Sci Rev* **44**, 48–56

Yancy CW, Jessup M, Bozkurt B, Butler J, Casey DE, Drazner MH, Fonarow GC, Geraci SA, Horwich T, Januzzi JL, et al. (2013): 2013 ACCF/AHA Guideline for the Management of Heart Failure: Executive Summary: A Report of the American College of Cardiology Foundation/American Heart Association Task Force on Practice Guidelines. *Circulation* **128**, 1810–1852

Yang J, Mani SA, Donaher JL, Ramaswamy S, Itzykson RA, Come C, Savagner P, Gitelman I, Richardson A, Weinberg RA (2004): Twist, a master regulator of morphogenesis, plays an essential role in tumor metastasis. *Cell* **117**, 927–939

Yki-Järvinen H, Wahlström T, Seppälä M (1985): Human endometrium contains relaxin that is progesterone-dependent. *Acta Obstet Gynecol Scand* **64**, 663–665

Yoshimatsu Y, Watabe T (2011): Roles of TGF-  $\beta$  Signals in Endothelial-Mesenchymal Transition during Cardiac Fibrosis. *Int J Inflamm* **2011**, 1–8

- Yu CH, Suriguga, Gong M, Liu WJ, Cui NX, Wang Y, Du X, Yi ZC (2017): High glucose induced endothelial to mesenchymal transition in human umbilical vein endothelial cell. *Exp Mol Pathol* 102, 377–383
- Yuan Y, Zhang Y, Han X, Li Y, Zhao X, Sheng L, Li Y (2017): Relaxin alleviates TGF $\beta$ 1-induced cardiac fibrosis via inhibition of Stat3-dependent autophagy. *Biochem Biophys Res Commun* 493, 1601–1607
- Zabalgaitia M, Berning J, Koren MJ, Støylen A, Nieminen MS, Dahlöf B, Devereux RB (2001): Impact of coronary artery disease on left ventricular systolic function and geometry in hypertensive patients with left ventricular hypertrophy (the LIFE study). *Am J Cardiol* 88, 646–650
- Zanotti S, Canalis E (2017): Parathyroid hormone inhibits Notch signaling in osteoblasts and osteocytes. *Bone* 103, 159–167
- Zeisberg EM, Kalluri R (2010): Origins of cardiac fibroblasts. *Circ Res* 107, 1304–12
- Zeisberg EM, Potenta S, Xie L, Zeisberg M, Kalluri R (2007a): Discovery of endothelial to mesenchymal transition as a source for carcinoma-associated fibroblasts. *Cancer Res* 67, 10123–8
- Zeisberg EM, Tarnavski O, Zeisberg M, Dorfman AL, McMullen JR, Gustafsson E, Chandraker A, Yuan X, Pu WT, Roberts AB, et al. (2007b): Endothelial-to-mesenchymal transition contributes to cardiac fibrosis. *Nat Med* 13, 952–61
- Zeisberg EM, Potenta SE, Sugimoto H, Zeisberg M, Kalluri R (2008): Fibroblasts in kidney fibrosis emerge via endothelial-to-mesenchymal transition. *J Am Soc Nephrol JASN* 19, 2282–7
- Zeisberg M, Neilson EG (2009): Biomarkers for epithelial-mesenchymal transitions. *J Clin Invest* 119, 1429–1437
- Zent J, Guo LW (2018): Signaling Mechanisms of Myofibroblastic Activation: Outside-in and Inside-Out. *Cell Physiol Biochem* 49, 848–868
- Zentner GE, Henikoff S (2013): Regulation of nucleosome dynamics by histone modifications. *Nat Struct Mol Biol* 20, 259–266
- Zhang Yong, Wu X, Li Y, Zhang H, Li Z, Zhang Ying, Zhang L, Ju J, Liu X, Chen X, et al. (2016): Endothelial to mesenchymal transition contributes to arsenic-trioxide-induced cardiac fibrosis. *Sci Rep* 6, 33787
- Zhong A, Mirzaei Z, Simmons CA (2018): The Roles of Matrix Stiffness and  $\beta$ -Catenin Signaling in Endothelial-to-Mesenchymal Transition of Aortic Valve Endothelial Cells. *Cardiovasc Eng Technol* 9, 158–167
- Zhou X, Chen X, Cai JJ, Chen LZ, Gong YS, Wang LX, Gao Z, Zhang HQ, Huang WJ,

- Zhou H (2015): Relaxin inhibits cardiac fibrosis and endothelial-mesenchymal transition via the Notch pathway. *Drug Des Devel Ther* 9, 4599–4611
- Zhou XL, Fang YH, Wan L, Xu QR, Huang H, Zhu RR, Wu QC, Liu JC (2019): Notch signaling inhibits cardiac fibroblast to myofibroblast transformation by antagonizing TGF- $\beta$ 1/Smad3 signaling. *J Cell Physiol* 234, 8834–8845
- Zhu P, Huang L, Ge X, Yan F, Wu R, Ao Q (2006): Transdifferentiation of pulmonary arteriolar endothelial cells into smooth muscle-like cells regulated by myocardin involved in hypoxia-induced pulmonary vascular remodelling. *Int J Exp Pathol* 87, 463–474
- Zhuang W, Li Z, Dong X, Zhao N, Liu Y, Wang C, Chen J (2019): Schisandrin B inhibits TGF- $\beta$ 1-induced epithelial-mesenchymal transition in human A549 cells through epigenetic silencing of ZEB1. *Exp Lung Res* 45, 157–166
- Zugck C, Müller A, Helms T, Wildau H, Becks T, Hacker J, Haag S, Goldhagen K, Schwab J (2010): Gesundheitsökonomische Bedeutung der Herzinsuffizienz: Analyse bundesweiter Daten. *DMW - Dtsch Med Wochenschr* 135, 633–638



---

## Acknowledgment

I would like to take this opportunity to express my deepest gratitude to the people who have supported me during my doctorate over the past years.

First, I especially would like to thank Prof. Dr. med. Elisabeth Zeisberg who gave me the opportunity to do my doctorate in her laboratory and whose unreserved help I could always rely on. Further thanks go to my supervisor PD PhD Xingbo Xu and his wife PhD Xiaoying Tan who enabled me to take my first independent steps in science. Thank you for your excellent supervision and support, which by far exceeds the usual supervisory relationship.

Further thanks go to the second member of my supervisory committee: Prof. Dr. med. Michael Zeisberg, who was always available for constructive comments and helpful discussions despite his clinical routine. Finally, I would like to thank him as the head of the department in which I am working, for giving me the opportunity to do the job I love.

I am very grateful for the scholarship provided by the German Heart Foundation (*Deutsches Zentrum für Herz-Kreislauf-Forschung e.V.*). Its support allowed me to concentrate on my scientific work and to participate in a supportive scientific network.

Furthermore, I would like to extend my thanks to the entire team of the laboratory. The working days and especially the common activities were always a pleasure, thanks to you. You always had an open ear for questions and were constantly there to help with words and deeds. I especially would like to thank our technicians Sarah, Annika, Katrin and Anika and all students with whom I have been able to spend working days in the laboratory since 2015.

---

## Curriculum vitae

My name is Tim Pascal Wilhelmi and I was born on 30.06.1993 in Wiesbaden in Hessa, Germany as the only child of Eva Wilhelmi and Alfred Wilhelmi. From 1999 to 2003 I attended the elementary school in Ockenheim. Thereupon, I went to the Sebastian-Münster-Gymnasium in Ingelheim, where I engaged, among other voluntary activities, as a student representative and coordinated the school medical service. In this way, my interest in medicine was awakened for the first time. After graduating from high school in 2012, I started a voluntary social year at the emergency medical service in Ingelheim.

In 2013, I received confirmation to study human medicine at the Georg-August University of Göttingen. With the successful completion of the first part of the medical examination, my interest in doing a doctorate grew. I wanted to gain experience in the laboratory and decided to look for a position in cardiological working groups. My strong interest in cardiology developed based on lectures in physiology and biochemistry and during my work for the emergency medical service. I applied for a doctoral position in the AG Zeisberg (Head: Prof. Dr. Elisabeth Zeisberg), where research focused on affection of the heart's stroma during cardiac diseases. After being accepted for my doctorate, I suspended my studies for two semesters in 2015-2016 and started my practical work in the laboratory. During this time, I successfully applied for a "Promotionsstipendium" of the German Heart Foundation (DZHK) and since then have been a member of the Young DZHK network.

After I had started my studies again, I was employed as a research assistant in the working group until the end of my studies and worked on various projects. I had the opportunity to present my project in a poster session at the 2nd DZHK Conference in Berlin in 2019. The project was published in the peer-reviewed journal "Theranostics" in 2020 under the title "Serelaxin alleviates cardiac fibrosis through inhibiting endothelial-to-mesenchymal transition via RXFP1". Furthermore, I had the opportunity to publish in terms of other projects as a co-author in "Nature Communications" (2018) and "FEBS Letters" (2016).

In 2020, I completed my medical studies with the medical examination with the overall grade 2.0. Since May 2021, I work as an assistant physician at the department of nephrology and rheumatology in the Universitätsmedizin Göttingen.

In July 2022, I married my wife.